

HYBRID METHODS FOR SIMULATION  
OF MUON IONIZATION COOLING CHANNELS

BY  
JOSIAH D. KUNZ

Submitted in partial fulfillment of the  
requirements for the degree of  
Doctor of Philosophy in Physics  
in the Graduate College of the  
Illinois Institute of Technology

Approved Chu/Pavel Snopok  
Advisor

Chicago, Illinois  
May 2017



## ACKNOWLEDGMENT

It goes without saying that I am grateful to God, who has guided me in my academic path and has allowed me to fulfil my dream of getting my Ph.D. in Physics. I would also like to thank my wife, Meredith Kunz, who has been by my side even before graduate school. I am very fortunate to have an advisor like Pavel Snopok, who puts in so much time and thought on my behalf. Pavel has worked with me on every turn. I could be no luckier than to have an advisor like him.

I would like to acknowledge the committee for their valuable time and selflessness: Dan Kaplan, Linda Spentzouris, Yagmur Torun, and Xiaofan Li. The Department of Energy is also acknowledged for funding me through Pavel.

On a less serious note, I would like to thank my late cat Scout, who slept on my lap through many of my COSY days. Although he did not make it to see the end result, he will not be forgotten. I would also like to thank my puppy Oliver for his patience with me while writing my thesis, and for keeping my mind fresh with breaks for playtime.

## TABLE OF CONTENTS

	Page
ACKNOWLEDGEMENT . . . . .	iii
LIST OF TABLES . . . . .	vi
LIST OF FIGURES . . . . .	ix
LIST OF SYMBOLS . . . . .	x
ABSTRACT . . . . .	xiv
 CHAPTER	
1. INTRODUCTION . . . . .	1
1.1. COSY Infinity . . . . .	3
1.2. Introduction to Matter-Dominated Lattices . . . . .	8
1.3. Emittance . . . . .	13
1.4. Looking Forward . . . . .	17
2. STOCHASTIC PROCESSES IN OTHER CODES . . . . .	20
2.1. Energy Straggling in ICOOL . . . . .	20
2.2. Multiple Scattering in ICOOL . . . . .	30
2.3. Energy Straggling in G4beamline . . . . .	38
2.4. Multiple Scattering in G4beamline . . . . .	42
3. STOCHASTIC PROCESSES IN COSY INFINITY . . . . .	48
3.1. Energy Straggling in COSY . . . . .	48
3.2. Multiple Scattering in COSY Infinity . . . . .	51
3.3. Transverse Displacement in COSY Infinity . . . . .	59
3.4. Temporal Displacement in COSY Infinity . . . . .	63
4. SOFTWARE IMPLEMENTATION . . . . .	67
4.1. User Input . . . . .	67
4.2. COSYScript Level . . . . .	69
4.3. FORTRAN Level . . . . .	70
4.4. Summary . . . . .	71
5. RESULTS . . . . .	72
5.1. Benchmark Against Other Codes . . . . .	72
5.2. Validation . . . . .	85
5.3. The Muon Ionization Cooling Experiment . . . . .	88

5.4. Summary . . . . .	100
APPENDIX . . . . .	100
A. DERIVATION OF TRANSVERSE EMITTANCE . . . . .	101
B. DERIVATION OF THE LANDAU ENERGY LOSS DISTRIBUTION . . . . .	106
C. DERIVATION OF IMPLEMENTED SCATTERING CROSS SECTION . . . . .	114
D. A BRIEF REVIEW OF RELEVANT PARTICLE PHYSICS . . . . .	126
E. EXPLICIT FORMS OF THE DIRAC GAMMA MATRICES AND PAULI MATRICES . . . . .	130
F. PROOFS OF USEFUL DIRAC GAMMA MATRIX TRACE IDENTITIES . . . . .	132
F.1. Proof of $(\gamma^5)^2 = I_4$ . . . . .	133
F.2. Proof of $\gamma^5 \gamma^\alpha = -\gamma^\alpha \gamma^5$ . . . . .	133
F.3. Proof of $\text{Tr}(\text{odd number of } \gamma \text{ matrices}) = 0$ . . . . .	134
F.4. Proof of $\text{Tr}(\gamma^\alpha \gamma^\beta) = 4\eta^{\alpha\beta}$ . . . . .	135
F.5. Proof of $\text{Tr}(\gamma^\alpha \gamma^\beta \gamma^\delta \gamma^\epsilon) = 4(\eta^{\alpha\beta} \eta^{\delta\epsilon} - \eta^{\alpha\delta} \eta^{\beta\epsilon} + \eta^{\alpha\epsilon} \eta^{\beta\delta})$ . . . . .	136
G. REPRODUCTION OF IMPLEMENTED CODE . . . . .	137
G.1. Example COSY Deck using ABSPOLY . . . . .	138
G.2. COSYScript . . . . .	143
G.3. FORTRAN . . . . .	154
BIBLIOGRAPHY . . . . .	191

## LIST OF TABLES

Table	Page
1.1 Energy loss table for muons in iron. . . . .	18
2.1 G4beamline scattering distribution parameters. . . . .	43
5.1 MICE Step IV coil parameters. . . . .	90
5.2 MICE Step IV initial distribution Gaussian parameters. . . . .	90
5.3 Run times for the MICE Step IV simulation. . . . .	94
5.4 Step size dependence for the absorber-coil section of the MICE Step IV lattice for liquid hydrogen. . . . .	96
5.5 Step size dependence for the MICE Step IV lattice. . . . .	99

## LIST OF FIGURES

Figure	Page
1.1 The current model of particle physics. . . . .	1
1.2 The reference orbit. . . . .	5
1.3 Example of some map $\mathcal{M}$ creating a bijection from $s_0$ to $s_1$ . . . . .	7
1.4 Example of two maps $\mathcal{M}(s_0, s_1)$ and $\mathcal{M}(s_1, s_2)$ . These two maps may be combined together to reduce to a single map, $\mathcal{M}(s_0, s_2)$ . . . . .	7
1.5 Classical muon–target interaction model. . . . .	8
1.6 Quantum muon–target interaction model. . . . .	9
1.7 Proposed muon accelerator schematics. . . . .	11
1.8 Cartoon of a cooling channel. . . . .	12
1.9 Vector diagram illustrating the principle of ionization cooling in Figure 1.8. Image courtesy of [14]. . . . .	13
1.10 $x$ - $\theta$ phase space examples. . . . .	14
1.11 Stopping power curve for antimuons on copper. . . . .	17
2.1 Classical model of particle passage through matter. . . . .	23
2.2 Example of the Landau function. . . . .	29
2.3 Quantum scattering model (repeated from Figure 1.6). . . . .	31
2.4 Two parts of Green’s function with their poles at $s = \pm k$ , altered to be closed by a semicircle at $ s  = \pm\infty$ . . . . .	35
3.1 $\lambda_{max}$ vs. $\langle \lambda \rangle$ over a variety of liquid hydrogen absorber lengths and initial beam momenta. . . . .	50
3.2 Example of the COSY cumulative angular distribution function. . . . .	54
3.3 Example of the first iteration of the COSY CDF algorithm. . . . .	56
3.4 Example of a muon entering an absorber with some nonzero initial angle. . . . .	57
3.5 Two examples of true paths. . . . .	60
3.6 2D histogram of $(x, p_x)$ phase space. . . . .	61

3.7	Cross section of Figure 3.6 at $p_x = 0.08 \text{ keV}/c$ . . . . .	62
3.8	Phase space portrait of Figure 3.6. . . . .	63
3.9	Sample simulation results for the implementation of the transverse coordinate correction algorithm. . . . .	63
3.10	Sample simulation results for the implementation of the temporal displacement algorithm discussed in this section. . . . .	66
4.1	A flowchart for the structure of the new COSY routines implemented in this work. . . . .	68
4.2	Cartoon example of some of the <b>ABSPOLY</b> parameters. . . . .	69
5.1	Muons of momentum $100 \text{ MeV}/c$ through 1 mm liquid hydrogen. .	73
5.2	Muons of momentum $100 \text{ MeV}/c$ through 10 mm liquid hydrogen.	74
5.3	Muons of momentum $100 \text{ MeV}/c$ through 100 mm liquid hydrogen.	75
5.4	Muons of momentum $200 \text{ MeV}/c$ through 1 mm liquid hydrogen. .	76
5.5	Muons of momentum $200 \text{ MeV}/c$ through 10 mm liquid hydrogen.	77
5.6	Muons of momentum $200 \text{ MeV}/c$ through 100 mm liquid hydrogen.	78
5.7	Muons of momentum $300 \text{ MeV}/c$ through 1 mm liquid hydrogen. .	79
5.8	Muons of momentum $300 \text{ MeV}/c$ through 10 mm liquid hydrogen.	80
5.9	Muons of momentum $300 \text{ MeV}/c$ through 100 mm liquid hydrogen.	81
5.10	Muons of momentum $400 \text{ MeV}/c$ through 1 mm liquid hydrogen. .	82
5.11	Muons of momentum $400 \text{ MeV}/c$ through 10 mm liquid hydrogen.	83
5.12	Muons of momentum $400 \text{ MeV}/c$ through 100 mm liquid hydrogen.	84
5.13	MuScat angular scattering results for 109 mm of liquid hydrogen compared against COSY (red), G4BL (green), and ICOOL (blue).	86
5.14	MuScat angular scattering results for 159 mm of liquid hydrogen compared against COSY (red), G4BL (green), and ICOOL (blue). .	87
5.15	MuScat angular scattering results for 3.73 mm of beryllium compared against COSY (red), G4BL (green), and ICOOL (blue). .	88
5.16	MICE Step IV cell. . . . .	89
5.17	MICE Step IV $x$ position results for 350 mm of liquid hydrogen. .	92

5.18	MICE Step IV $x$ angle results for 350 mm of liquid hydrogen. . . . .	92
5.19	MICE Step IV final energy results for 350 mm of liquid hydrogen. . . . .	93
5.20	MICE Step IV $x$ position results for 65 mm of lithium hydride. . . . .	94
5.21	MICE Step IV $x$ angle results for 65 mm of lithium hydride. . . . .	95
5.22	MICE Step IV final energy results for 65 mm of lithium hydride. . . . .	95
5.23	Absorber-coil simulation results for $x$ with $10^5$ muons and a 5 step propagation. . . . .	97
5.24	Absorber-coil simulation results for $\theta_x$ with $10^5$ muons and a 5 step propagation. . . . .	97
5.25	Absorber-coil simulation results for the final energy with $10^5$ muons and a 5 step propagation. . . . .	98
5.26	MICE simulation results for $x$ with $10^5$ muons at 5th order and 50 steps. . . . .	99
5.27	MICE simulation results for $\theta_x$ with $10^5$ muons at 5th order and 50 steps. . . . .	100
A.1	Sample scatterplot of a bivariate Gaussian with its projected ellipse. . . . .	104
B.1	Plot of $\int w(u)(1 - e^{-pu}) du$ . . . . .	111
C.1	Feynman diagram for electron-muon scattering. . . . .	116
C.2	Mathematical interpretation the three branches of the Feynman diagram in Figure C.1. . . . .	117
C.3	COSY treatment of muon-electron scattering. . . . .	124

## LIST OF SYMBOLS

Symbol	Definition
$\mathcal{A}, \mathcal{B}$	Matrix, general
$a, b_r, d_r, p_g, q_g$	GEANT4 angular parameters
$b$	Impact parameter
$b_c$	COSY offset of scattering tail
$C, C_i$	Normalization constant; shell correction parameter)
$C_{Euler}$	Euler's constant ( $\approx 0.577$ )
$c$	Speed of light in a vaccuum
$\langle dE/dx \rangle$	Energy loss per unit length, mean (Bethe Bloch)
$E$	Energy (general; context dependent)
$e$	Fundamental charge (such that $z_{ch} = eQ$ )
$e^-, e^+$	Electron or antielectron
$F$	Distribution function antiderivative (general; context dependent)
$f$	Distribution function (general; context dependent)
$f_i$	Oscillator strengths
$g(E)$	Energy loss distribution function
$g(u)$	Angular distribution function
$H$	Distribution function antiderivative (general; context dependent)
$h$	Distribution function (general; context dependent); Planck's constant
$h_i$	Highland corrections ( $i = 1, 2$ )

$\hbar$	Planck's constant divided by $2\pi$
$I$	Ionization energy (mean)
$I_j$	Unit matrix of rank $j$
$K, K_i$	Constant (context dependent)
$L$	Length (of absorber or step size)
$\ell$	Time-of-flight in units of length (COSY coordinate)
$M$	Moments of a function
$\mathcal{M}$	Scattering amplitude; transfer map
$m$	Mass (general; context dependent)
$m_e$	Electron mass
$m_\mu$	Muon mass
$N$	Atomic density
$N_A$	Avagadro's Number
$N_{el}$	Electron density
$P$	Four-momentum
$P_k$	Legendre polynomials
$p$	Momentum (total)
$(p_x, p_y, p_z)$	Beamline momentum coordinate system
$Q_i$	Charge number of particle $i$
$r_e$	Electron radius
$s$	Arc length coordinate
$T$	Transverse coordinate

$T_{max}$	Maximum transferrable kinetic energy
$t$	Time (variable)
$t_z$	True path length
$U$	Spinor
$u$	Angular cosine variable ( $u = \cos \theta$ ); dummy variable
$u_0$	Characteristic cosine variable
$\vec{v}$	Unit vector
$v$	Velocity
$w$	Weight for a distribution function (context dependent)
$X_0$	Radiation length
$(x, y, z)$	Beamline position coordinate system
$Z$	Atomic charge
$z_{ch}$	Electric charge
$z_g$	Geometric path length
$\alpha$	Dummy variable
$\beta$	Relativistic velocity ( $\beta = v/c$ )
$\gamma$	Lorentz factor
$\gamma^\alpha$	Dirac gamma matrix
$\delta$	Density correction parameter; Dirac function
$\epsilon$	Energy loss fluctuation ( $\epsilon = \Delta E$ ); emittance
$\zeta$	COSY amplitude of scattering tail

$\eta$	Minkowski metric
$\theta$	Scattered angle
$\theta_0$	Angular distribution Gaussian width
$\kappa$	Vavilov limit parameter
$\lambda$	Landau parameter
$\lambda_k$	Transport free mean paths, $k^{th}$ value
$\lambda_v$	Vavilov parameter
$\mu$	Mean; muon
$\nu_e, \bar{\nu}_e$	Electron neutrino or electron antineutrino
$\nu_\mu$	Muon neutrino
$\pi$	Circle constant
$\rho$	Density
$\Sigma$	Cross section
$\sigma$	Standard deviation
$\sigma^j$	Pauli matrices
$\phi$	Laplace transformed function
$\psi$	Wavefunction, time-independent component
$\Omega$	Solid angle
$*$	Complex conjugate
$\dagger$	Transpose conjugate
$T$	Transpose of a matrix

## ABSTRACT

COSY Infinity is an arbitrary-order beam dynamics simulation and analysis code. It can determine high-order transfer maps of combinations of particle optical elements of arbitrary field configurations. For precision modeling, design, and optimization of next-generation muon beam facilities, its features make it a very attractive code. New features are being developed for inclusion in COSY to follow the distribution of charged particles through matter. To study in detail some of the properties of muons passing through material, the transfer map approach alone is not sufficient. The interplay of beam optics and atomic processes must be studied by a hybrid transfer map–Monte Carlo approach in which transfer map methods describe the average behavior of the particles in the accelerator channel including energy loss, and Monte Carlo methods are used to provide small corrections to the predictions of the transfer map accounting for the stochastic nature of scattering and straggling of particles. The advantage of the new approach is that it is very efficient in that the vast majority of the dynamics is represented by fast application of the high-order transfer map of an entire element and accumulated stochastic effects as well as possible particle decay. The gains in speed shown in this work are expected to simplify the optimization of muon cooling channels which are usually very computationally demanding due to the need to repeatedly run large numbers of particles through large numbers of configurations. This work describes the development of the required algorithms and their application to the simulation of muon ionization cooling channels. The code is benchmarked against other codes, validated with experimental results, and predicts results for current muon ionization cooling efforts.

## CHAPTER 1

### INTRODUCTION

Muons ( $\mu$ ) were first discovered experimentally in 1947 by Powell *et al.* [1] who were looking for the Yukawa meson. It is now known that muons fit into a particle group called leptons, and fit into the standard model (along with other fundamental particles) as shown in Figure 1.1.

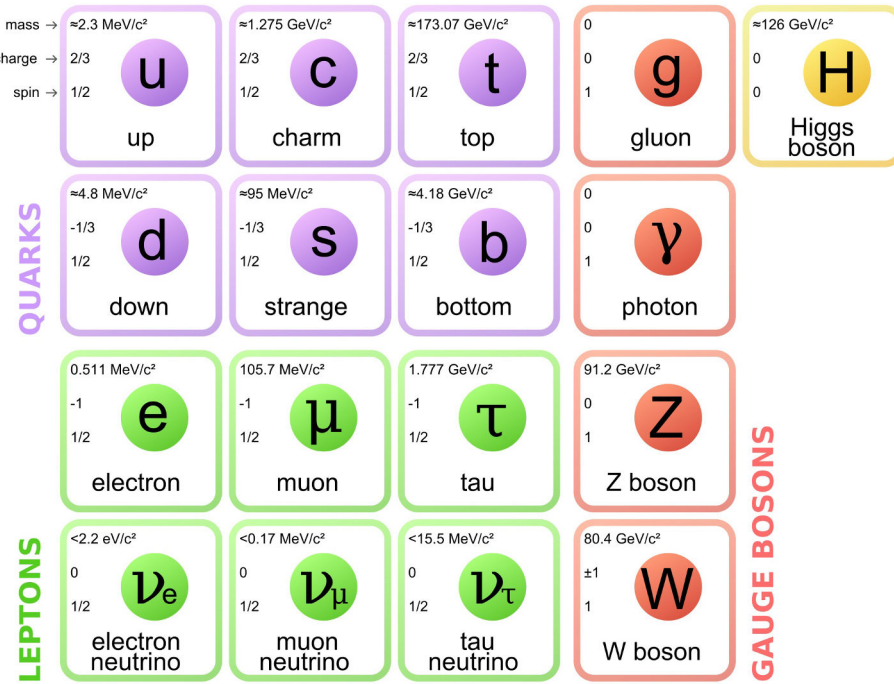


Figure 1.1. The current model of particle physics. Image courtesy of [2].

Similar to the electron ( $e$ ), the muon carries a fundamental charge of  $\pm 1$ , a total spin of  $1/2$ , and observes the electromagnetic and weak forces. Moreover, the muon also has a corresponding neutrino: the muon neutrino ( $\nu_\mu$ ). However, the muon ( $\text{mass} = 105.7 \text{ MeV}/c^2$ ) is about 200 times heavier than the electron ( $\text{mass} = 0.511 \text{ MeV}/c^2$ ). Indeed, sometimes it is useful to think of a muon simply as a heavy electron, but the mass implies several unique characteristics. One of these is the instability of muons, and results in muons decaying into an electron, an electron antineutrino, and

a muon neutrino:

$$\mu \rightarrow e + \bar{\nu}_e + \nu_\mu.$$

This is quite interesting, as it means muons are a double-edged sword. On the one hand, their point-like nature means that muon collisions are clean. That is to say, muon colliders have a great advantage over, e.g., proton colliders since protons are composed of three quarks. Each quark may have a different flavor or energy level and hence adds more variables to the analysis. Furthermore, each quark is bound, and so gluon interactions must also be considered. These quarks and gluons may undergo hadronization when interacting with one another, creating a plethora of possible hadrons. Hadronization is not fully understood, and so these sprays of hadrons are typically lumped together as a single “jet.” While there are many working models for jet analysis, none are exact. Conversely, any data from muon interactions will have relatively little noise and will not produce jets.

Clean collisions can also be achieved with linear electron colliders. Yet unlike the electron, the muon does not emit a large amount of synchrotron radiation as it is accelerated. This is because the power irradiated by a particle due to synchrotron radiation is inversely proportional to the mass of the particle to the fourth power [3]:

$$P \propto 1/m^4.$$

Therefore, the relative power loss due to synchrotron radiation for electrons and muons is  $P_e/P_\mu \propto m_\mu^4/m_e^4 \approx 1.8 \times 10^9$ . Since muons lose power via synchrotron radiation at roughly one-billionth the rate of electrons, it is more efficient to have a circular muon accelerator than a circular electron accelerator.

However, there is one problem with a muon accelerator. A rest frame lifetime of  $2.2 \mu\text{s}$  requires the muons to be accelerated quickly before they decay. This is a challenge for circular colliders that require a high-intensity beam.

Overall, it appears that there are several advantages and one key disadvantage: the short lifetime of the muon. However, this is a disadvantage only for muon colliders. Another application, which turns the moderately short lifetime into an advantage, is a neutrino factory. This is a facility that is dedicated to the output of a neutrino beam. Muons have two primary advantages over fission reactor neutrino sources, which only produce electron neutrinos. The first is that muons decay into exactly two flavors of neutrino: electron and muon. Therefore, the initial composition of the neutrino beam would be well-defined. This is important since neutrinos can change their flavors over time, and having a well-defined mixed beam provides more data. Secondly, since neutrinos have no electric charge, they cannot be manipulated via electromagnetic focusing methods. However, the beam of muons can be focused into a high-intensity beam, and the intensity of the neutrino beam will reflect this. When compared to  $\pi^\pm$  neutrino sources, which also produce both muon and electron neutrinos, muons have the benefit of having a lifetime that is two orders of magnitude longer. This means that unlike pions, muons can be collected and focused in a feasible amount of time.

## 1.1 COSY Infinity

COSY Infinity is a beamline simulation tool used in the design, analysis, and optimization of particle accelerators [4]. COSY uses the transfer map approach, which evaluates the overall effect of a system of beamline elements on a beam of particles using differential algebra. This involves expanding an ordinary differential equation into multivariate Taylor polynomials up to arbitrary order [5]. Each particle in this work is represented by its coordinates as a phase space vector. The form of phase

space vectors used in this work is

$$\mathbf{Z} = \begin{pmatrix} x \\ y \\ l = k(t - t_0) \\ a = p_x/p_0 \\ b = p_y/p_0 \\ \delta = (E - E_0)/E_0 \end{pmatrix}, \quad (1.1)$$

where the coordinates are transverse positions  $(x, y)$ , time-of-flight in units of length  $(l)$ , transverse angles w.r.t. the reference particle  $(a, b)$ , and kinetic energy deviations w.r.t. the reference particle  $(\delta)$ .  $k = -v_0\gamma/(1 + \gamma)$  converts time into distance,  $p_x$  and  $p_y$  are the  $x$  and  $y$  momenta,  $p$  (no subscript) is the total momentum, and  $E$  is the kinetic energy. The 0 subscript in the definitions denotes the reference particle properties.

In beam physics, phase space vectors  $\mathbf{Z}$  are subject to physics processes. This effect can usually be represented by a differential equation. For example, a non-relativistic particle in an electromagnetic field is subject to the force law [3]

$$\mathbf{F} = Q(\mathbf{E} + \mathbf{v} \times \mathbf{B}),$$

where  $\mathbf{F}$  is the force,  $\mathbf{E}$  and  $\mathbf{B}$  are the electric and magnetic fields,  $Q$  is the charge, and  $\mathbf{v}$  is the velocity. In terms of the momentum, this is

$$\frac{d}{dt}\mathbf{p} = Q(\mathbf{E} + \frac{1}{m}\mathbf{p} \times \mathbf{B}).$$

Fortunately, any arbitrary order ordinary differential equation (ODE) containing the phase space vector  $\mathbf{Z}$  can be rewritten as a first-order ODE [5]. For an order

$n$  ODE, a first-order ODE is constructed by introducing  $n - 1$  new variables. This is to say that

$$\frac{d^n}{dt^n} \mathbf{Z} = \mathbf{f} \left( \frac{d^0}{dt^0} \mathbf{Z}, \dots, \frac{d^{n-1}}{dt^{n-1}} \mathbf{Z} \right)$$

can be rewritten as

$$\frac{d}{dt} \begin{pmatrix} \mathbf{Z} \\ \mathbf{Z}_1 \\ \vdots \\ \mathbf{Z}_{n-1} \end{pmatrix} = \begin{pmatrix} \mathbf{Z}_1 \\ \mathbf{Z}_2 \\ \vdots \\ \mathbf{f}(\mathbf{Z}, \dots, \mathbf{Z}_{n-1}) \end{pmatrix}.$$

Here,  $\mathbf{f}$  represents the physics processes. For the Maxwell's equations example, the equation is already first order in  $a$  and  $b$ , with the momentum component of  $\mathbf{f}$  as

$$\mathbf{f}(\mathbf{p}) = Q(\mathbf{E} + \frac{1}{m} \mathbf{p} \times \mathbf{B}) = Q(\mathbf{E} + \frac{1}{m} [ap_0 \hat{x} + bp_0 \hat{y} + p_z \hat{z}] \times \mathbf{B}).$$

Furthermore, COSY does not use time as the independent variable, but rather arc length  $s$  (see Figure 1.2).

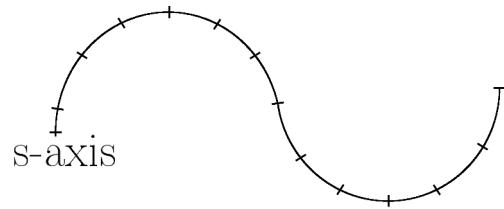


Figure 1.2. The reference orbit. Figure courtesy of [6].

If there exists a unique evolution of  $\mathbf{Z}$  then it is possible to construct the so-called transfer map  $\mathcal{M}$ . Mathematically, this relationship is  $\mathbf{Z}(s) = \mathcal{M}(s_0, s) * \mathbf{Z}(s_0)$ , with  $*$  representing the application of the transfer map to the phase space vector  $\mathbf{Z}$  at  $s_0$ .

It is possible to construct a transfer map for most cases in beamline physics. This is because most beamline elements follow differential equations which yield unique solutions dependent on initial conditions (such as Maxwell's equations). If there does not exist a unique evolution of  $\mathbf{Z}$  then it is not possible to construct the transfer map. Systems which produce a unique evolution of  $\mathbf{Z}$  are called "deterministic."

An example of the relationship between the initial phase space vector, the transfer map, and the final phase space vector can be seen in Figure 1.3. The initial phase space occupied by the beam of particles is at the coordinate  $s_0$ . Physically, there exists some deterministic beamline element between  $s_0$  and  $s_1$ . This element can be represented by the map  $\mathcal{M}$ , which creates a bijection for the phase space vectors  $\mathbf{Z}(s_0)$  and  $\mathbf{Z}(s_1)$  between the initial coordinate  $s_0$  and the final coordinate  $s_1$ .

Entire lattices may also be represented by a single transfer map. This is done by dividing the lattice into its base components or elements. A transfer map for each corresponding element may then be produced. For two example elements between coordinates  $s_0$  and  $s_2$  (see Figure 1.4), the composition of two maps yields another map:  $\mathcal{M}(s_1, s_2) \circ \mathcal{M}(s_0, s_1) = \mathcal{M}(s_0, s_2)$ . Therefore, it is possible to simplify the middle part  $s_1$ . In this way, the transfer maps from small components build up into a single transfer map for the whole system. Computationally this is advantageous because once calculated, it is much faster to apply a single transfer map to a distribution of particles than to simulate that same distribution through many meters of individual lattice elements.

Along with the tracking of particles through a lattice, COSY also has a plethora of analysis and optimization tools, including (but not limited to) lattice aberration and correction tools, support for Twiss parameters, support for tunes and nonlinear tune shifts, built-in optimizers for lattice design, and spin tracking.

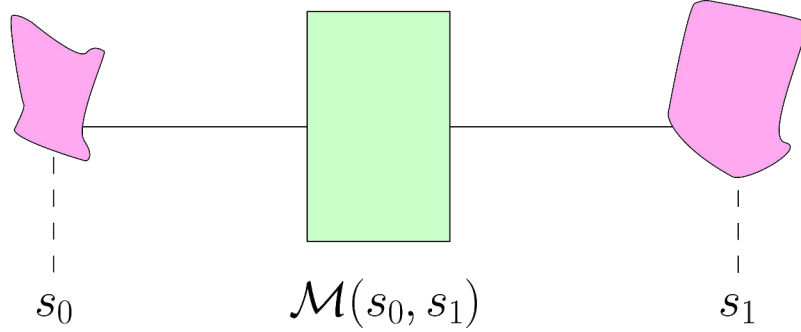


Figure 1.3. Example of some map  $\mathcal{M}$  creating a bijection from  $s_0$  to  $s_1$ .

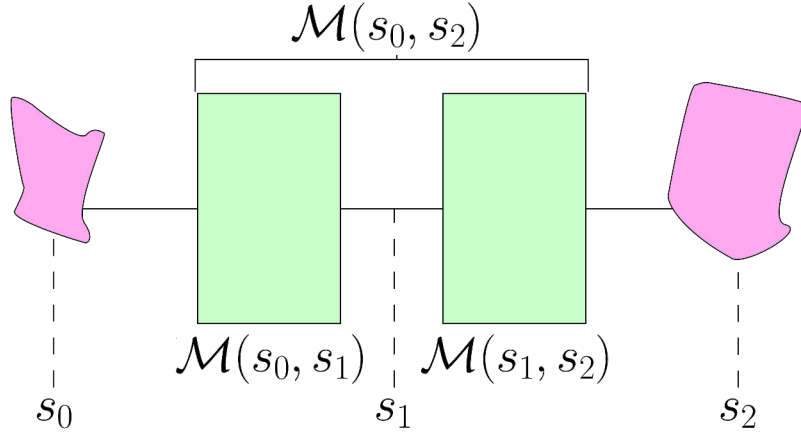


Figure 1.4. Example of two maps  $\mathcal{M}(s_0, s_1)$  and  $\mathcal{M}(s_1, s_2)$ . These two maps may be combined together to reduce to a single map,  $\mathcal{M}(s_0, s_2)$ .

Valid elements are any beamline elements that are deterministic. Elements used in this study are magnetic multipoles (dipoles, quadrupoles, etc.), solenoidal coils, radiofrequency (RF) cavities, and drifts. Currently supported elements in COSY include but are not limited to: various magnetic and electric multipoles (with or without fringe effects), homogeneous and inhomogeneous bending elements, Wien

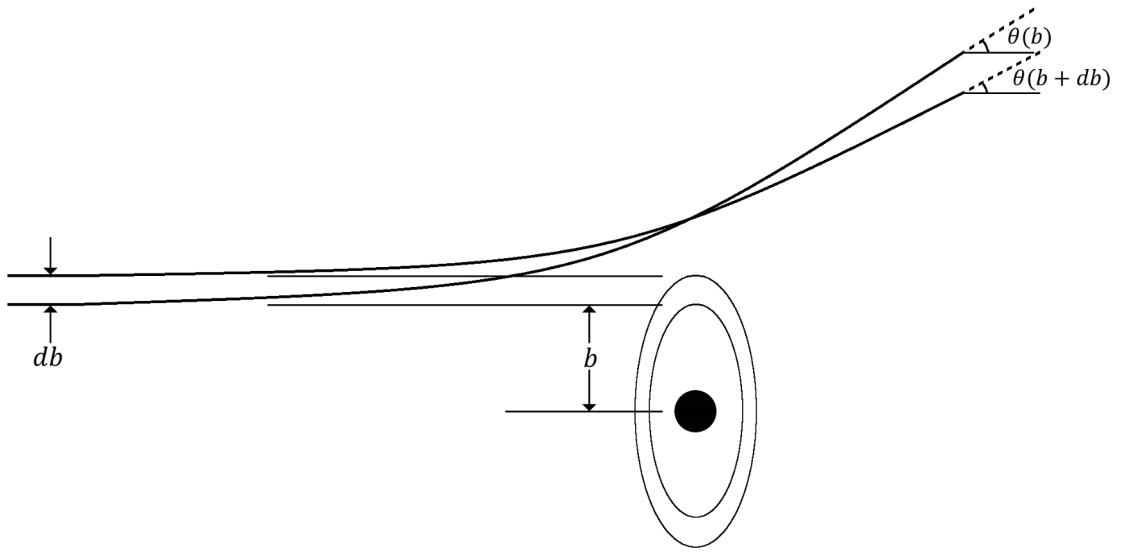


Figure 1.5. Classical muon–target interaction model courtesy of [9].

filters, wigglers and undulators, cavities, cylindrical electromagnetic lenses, general particle optical elements, and deterministic polynomial absorbers of arbitrary order.

## 1.2 Introduction to Matter-Dominated Lattices

**1.2.1 Introduction to Stochastic Effects.** This section introduces stochastic effects, or effects that are intrinsically random. These effects are in contrast to deterministic effects, which are not random and hence can be predicted exactly.

This work concerns the interactions between a muon beam and some stationary target called the “absorber”—typically a cylinder or wedge of a material with low nuclear charge ( $Z$ ) such as liquid hydrogen or lithium hydride. The simplest model of a beam interacting with some stationary target can be found in several textbooks [7,8], with the model from [9] illustrated in Figure 1.5.

In this figure,  $b$  is referred to as the impact parameter and is measured with respect to the particle’s initial trajectory. For a beam of noninteracting particles and a perfectly stationary target, classical mechanics suggests that this is a purely

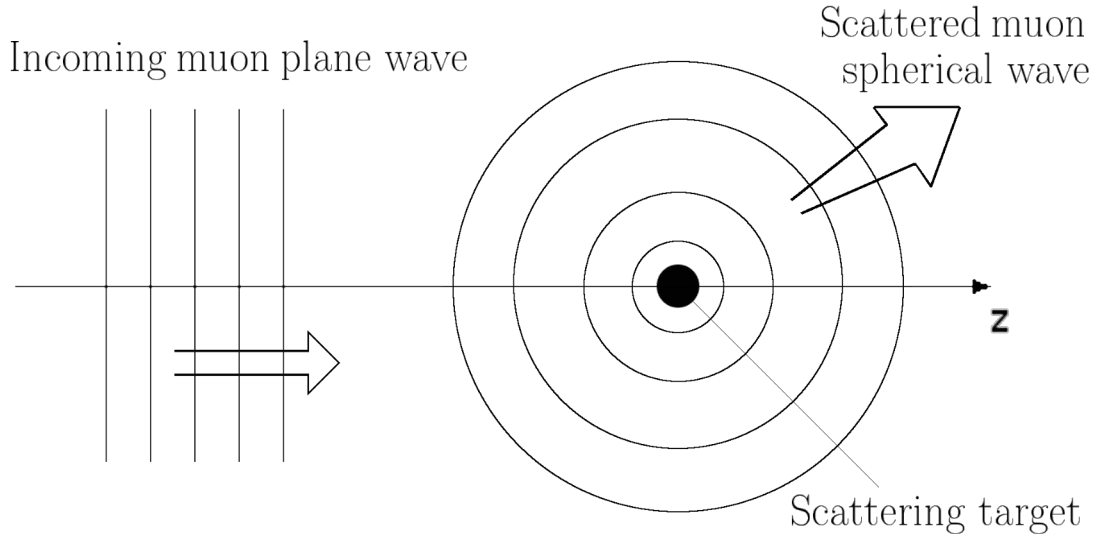


Figure 1.6. Quantum muon–target interaction model. The incoming particle wavefunction is represented as a plane wave and is scattered locally as a spherical wave. Image courtesy of [8].

deterministic problem (see, e.g., “hard-sphere scattering” in [8]); the particle with a smaller impact parameter  $b$  deflects more than its neighbor with a slightly larger impact parameter  $b + db$ . Since this model is entirely based on initial conditions, it would be relatively easy to implement these effects into the map methods of COSY Infinity. However, reality does not follow the model of Figure 1.5. A more accurate model is illustrated by Figure 1.6. Here the target is still approximated as fixed, but the incident particle is now approximated as a traveling plane wave and the scattered particle as a spherical wave (at least locally). It is shown later that this model predicts

1. a spectrum of energy loss  $\omega(\epsilon)$  which yields the probability of losing an amount of energy  $\epsilon$  (see Section 2.1), and
2. a scattering amplitude which gives the shape of the probability distribution of scattering in a given direction  $\theta$  (see Section 2.2).

Hence quantum theory suggests that even if two identical particles have identical initial conditions their final conditions are not the same.

**1.2.2 Muon Ionization Cooling.** In Section 1.1, the primary disadvantage to the considered muon-based accelerator was the muon lifetime ( $2.2 \mu\text{s}$  at rest). This is expected to be far too short a timespan to be useful in a traditional accelerator scheme since the muons must be collected, focused, and accelerated. For the moment, observe the two proposed schematics in Figure 1.7 [10]. The section labeled “Proton Driver” produces protons, which will eventually yield muons. This is essential since muons do not naturally occur in great quantities at a convenient extraction point. In order to create muons, the protons strike some large target (which must be optimized to produce the highest yield), resulting in a spray of protons, muons, electrons, and pions (even shorter-lived particles consisting of a quark-antiquark pair). To further optimize this process, it is advantageous to let the pions decay into muons via  $\pi^+ \rightarrow \mu^+ + \nu_\mu$ . The resulting ensemble of muons is then split up into bunches. The next section in Figure 1.7 is the focus of this thesis. For now, it is simply addressed as the “cooling channel” and delved into later. Cooling the beam simply means reducing the beam’s phase space volume. The purpose of cooling is to increase the density of the resulting beam. This lets the beam fit into smaller components such as magnets and RF cavities, which are less expensive than larger ones. However, this increase in density also increases the luminosity of the beam in the long run. For a collider, this means more collisions; for a neutrino factory, this means more neutrino counts in the detectors (since neutrinos are neutral, there is no way to focus a neutrino beam once created). After the beam of muons is focused it is accelerated to an appropriate energy. For a neutrino factory, this is  $\gtrsim 5 \text{ GeV}$ , and the muon and antimuon beams are allowed to decay in a storage ring. For a muon collider, the center-of-momentum energy is  $\sim 126 \text{ GeV}$  for a Higgs factory or up to  $10 \text{ TeV}$  for high energy studies.

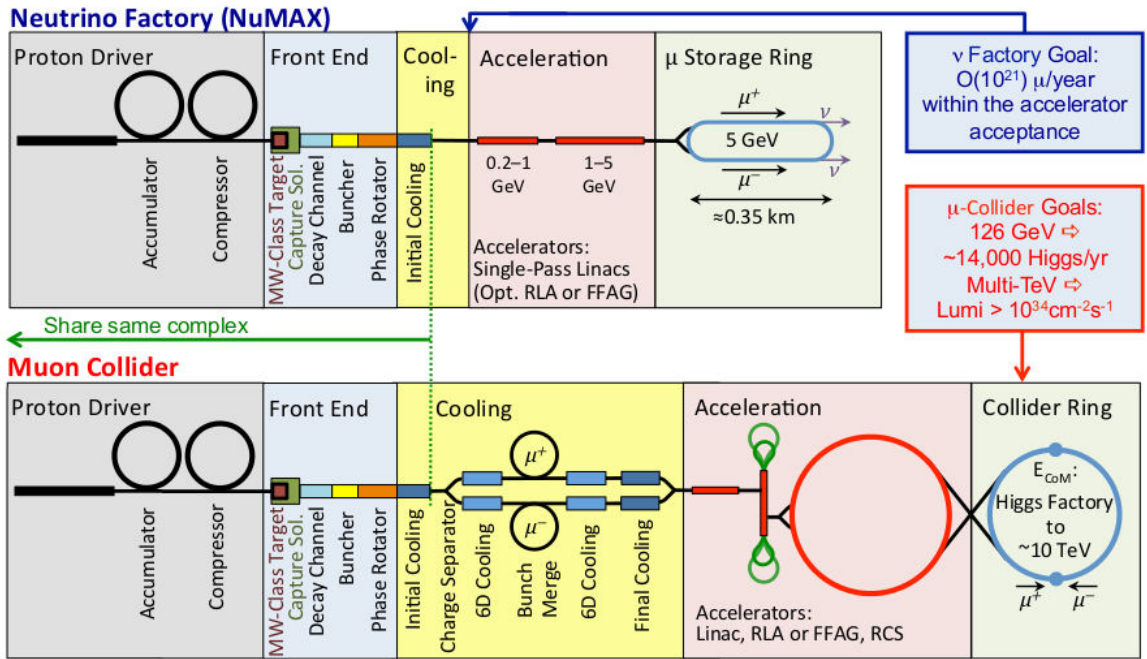


Figure 1.7. Proposed muon accelerator schematics. The neutrino factory (top) is designed to produce high-intensity beams of neutrinos. The muon collider (bottom) is designed to produce high energy high-intensity beams of muons for, e.g., Higgs production. The muon collider demands more cooling and acceleration than the neutrino factory due to the higher intensity and energy threshold requirements of high energy collision physics. Image courtesy of [10].

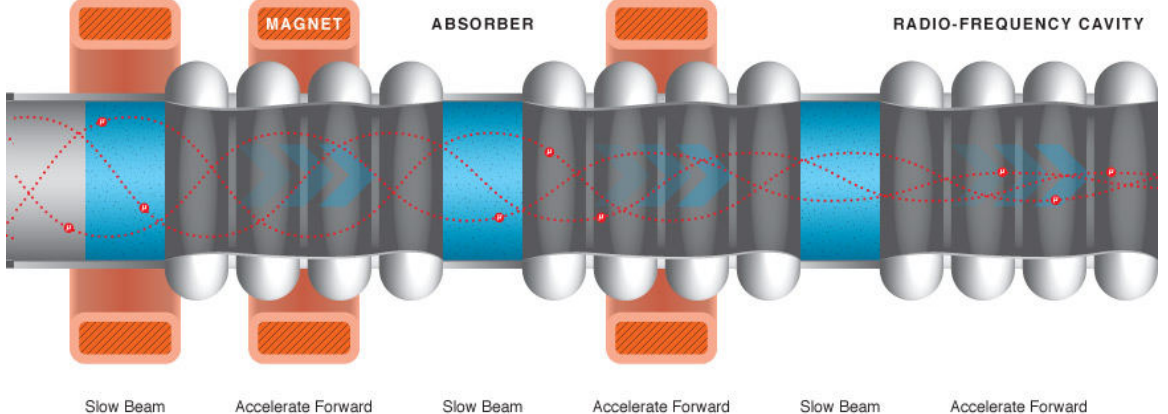


Figure 1.8. Cartoon of a cooling channel, courtesy of [10].

The cooling channel is the crux of the entire operation for either purpose. Ionization cooling is the only cooling technique fast enough to work within the average muon lifetime. Ionization cooling requires the beam to deposit its energy in matter, thus ionizing the matter.

While the idea behind ionization cooling has been around since at least 1956 [11,12], it did not appear to be a viable option until roughly 1970 [13]. It was believed that multiple scattering effects would mask any cooling benefits. Scattering is a quantum effect in which two objects are deflected when they are in close proximity and hence is intrinsically random. This means that while the energy deposition reduced the beam's phase space, the beam would also grow in the transverse direction due to this multiple scattering.

Now, this seems to be quite the opposite of what is intended; ionization cooling potentially produces a slow, fat beam, and an effective muon beam should be narrow and fast so that the Lorentz boost keeps the muons from decaying. Fortunately, these problems can be solved simultaneously. The overall cooling scheme is presented in Figure 1.8 and the vector describing the change in momentum is depicted in Figure 1.9.

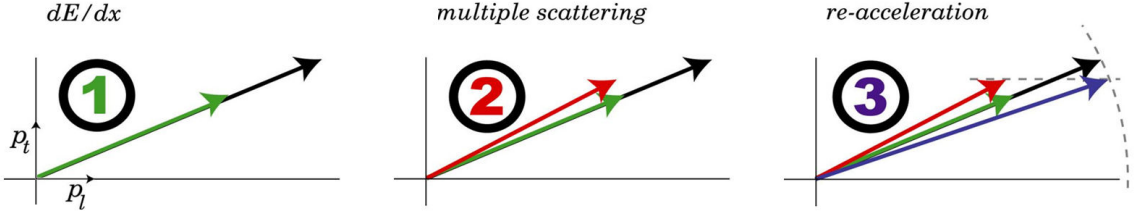


Figure 1.9. Vector diagram illustrating the principle of ionization cooling in Figure 1.8. Image courtesy of [14].

The key is to use a cell which contains both the ionizing material and a radio frequency cavity. To understand why this solves the problem of potentially producing a beam with a large transverse phase space, it is necessary to observe Figure 1.9. In Figure 1.9, the longitudinal momentum ( $p_l$ ) is plotted against the transverse momentum ( $p_t$ ).

1. Beam deposits energy in material, reducing the momentum in all directions.
2. Multiple scattering effects are observed. The transverse phase space increases (or “heats up”). By a clever choice of absorbing material (as discussed in the next section), the growth of the transverse phase space is kept to a minimum at this stage.
3. The beam is re-accelerated by radiofrequency cavities, increasing the longitudinal momentum only. The result is a reduction in transverse momentum (i.e., blue vector compared to black vector). This solves the problem of having a large transverse phase space. Moreover, re-acceleration alleviates the problem of decay: after the beam loses energy, it gains that much energy again, and so the Lorentz boost stays constant on average. This also allows for the use of the same cooling cell repeatedly without need to modify it.

### 1.3 Emittance

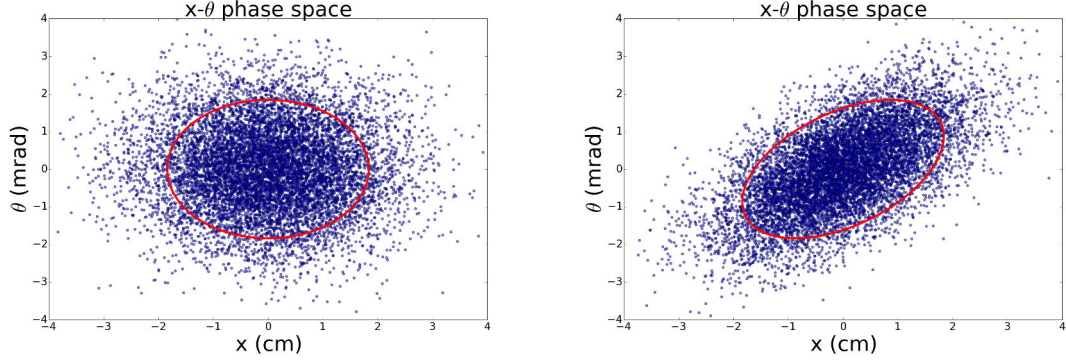


Figure 1.10.  $x$ - $\theta$  phase space examples. Left: example beam with no  $x$ - $\theta$  correlation ( $\langle x\theta \rangle = 0$ ). Right: example beam with significant  $x$ - $\theta$  correlation ( $\langle x\theta \rangle = 0.8$ ).

Emittance ( $\epsilon$ ) is a measure of the volume of phase space occupied by the beam. It is sometimes beneficial to normalize the emittance by the relativistic factors,  $\gamma$  and  $\beta$ . This is useful because when a beam accelerates the transverse angles decrease. This results in a reduction of  $\epsilon_x$  (where  $x$  represents the general transverse direction) even though transverse phase space was not directly manipulated. However,  $\epsilon_x^N$  stays constant when a beam accelerates, and hence gives an invariant measure characterizing the beam. The relevant transverse emittance is

$$\epsilon_x^N = \beta\gamma\epsilon_x = \beta\gamma\sqrt{\langle x^2 \rangle \langle \theta^2 \rangle - \langle x\theta \rangle^2}. \quad (1.2)$$

Here, azimuthal symmetry is assumed, and so  $x$  represents the general transverse position, and  $\theta = \sin^{-1} p_x/p$  is the projection of the divergence angle of the particle trajectory onto the  $x$ - $z$  plane, where  $z$  is the longitudinal Cartesian coordinate.

The full derivation of the emittance in Eq. (1.2) can be found in Appendix A. Qualitatively, if there exists no cross-dependence in  $x$  and  $\theta$ , then the distribution should be a non-tilted ellipse. Then the emittance is proportional to the geometric mean,  $\sqrt{\langle x^2 \rangle \langle \theta^2 \rangle}$ . However, if there is some cross-dependence, then the result is a tilted ellipse. For a sample comparison of tilted vs. non-tilted ellipses, see Figure 1.10. Here, the emittance is outlined in red.

The goal is to observe the evolution of the emittance through an absorber. Taking the expression for the rate of change of normalized transverse emittance over a length  $z$  from [15] results in

$$\frac{d\epsilon_x^N}{dz} = \frac{\beta_\perp}{2} \frac{E_s^2}{\beta^3 Emc^2} \frac{1}{X_0} - \frac{1}{\beta} \left| \left\langle \frac{dE}{dz} \right\rangle \right| \frac{\epsilon_x^N}{E},$$

where  $\beta = v/c$  is the velocity in units of  $c$ ,  $\beta_\perp$  is the transverse betatron function,  $E_s$  is a characteristic energy (usually taken as 14 MeV),  $E$  is the (mean) energy of the beam,  $m$  is the mass of the beam species,  $X_0$  is the radiation length of the absorber material, and  $\langle dE/dz \rangle$  is the mean energy loss of the beam through the absorber. The first term represents “heating” and the second term represents “cooling” in the transverse plane.

The first term is

$$\frac{d\epsilon_x^N}{dz}(\text{heat}) = \frac{\beta_\perp}{2} \frac{E_s^2}{\beta^3 Emc^2} \frac{1}{X_0}. \quad (1.3)$$

Now it is clearer why this is referred to as the heating term. Since the derivative of emittance is positive, this part represents emittance growth. Moreover, to reduce this growth, it is necessary to have highly energetic particles through a material with a large radiation length (typically  $X_0$  increases with decreasing nuclear charge  $Z$ ).

The second term is

$$\frac{d\epsilon_x^N}{dz}(\text{cool}) = -\frac{1}{\beta} \left| \left\langle \frac{dE}{dz} \right\rangle \right| \frac{\epsilon_x^N}{E}. \quad (1.4)$$

Similarly as for the heating term, it is now understandable why this is referred to as the cooling term. The rate of change of the normalized transverse emittance is negative, and so the transverse phase space shrinks. The shape of the cooling term is determined by the average energy loss,  $|\langle \frac{dE}{dz} \rangle|$ . A good example of an average energy loss curve can be seen in Figure 1.11 [16]. For this example, there are several effects noted in Figure 1.11. One may be tempted to think that based on Eq. (1.4) the most

cooling should occur in the Anderson-Ziegler regime at  $\beta\gamma \sim 0.01$ . This may seem correct since there is a  $1/E$  dependence in Eq. (1.4), and so the high energy part of the curve is not advantageous. Indeed, for  $\rho = 8.92 \text{ g/cm}^3$  it is easy to see that at  $\beta\gamma = 0.01$

$$\frac{d\epsilon_x^N}{dz}(\text{cool}) \approx -900 \text{ cm}^{-1} \cdot \epsilon_x^N.$$

However, a better approach is to build a cooling cell with the minimum ionization point in mind (in the Bethe regime, where  $\beta\gamma \sim 2$ ). At the peak ( $\beta\gamma \sim 0.01$ ), the muon beam slows down considerably through a single cooling cell, and one is at risk of losing the beam to decay. Moreover, Figure 1.11 only depicts the stopping power, not the actual energy loss that individual particles experience. The individual energy loss is a stochastic effect, and the distribution of energy losses broadens with decreasing beam energy.<sup>1</sup> Moreover, the average of the final energy distribution is smaller for lower energy particles. These facts combined mean that at lower energies, there are more particles that stop completely.

Finally, Eq. (1.3) suggests that higher energies are better since they reduce the heating term. For these reasons, it is apparent that a muon cooling cell should be made of low- $Z$  materials such as liquid hydrogen or lithium hydride and operate in the range of momenta between  $100 \text{ MeV}/c$  and  $400 \text{ MeV}/c$ .

When particles impinge upon a fixed target, they lose some of their energy. For massive particles like muons, there are a number of major effects that contribute. However, it is important to note that in the muon cooling regime only ionization contributes significantly to the energy loss. To see this, take for an example the

---

<sup>1</sup>This may be seen via the variance-like term (defined in Eq. (2.11)) inside the definition of the Landau parameter (defined in Eq. (B.8)).

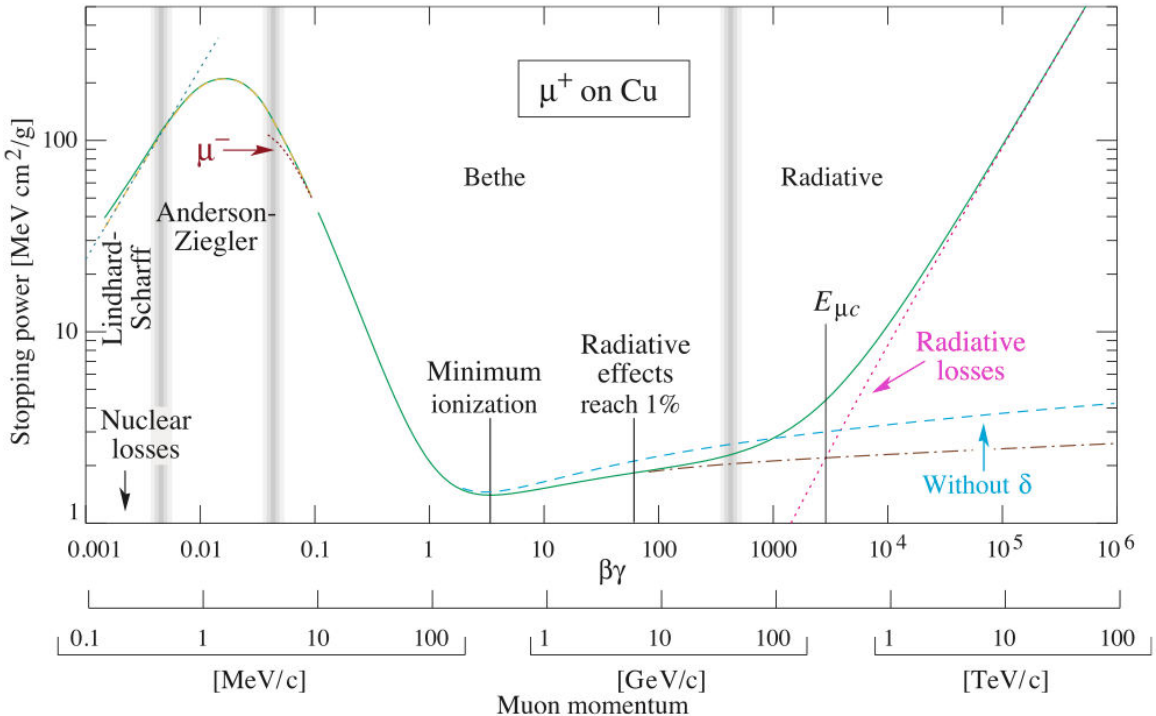


Figure 1.11. Stopping power curve for antimuons on copper, courtesy of [16].

relatively heavy element of iron.<sup>2</sup> In Table 1.1, the energy loss contributions of these four effects can be seen. However, the non-ionization effects start to contribute only at an initial beam kinetic energy of 1.40 GeV—far outside of the muon cooling regime.

This is a good example because all of the cooling materials currently being considered have less muon stopping power than iron. This means that iron represents the maximum contribution of non-ionization energy loss per initial beam energy; that is, the non-ionization effects begin to emerge at much higher energies for lighter materials such as liquid hydrogen. Note that Figure 1.11 may also be useful when discussing this subject, as the minimum ionization regime is explicitly characterized.

## 1.4 Looking Forward

<sup>2</sup>While iron would not likely be used as an absorber material, it serves as an exaggerated example due to its  $Z$  value of 26.

Table 1.1. Energy loss table for muons in iron, courtesy of [17]. The first two columns show  $T$ , the kinetic energy of the beam, and  $p$ , the corresponding momentum of the beam. The next four columns show the various contributions to energy loss, with column 7 giving the total energy loss. Finally, column 8 shows the range of muons through the material calculated by the continuous slowing down approximation.

$T$ MeV	$p$ MeV/ $c$	Ionization	Brems	Pair prod MeV cm $^2$ /g	Photonucl	Total	Range g/cm $^2$
10	47.04	5.494				5.494	1.025
14	56.16	4.321				4.321	1.854
20	68.02	3.399				3.399	3.437
30	85.09	2.654				2.654	6.812
40	100.3	2.274				2.274	10.91
80	152.7	1.717				1.717	31.78
100	176.4	1.616				1.616	43.82
140	221.8	1.516				1.516	69.50
200	286.8	1.463				1.463	109.9
300	391.7	1.452				1.453	178.7
400	494.5	1.467				1.467	247.2
800	899.5	1.548				1.548	512.4
1000	1101	1.581	0.001			1.582	640.2
1400	1502	1.635	0.001		0.001	1.637	888.5

This work uses basic principles to successfully implement muon ionization cooling simulation tools in COSY Infinity. The algorithms which have been implemented are derived from first principles or other codes. The derivations for other codes can be found in Chapter 2 and novelly for this work in Chapter 3. Furthermore, these algorithms are augmented by fitting the results to experimental data and benchmarking against external sources. The results of benchmarking and validation are discussed in Chapter 5, wherein it is shown that the new routines in COSY produce robust, accurate, and fast simulations.

## CHAPTER 2

### STOCHASTIC PROCESSES IN OTHER CODES

In this chapter, the two major stochastic processes—energy straggling and multiple scattering—are detailed. Because there are so many models for these two key processes, two case studies are shown as a frame for their derivations: ICOOL [18] and G4beamline [19]. Both of these codes use particle-by-particle propagation and do not use the transfer map method discussed in Section 1.1.

The first case study is ICOOL [18] and covers the classic models. Much of the classic theory is also used in the new COSY routines. Consequently, the sections concerning ICOOL serve as a foundation for the derivations in Chapter 3. ICOOL was created at Brookhaven National Laboratory for the benefit of the members of the Neutrino Factory and Muon Collider Collaboration, who specifically study ionization cooling problems.

The second case study is G4beamline [19], which is based on GEANT4 [20]. GEANT4 implements a more novel approach. Many of the routines use empirically-tuned parameters. Consequently, G4beamline is accurate for a variety of particles over a wide range of energies. It should be noted that muons, for which there is little experimental data available, are usually grouped with protons as heavy charged particles. Therefore, for lack of experimental data, muons use the same routines as protons.

#### **2.1 Energy Straggling in ICOOL**

ICOOL [18] employs four straggling models, three of which were used in these muon simulations studies. Discussed below, these are

1. Gaussian (Bohr),
2. Landau distribution, and

3. Vavilov distribution (with appropriate limits).

The fourth model was not considered for this study.

**2.1.1 Gaussian (Bohr) Straggling Model.** The first model uses a Gaussian function to model the energy loss distribution. Recall that Gaussian distributions are defined by two parameters: the standard deviation  $\sigma$  and the mean  $\mu$ .

According to [20], the first of these is given by:

$$\sigma^2 = 2\pi e^2 N_A T_c \frac{Z\rho L}{A} \frac{1 - \beta^2/2}{\beta}, \quad (2.1)$$

where  $e$  is the fundamental electric charge,  $N_A$  is Avogadro's number,  $T_c$  the kinetic energy cut of  $\delta$ -electrons,<sup>3</sup>  $Z$  the nuclear charge,  $\rho$  the density of the material,  $L$  the length of the material,  $A$  the nuclear mass, and  $\beta = v/c$  the velocity in units of  $c$ .

The mean comes from the Bethe-Bloch equation [21], which is derived here and yields Eq. (2.5). The derivation is the so-called classical derivation, which applies first principles and mechanically derives an expression. The classically-derived intermediate equation is then subject to modern corrections, which account for the approximations made or phenomena neglected by the classical derivation.

### *Classical Derivation*

The process begins with a particle of charge  $e$  moving through a material. It is assumed that the mass of the incoming particle is much greater than the mass of the electron since scattering is neglected in this derivation. Moreover, the electron must either be at rest and fixed into place (which is nonphysical) or the collision time of the particle and electron must be very small compared to the electron orbital time.

---

<sup>3</sup> $\delta$ -electrons are secondary electrons which also cause ionization. If the primary ionization source (muons in this study) has enough energy to produce  $\delta$ -electrons, the cascading effect is significant, and hence is a limit for the Gaussian model.

The longitudinal ( $z$ ) axis is aligned with the particle velocity such that  $v_x = v_y = 0$ . The momentum transfer  $\Delta p$  from the incoming particle to the orbiting electron is sought via

$$\Delta p = \int_{-\infty}^{\infty} F dt.$$

The first observation is that the net change in the longitudinal force on the particle is zero. This is true since the particle feels an average force “forward” just as much as it feels a force “backward” due to symmetry. Explicitly, this is equivalent to saying that  $F_z(z) = -F_z(-z)$ .

For this reason, any change in momentum is solely due to the transverse force. Again following Figure 2.1,

$$\Delta p = \int_{-\infty}^{\infty} F_x dt = \int_{-\infty}^{\infty} F_x \frac{dz}{v} = \int_{-\infty}^{\infty} F \cos \theta \frac{dz}{v},$$

Observe from Figure 2.1 that  $\cos \theta = b/r$ . Then

$$\Delta p = \int_{-\infty}^{\infty} \frac{e^2}{r^2} \frac{b}{r} \frac{dz}{v} = \int_{-\infty}^{\infty} \frac{e^2}{z^2 + b^2} \frac{b}{\sqrt{z^2 + b^2}} \frac{dz}{v} = \frac{e^2 b}{v} \int_{-\infty}^{\infty} \frac{1}{(z^2 + b^2)^{3/2}} dz.$$

By substitution of the following

$$\begin{aligned} z &= b \tan \theta, & dz &= b \sec^2 \theta d\theta, \\ z = -\infty &\rightarrow \theta = \frac{-\pi}{2}, & z = \infty &\rightarrow \theta = \frac{\pi}{2}. \end{aligned}$$

the integral becomes

$$\Delta p = \frac{e^2 b}{v} \int_{-\pi/2}^{\pi/2} \frac{b \sec^2 \theta d\theta}{(b^2(\tan^2 \theta + 1))^{3/2}} = \frac{e^2 b}{v} \int_{-\pi/2}^{\pi/2} \frac{d\theta}{b^2 |\sec \theta|},$$

or simply,

$$\Delta p = \frac{2e^2}{vb}.$$

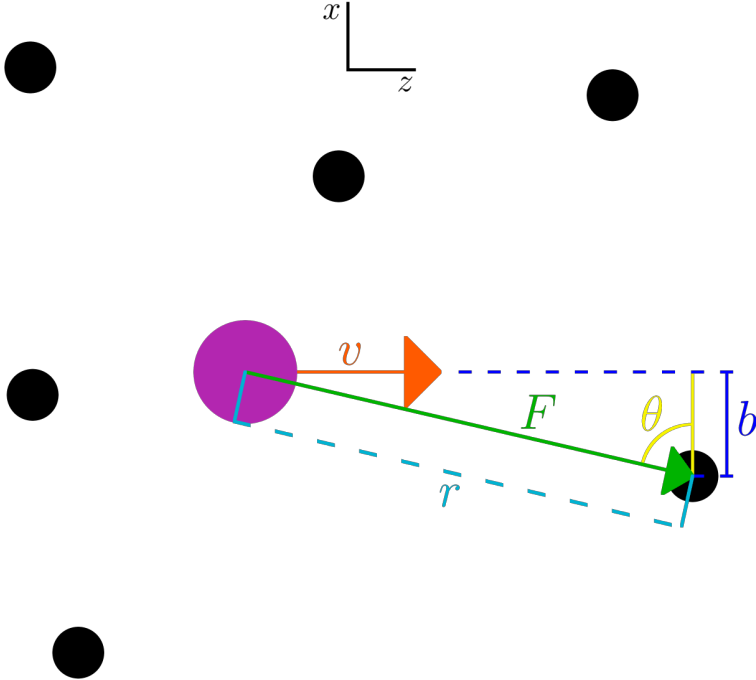


Figure 2.1. Classical model of particle passage through matter.

This non-relativistic approach yields the energy loss for the interaction between a muon and a single bound electron:

$$\epsilon = \frac{\Delta p^2}{2m_e} = \frac{2e^4}{v^2 b^2 m_e}. \quad (2.2)$$

Here, it is useful to note that if the interaction of the muon with the nucleus were desired,  $\epsilon$  for a single interaction would be proportional to  $Z^2/m_{nuc}$  and would be added on to Eq. (2.2). However, since  $1/m_e \gg 1/m_{nuc}$  the second term is disregarded.

Observe from Figure 2.1 that only a single electron has been considered for Eq. (2.2). For multiple electrons, the average electron density is  $N_{el} = N_A \cdot Z\rho/A$ , where  $N_A$  is Avogadro's number,  $Z$  the nuclear charge,  $\rho$  the density of the material, and  $A$  the nuclear mass. From this expression the average energy loss may be obtained. The cylindrical symmetry of the system is exploited by integrating the single electron interaction in cylindrical coordinates, with  $\theta$  as the cylindrical angle,  $b$  (the impact parameter) as radius, and  $z$  as length. The bounds are  $\theta \in [0, 2\pi]$ ,  $z \in [0, L]$

(where  $L$  is the total length of material traversed), and  $b \in [b_{min}, b_{max}]$  (which is discussed shortly). Then

$$\begin{aligned}\langle \epsilon \rangle &= \int_{b_{min}}^{b_{max}} \int_0^L \int_0^{2\pi} \frac{2e^4}{v^2 b^2 m_e} N_{el} d\theta dz b db \\ &= \frac{4\pi N_A e^4 Z \rho L}{v^2 m_e} \frac{A}{A} \int_{b_{min}}^{b_{max}} \frac{db}{b} \\ \langle \epsilon \rangle &= \frac{4\pi N_A e^4 Z \rho L}{v^2 m_e} \ln \frac{b_{max}}{b_{min}}.\end{aligned}\quad (2.3)$$

It is reasoned that  $b_{min}$  comes from the maximum amount of energy ( $T_{max}$ ) which a muon may impart to an electron. This quantity is derived later and can be seen in Eq. (2.8), but is only symbolic here. Similarly, the minimum transferrable energy is taken as the mean ionization energy,  $I$ , which is usually an empirical value. Any energy below this value does not transfer, since this is the minimum amount of energy to free the electron from its orbit. Then

$$\begin{aligned}\epsilon_{max} &= \frac{2e^4}{v^2 b_{min}^2 m_e} = T_{max}, \\ b_{min} &= \frac{e^2}{v} \sqrt{\frac{2}{m_e T_{max}}}, \\ \epsilon_{min} &= \frac{2e^4}{v^2 b_{max}^2 m_e} = T_{min} = I, \\ b_{max} &= \frac{e^2}{v} \sqrt{\frac{2}{m_e I}}.\end{aligned}$$

Once the bounds have been obtained, the integral in Eq. (2.3) becomes

$$\langle \epsilon \rangle = \frac{2\pi N_A e^4 Z \rho L}{v^2 m_e} \ln \frac{T_{max}}{I}. \quad (2.4)$$

### *Modern Corrections*

There are a number of corrections to the Bethe-Bloch equation as it appears in [4]. The first is a correction under the logarithm due to the relativistic flattening of the incoming particle's electric field. This factor is  $2m_e \beta^2 \gamma^2 / I$  [4]. Another correction

is known as the density correction  $\delta$  and arises due to the polarization of the material [4]. This is important for high energies since it can limit the range of the flattened electric field in the material. The last correction is the shell correction  $C$  and accounts for the fact that the electron is not at rest (or the interaction time is not much faster than the electron orbit) [4]. This is important for low energies. These corrections may or may not have a large impact on these medium energy studies since the logarithmic and density corrections arise at high energies and the shell correction occurs at low energies. Finally, in its more familiar form, the constants in Eq. (2.4) are condensed into a single constant  $K = \frac{2\pi e^4 N_A}{m_e} \approx 0.154 \text{ MeV} \cdot \text{cm}^2/\text{g}$ . Since the model assumes natural units (i.e.,  $c = 1$ ),  $v^2$  is usually replaced with  $\beta^2$ . Moreover, to avoid confusion  $\langle \epsilon \rangle$  is given a negative sign in order to emphasize energy *loss*.

The ultimate result is the Bethe-Bloch equation for the average energy lost by a particle traversing some medium with correction factors:

$$\langle \epsilon \rangle = -\frac{K}{\beta^2} \frac{Z\rho L}{A} \left( \ln \frac{2m_e\beta^2\gamma^2 T_{max}}{I^2} - 2\beta^2 - \delta - 2\frac{C}{Z} \right). \quad (2.5)$$

According to the Particle Data Group [16], this equation is generally accurate for intermediate  $Z$  materials (within a few % when compared to experimental data) in the energy regime of  $0.1 \lesssim \beta\gamma \lesssim 1000$ . The lower limit of this equation is reached when the incoming particle velocity is comparable to the atomic electron velocities, and the upper limit is attained due to radiative effects, and both limits exhibit some  $Z$  dependence. Figure 1.11 depicts this region with muons on copper. Clearly, the region typically used for muon ionization cooling ( $100 \text{ MeV}/c < p_\mu < 1000 \text{ MeV}/c$ ) falls in the middle of the Bethe-Bloch region.

### *Derivation of $T_{max}$*

Although  $T_{max}$  is used symbolically in many equations, here it is derived explicitly from a relativistic point of view. This derivation yields Eq. (2.8) and works in natural units such that  $c = 1$ . Conservation of energy for a muon incident upon an electron at rest requires that

$$\begin{aligned} E_\mu + m_e &= E_{\mu,f} + E_e, && \text{or} \\ \sqrt{p_\mu^2 + m_\mu^2} + m_e &= \sqrt{p_{\mu,f}^2 + m_\mu^2} + T_e + m_e, && \text{or} \\ p_{\mu,f}^2 &= p_\mu^2 + T_e^2 - 2T_e\sqrt{p_\mu^2 + m_\mu^2}, \end{aligned} \quad (2.6)$$

with

$$\begin{aligned} E_e &= T_e + m_e = \sqrt{p_e^2 + m_e^2}, && \text{or} \\ p_e^2 &= (T_e + m_e)^2 - m_e^2, \end{aligned} \quad (2.7)$$

where  $T_e$  is the final kinetic energy of the electron,  $p_\mu$  the initial muon momentum,  $m_\mu$  the mass of the muon, and  $p_{\mu,f}$  the final muon momentum.

Conservation of momentum requires that

$$\begin{aligned} \vec{p}_\mu &= \vec{p}_{\mu,f} + \vec{p}_e, && \text{or} \\ p_{\mu,f}^2 &= p_\mu^2 + p_e^2 - 2p_\mu p_e \cos \alpha, \end{aligned}$$

where  $\alpha$  is the angle between the initial muon momentum and the final electron momentum. Using Eq. (2.7) for  $p_e$  on the right-hand side this becomes

$$p_{\mu,f}^2 = p_\mu^2 + (T_e + m_e)^2 - m_e^2 - 2p_\mu \cos \theta \sqrt{(T_e + m_e)^2 - m_e^2}.$$

Now substitution of Eq. (2.6) for  $p_{\mu,f}^2$  on the left-hand side yields

$$p_\mu^2 + T_e^2 - 2T_e\sqrt{p_\mu^2 + m_\mu^2} = p_\mu^2 + (T_e + m_e)^2 - m_e^2 - 2p_\mu \cos \theta \sqrt{(T_e + m_e)^2 - m_e^2}.$$

For maximum energy (i.e., to attain  $T_e = T_{max}$ ),  $\cos \theta = 1$ , which is representative of a head-on collision. Then

$$\begin{aligned} T_{max}^2 - 2T_{max}\sqrt{p_\mu^2 + m_\mu^2} &= T_{max}^2 + 2T_{max}m_e - 2p_\mu\sqrt{T_{max}^2 + 2T_{max}m_e} \\ -2T_{max}(\sqrt{p_\mu^2 + m_\mu^2} + m_e) &= -2p_\mu\sqrt{T_{max}^2 + 2T_{max}m_e} \\ \sqrt{p_\mu^2 + m_\mu^2} + m_e &= p_\mu\sqrt{1 + \frac{2m_e}{T_{max}}}. \end{aligned}$$

Substituting the initial muon energy  $E_\mu = \sqrt{p_\mu^2 + m_\mu^2} = \gamma m_\mu$  and the initial muon momentum  $p_\mu^2 = E_\mu^2 - m_\mu^2 = m_\mu^2(\gamma^2 - 1) = m_\mu^2\gamma^2\beta^2$  results in

$$\begin{aligned} \gamma m_\mu + m_e &= m_\mu \gamma \beta \sqrt{1 + \frac{2m_e}{T_{max}}} \\ (\gamma m_\mu + m_e)^2 &= m_\mu^2 \gamma^2 \beta^2 \left(1 + \frac{2m_e}{T_{max}}\right). \end{aligned}$$

Finally, solving for the maximum transferrable energy from an incident muon to an electron at rest, it is found that

$$T_{max} = \frac{2m_e\beta^2\gamma^2}{1 + 2\gamma\frac{m_e}{m_\mu} + (\frac{m_e}{m_\mu})^2}. \quad (2.8)$$

**2.1.2 Landau Straggling Model.** The second ICOOL straggling model selects an energy loss from a Landau distribution [22]. This derivation is particularly important since it is the same model that was implemented into COSY in this work. The derivation may be seen in Appendix B. The result is Eq. (2.9) and is reproduced here:

$$f(\lambda) = \frac{1}{2\pi i \xi} \int_{K-i\infty}^{K+i\infty} \exp(u \ln u + \lambda u) du, \quad (2.9)$$

where  $u$  is a dummy variable,  $K > 0$  is a small real constant, and  $\lambda$  is the variable of interest, defined as

$$\lambda \equiv \frac{\epsilon - \langle \epsilon \rangle}{\xi} - (1 - C_{Euler}) - \beta^2 - \ln(\xi/T_{max}). \quad (2.10)$$

$\lambda$  is made up of several physical parameters which are defined thusly:  $\epsilon$  is the energy loss,  $\xi$  a width parameter in units of energy,  $C_{Euler} \approx 0.577$  the Euler constant,  $\beta$

the velocity of the incident particle in units of  $c$ , and  $T_{max}$  the maximum transferable energy to a single electron from Eq. (2.8). The significance of  $\xi$  will be discussed shortly, and it is defined as

$$\xi = \frac{2\pi r_e^2 m_e N_A Z \rho L}{\beta^2 A}. \quad (2.11)$$

Here,  $r_e$  is the classical electron radius,  $m_e$  the electron mass,  $N_A$  Avogadro's number,  $Z$  the nuclear charge,  $\rho$  the density of the material,  $L$  the length of the material,  $A$  the nuclear mass, and  $\beta = v/c$  the velocity in units of  $c$ .

An analogy to the Gaussian distribution function may be drawn. It is then convenient to define

$$\begin{aligned} \mu_L &= \xi (\langle \epsilon \rangle - (1 - C_{Euler}) - \beta^2 - \ln(\xi/T_{max})) , \\ \sigma_L &= \xi , \end{aligned}$$

and hence,

$$\lambda = \frac{\epsilon - \mu_L}{\sigma_L}.$$

Now it can be seen that  $\mu_L$  is the peak-position-like term and  $\sigma_L$  is the width-like term.<sup>4</sup> As mentioned in Section 1.3, the lower the energy, the more broad the Landau distribution. Figure 2.2 shows the Landau distribution with parameters  $(\mu_L, \sigma_L) = (3.98, 0.416)$ . This corresponds to the distribution for a muon of momentum 200 MeV/ $c$  through 30 cm of liquid hydrogen. Observe that the actual energy loss  $\epsilon$  has a small, yet non-zero chance to gain energy ( $\epsilon < 0$ ). In practice, however,  $\epsilon$  is required to be positive.

---

<sup>4</sup>Note that  $\sigma_L = \xi$  does not affect the peak position, and so it is fair to compare it to the Gaussian "width." However, changing  $\xi$  also changes  $\mu_L$  since  $\mu_L$  is a function of  $\xi$ . Therefore,  $\mu_L$  cannot be regarded loosely as a "peak position" parameter.

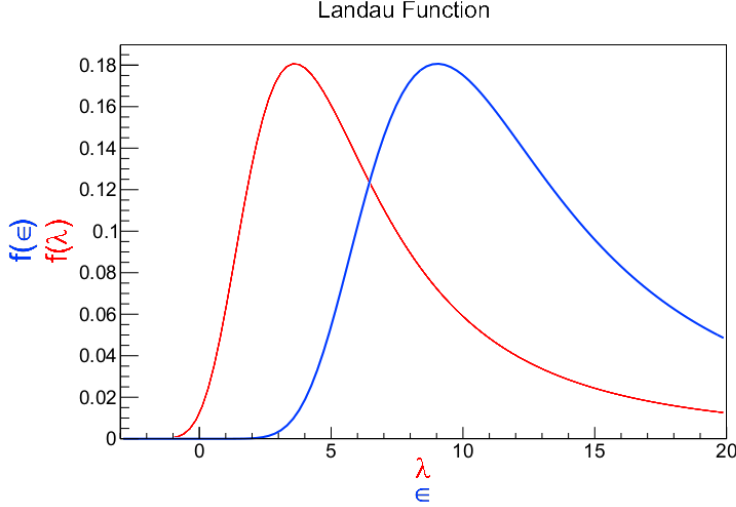


Figure 2.2. Example of the Landau distribution for a muon of momentum  $200 \text{ MeV}/c$  through  $30 \text{ cm}$  of liquid hydrogen. In red, the Landau distribution as a function of the parameter  $\lambda$  can be seen. In blue, the Landau distribution as a function of the actual energy loss  $\epsilon$  is illustrated.

In summary, the ICOOL Landau model uses the mean energy loss from the Bethe-Bloch equation (Eq. (2.5)). The routine then adds noise based on the Landau distribution with parameters  $(\mu_L, \sigma_L) = (0, 1)$ , which has a mode of zero. In this way, the average value of energy loss as predicted by Bethe-Bloch theory is maintained. The average value plus noise is then accepted as the total energy loss of the particle.

**2.1.3 Vavilov Straggling Model.** The Vavilov model [23] is similar to the Landau model, except that the thickness of the absorber is not required to be small enough such that the energy loss is small compared to the initial energy. The derivation is also similar, except that Vavilov introduced a limit on the maximum transferable energy due to a single collision (recall that in Landau theory the upper limit was  $\infty$ ).

The result is

$$f(\lambda_v, \kappa, \beta^2) = \frac{1}{\xi} \phi_v(\lambda_v, \kappa, \beta^2), \quad (2.12)$$

where

$$\begin{aligned}
\phi_v(\lambda_v, \kappa, \beta^2) &= \frac{1}{2\pi i} \int_{K+i\infty}^{K-i\infty} \phi(p, \kappa, \beta^2) e^{\lambda p}, \\
\phi(p, \kappa, \beta^2) &= \exp[\kappa(1 + \beta^2 \gamma)] \exp[\psi(p, \kappa, \beta^2)], \\
\psi(p) &= p \ln \kappa + (p + \beta^2 \kappa)[\ln(p/\kappa) + E_1(p/\kappa)] - \kappa e^{-p/\kappa}, \\
E_1(p) &= \int_{\infty}^z \frac{e^{-u}}{u} du \quad (\text{the exponential integral}), \\
\lambda_v &= \kappa \left( \frac{\epsilon - \langle \epsilon \rangle}{\xi} - (1 - C_{Euler}) - \beta^2 \right) = \kappa(\lambda + \ln \kappa), \text{ and} \\
\kappa &= \xi/T_{max}.
\end{aligned}$$

While this function in theory is universal for the needs of this study, clearly such a distribution function requires numerical methods, and as such is computationally more costly than the Landau method. Fortunately, the Vavilov distribution converges to either the Landau distribution (for  $\kappa \rightarrow 0$ ) or a Gaussian distribution (for  $\kappa \rightarrow \infty$ ) at its extrema. The cutoffs for these extrema in practice are

$$\phi_v = \begin{cases} \text{Landau via Eq. (2.9)} & \kappa \leq 0.01 \\ \text{Vavilov via Eq. (2.12)} & 0.01 < \kappa < 10 \\ \text{Gaussian via } Gaus(\langle \epsilon \rangle, \sigma) \text{ in Eqns. 2.5 and 2.1} & 10 \leq \kappa \end{cases}$$

## 2.2 Multiple Scattering in ICOOL

ICOOL version 3.30 [18] boasts a total of seven models of multiple scattering:

1. Gaussian ( $\sigma$  determined by Rossi-Greisen model),
2. Gaussian ( $\sigma$  determined by Highland model),
3. Gaussian ( $\sigma$  determined by Lynch-Dahl model),
4. Bethe version of Molière distribution with Rutherford limit,

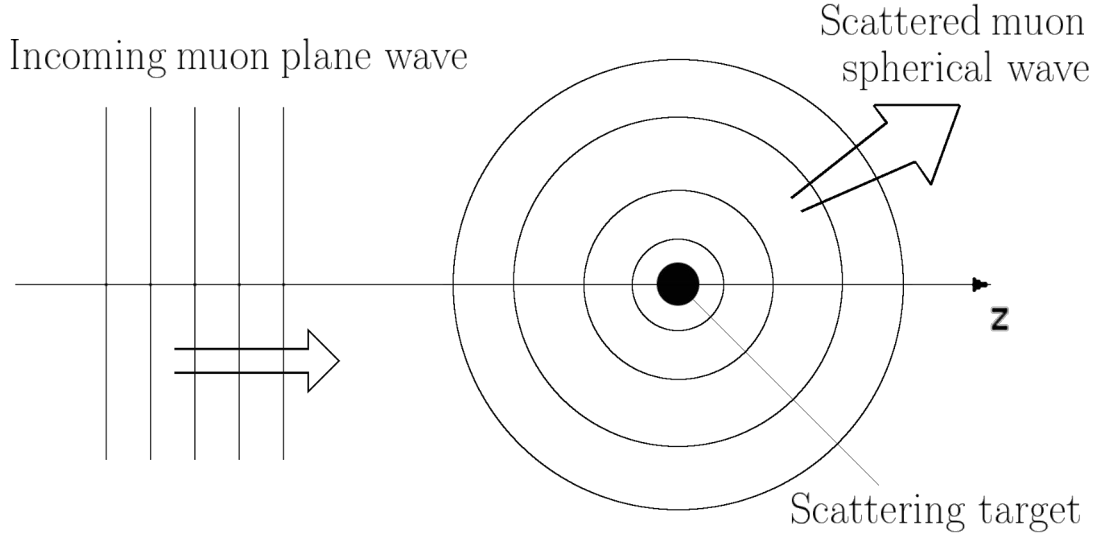


Figure 2.3. Quantum scattering model (repeated from Figure 1.6).

5. Rutherford,
6. Fano with Rutherford limit, and
7. Tollestrup with Rutherford limit.

The scattering model used in this work is Fano with Rutherford limit, which is also the default scattering model in ICOOL. The following is a derivation of the Rutherford model accompanied by a brief discussion of the Fano model. Unless otherwise stated, the derivation of the Rutherford model closely follows [8].

The Rutherford model is used in part in four out of the seven models because it is so robust. The derivation can be carried out using the Coulomb potential, classical mechanics, the Born approximation, and quantum field theory, with the quantum mechanics Born approximation being the weapon of choice here. Recall that the quantum model used in this work is shown schematically in Figure 2.3. Here there is an incoming plane wave (mathematically represented by  $e^{ikz}$ ) and a spherical wave

(represented by  $e^{ikr}/r$ ), where  $r$  and  $z$  are the coordinates,  $i$  the imaginary unit, and  $k$  the wave number, classically related to the energy as  $k = \sqrt{2mE}/\hbar$ . Then basic quantum mechanics suggests that the solution to the Schrödinger equation has the form

$$\psi(r, \theta) \approx A \left( e^{ikz} + f(\theta) \frac{e^{ikr}}{r} \right), \quad (2.13)$$

where  $A$  is the total amplitude and  $f(\theta)$  is the scattering amplitude. The probability of the particle scattering in a particular direction is given by the amplitude squared,  $|f(\theta)|^2$ , and is the object of this derivation. Now,  $\psi$  solves the differential (time-independent) Schrödinger equation, which usually has the form

$$-\frac{\hbar^2}{2m} \nabla^2 \psi + V\psi = E\psi,$$

where  $V$  is the system potential and  $E$  is the energy of the wavefunction. This can be expressed alternatively by assigning  $Q \equiv V\psi \cdot 2m/\hbar^2$  and recalling that  $k = \sqrt{2mE}/\hbar$ . Then

$$(\nabla^2 + k^2)\psi = Q. \quad (2.14)$$

The strategy is to solve Eq. (2.14) for  $\psi$ . A comparison of the solutions for  $\psi$  from Eqns. 2.13 and 2.14 yields the scattering amplitude  $f(\theta)$ . However, if Eq. (2.14) is solved for  $\psi$  then it suggests that  $\psi$  will be in integral form since Eq. (2.14) is a differential equation. Therefore, some special techniques are required. Note that it does not matter at this point that  $Q$  is a function of  $\psi$ , since the task is to compare the integrated solution of Eq. (2.14) with that of Eq. (2.13). Moving forward, observe that Eq. (2.14) may again be rewritten as

$$(\nabla^2 + k^2)\psi(\vec{r}) = Q(\vec{r}) = \int \delta^3(\vec{r} - \vec{r}_0)Q(\vec{r}_0)d^3\vec{r}_0. \quad (2.15)$$

Now it is natural to guess that there exists some function  $G(\vec{r})$  such that

$$\psi(\vec{r}) = \int G(\vec{r} - \vec{r}_0)Q(\vec{r}_0)d^3\vec{r}_0, \quad (2.16)$$

in which case

$$(\nabla^2 + k^2)\psi(\vec{r}) = (\nabla^2 + k^2) \int G(\vec{r} - \vec{r}_0) Q(\vec{r}_0) d^3 \vec{r}_0,$$

or

$$(\nabla^2 + k^2)\psi(\vec{r}) = \int [(\nabla^2 + k^2)G(\vec{r} - \vec{r}_0)] Q(\vec{r}_0) d^3 \vec{r}_0. \quad (2.17)$$

Combining Eqns. 2.15 and 2.17, it can be seen that

$$\int \delta^3(\vec{r} - \vec{r}_0) Q(\vec{r}_0) d^3 \vec{r}_0 = \int [(\nabla^2 + k^2)G(\vec{r} - \vec{r}_0)] Q(\vec{r}_0) d^3 \vec{r}_0.$$

Consequently, one comes to the conclusion that

$$(\nabla^2 + k^2)G(\vec{r}) = \delta^3(\vec{r}). \quad (2.18)$$

If Eq. (2.18) seems familiar, it is because this is the Helmholtz equation with a delta function source.  $G(\vec{r})$  is the Green's function for the Helmholtz equation, and in this case it is the response to the delta function source. Now, if one accepts that there exists a well-known particular solution for Eq. (2.18), then one could skip forward to the solution in Eq. (2.21); however, it is also derived subsequently.

The usual strategy in solving systems like Eq. (2.18) is to Fourier transform both the Green's function and the delta function. Then creating the dummy variable  $\vec{s}$ , the transform yields

$$G(\vec{r}) = \frac{1}{(2\pi)^{\frac{3}{2}}} \int e^{i\vec{s}\cdot\vec{r}} g(\vec{s}) d^3 \vec{s},$$

and

$$\delta^3(\vec{r}) = \frac{1}{(2\pi)^3} \int e^{i\vec{s}\cdot\vec{r}} d^3 \vec{s}.$$

Then from Eq. (2.18),

$$\frac{1}{(2\pi)^{\frac{3}{2}}} \int (k^2 e^{i\vec{s}\cdot\vec{r}} - s^2 e^{i\vec{s}\cdot\vec{r}}) g(\vec{s}) d^3 \vec{s} = \frac{1}{(2\pi)^3} \int e^{i\vec{s}\cdot\vec{r}} d^3 \vec{s},$$

it is clear that  $g(\vec{s}) = 1/(2\pi)^{3/2}(k^2 - s^2)$ . Now all that is left is to find  $G(\vec{r})$  from its transformation:

$$G(\vec{r}) = \frac{1}{(2\pi)^3} \int e^{i\vec{s}\cdot\vec{r}} \frac{d^3 \vec{s}}{k^2 - s^2}$$

$$G(\vec{r}) = \frac{1}{(2\pi)^3} \int_0^\infty \frac{s}{k^2 - s^2} \left( \int_0^\pi e^{isr \cos \theta} \sin \theta d\theta \right) ds \int_0^{2\pi} d\phi.$$

The integration over  $\phi$  is trivial, and the integration over  $\theta$  can be done via  $u$  substitution, with  $u = \cos \theta$ . The last integral is over  $s$ , and is

$$G(\vec{r}) = \frac{1}{2\pi^2 r} \int_0^\infty \frac{s \sin sr}{k^2 - s^2} ds = \frac{1}{4\pi^2 r} \int_{-\infty}^\infty \frac{s \sin sr}{k^2 - s^2} ds.$$

This integral is not simple to solve, but it does have two poles at  $s = k$  and  $s = -k$ , which implies the technique of choice should be to use Cauchy's integral formula for simple poles<sup>5</sup>:

$$\oint \frac{f(z)}{z - z_0} dz = 2\pi i f(z_0), \quad (2.19)$$

where the integral is done over some path in the complex plane and  $z_0$  is the pole of interest which lies within the closed path (note: the integral is zero if there exist no poles in the enclosed path). It follows then that  $f(z)$  is not simply any function, but necessarily a complex function. For this reason, the (strictly real) Green's function integral should be split up into two (strictly complex) functions, as depicted by Figure 2.4. This can be done by expanding the  $\sin sr$  term and factoring  $k^2 - s^2$ :

$$G(\vec{r}) = \frac{i}{8\pi^2 r} \left[ \int_{-\infty}^\infty \frac{se^{isr}}{(s - k)(s + k)} ds - \int_{-\infty}^\infty \frac{se^{-isr}}{(s - k)(s + k)} ds \right]. \quad (2.20)$$

Observe that in Eq. (2.20) the path integrals at  $|s| = \pm\infty$  have been left out. This is because they do not contribute to the integral since the first integrand corresponds to the left side of Figure 2.4 and goes like  $e^{isr}$ , hence going to zero at large positive imaginary numbers. Similarly, the second integrand goes like  $e^{-isr}$  and goes to zero at large negative imaginary numbers.

---

<sup>5</sup>This touches an area of mathematics known as the calculus of residues, and is based on the Laurent series.

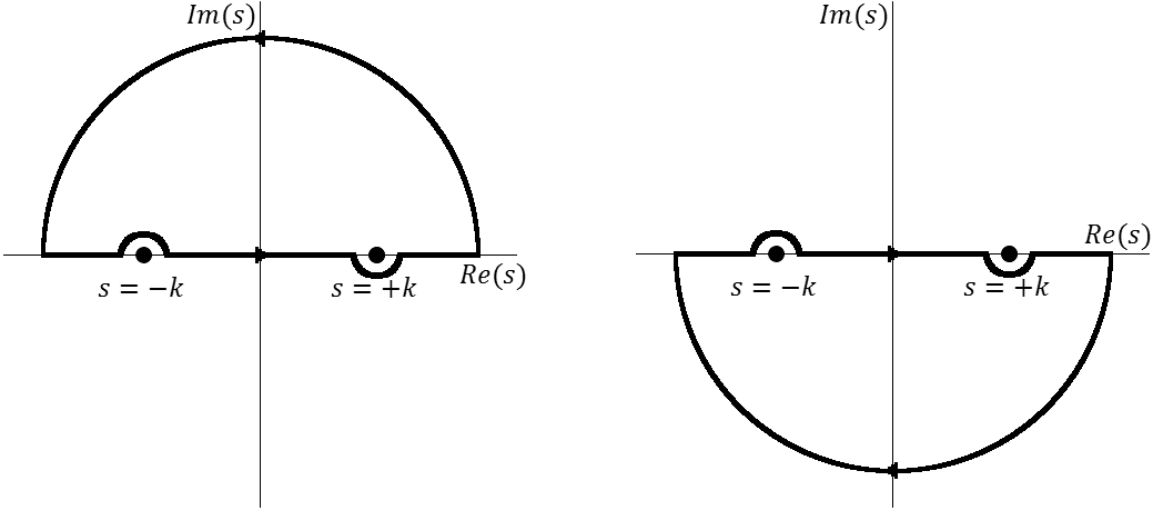


Figure 2.4. Two parts of Green's function with their poles at  $s = \pm k$ , altered to be closed by a semicircle at  $|s| = \pm \infty$ .

Combining Eqns. 2.19 and 2.20, it can be seen that

$$G(\vec{r}) = \frac{i}{8\pi^2 r} [(i\pi e^{ikr}) - (-i\pi e^{ikr})] = -\frac{e^{ikr}}{4\pi r}.$$

This is a particular solution to the inhomogeneous Helmholtz equation. To get a general solution, the solution to the homogeneous Helmholtz equation must be added:

$$G(\vec{r}) = G_0(\vec{r}) - \frac{e^{ikr}}{4\pi r}; \quad (2.21)$$

that is,  $G_0(\vec{r})$  solves  $(\nabla^2 + k^2)G_0(\vec{r}) = 0$ .

Using Eq. (2.16) in conjunction with Eq. (2.21) gives rise to the *integrated* time-independent Schrödinger equation:

$$\psi(\vec{r}) = \psi_0(\vec{r}) - \frac{m}{2\pi\hbar^2} \int \frac{e^{ik|\vec{r}-\vec{r}_0|}}{|\vec{r}-\vec{r}_0|} V(\vec{r}_0) \psi(\vec{r}_0) d^3\vec{r}_0. \quad (2.22)$$

That is, nothing has been said about the potential and so this equation is quite general. Eq. (2.22) gives the recursive form for  $\psi$ . Let  $g = -me^{ik|\vec{r}-\vec{r}_0|}/2\pi\hbar^2|\vec{r}-\vec{r}_0|$  so that

$$\psi(\vec{r}) = \psi_0(\vec{r}) + \int g V(\vec{r}_0) \psi(\vec{r}_0) d^3\vec{r}_0.$$

Then Eq. (2.22) says that

$$\psi = \psi_0 + \int gV\psi d^3\vec{r}_0 = \psi_0 + \int gV \left( \psi_0 + \int gV\psi d^3\vec{r}'_0 \right) d^3\vec{r}_0.$$

Applying this recursion several times gives the Born series:

$$\psi = \psi_0 + \int gV\psi_0 + \iint gVgV\psi_0 + \iiint gVgVgV\psi_0 + \dots$$

The zeroth term is exact if there is no scattering whatsoever (i.e.,  $V = 0$ ) and the first term is accurate if the scattering potential is “weak” (that is, if  $V$  is small enough for the second term to be neglected). For the purposes of this derivation, first order is a sufficient approximation for  $\psi$ . Then

$$\psi = \psi_0 + \frac{m}{2\pi\hbar^2} \int \frac{e^{ik|\vec{r}-\vec{r}_0|}}{|\vec{r}-\vec{r}_0|} V(\vec{r}_0) \psi_0(\vec{r}_0) d^3\vec{r}_0.$$

Recall that the strategy was to compare this solution of the Helmholtz equation with the wavefunction from the quantum scattering model (Eq. (2.13)) in order to find the scattering amplitude,  $f(\theta)$ . Doing so yields

$$f(\theta) = -\frac{r}{e^{ikr}} \frac{m}{2\pi\hbar^2 A} \int \frac{e^{ik|\vec{r}-\vec{r}_0|}}{|\vec{r}-\vec{r}_0|} V(\vec{r}_0) \psi_0(\vec{r}_0) d^3\vec{r}_0.$$

The Coulomb potential goes as  $1/r^2$ , and as such  $V(\vec{r}_0)$  is localized about  $\vec{r}_0 = 0$ . Since particles are observed far away from their scattering centers, it is advantageous to make use of the fact that component-wise  $\vec{r} \gg \vec{r}_0$ . However, care must be used, since one must evaluate the exponential and non-exponential terms separately, for they are of different orders. For the non-exponential terms, this is simple, since

$$\frac{r}{|\vec{r}-\vec{r}_0|} \approx 1.$$

The exponential terms look like

$$e^{ik(|\vec{r}-\vec{r}_0|-r)},$$

and so it is useful to expand the absolute value as

$$|\vec{r} - \vec{r}_0|^2 = r^2 + r_0^2 - 2\vec{r} \cdot \vec{r}_0 \approx r^2 \left( 1 - 2\frac{\vec{r} \cdot \vec{r}_0}{r^2} \right),$$

or simply

$$|\vec{r} - \vec{r}_0| \approx r - \hat{r} \cdot \vec{r}_0.$$

This leaves

$$f(\theta) = \frac{m}{2\pi\hbar^2} \int e^{-ik\hat{r} \cdot \vec{r}_0} V(\vec{r}_0) e^{ik\hat{z} \cdot \vec{r}_0} d^3 \vec{r}_0. \quad (2.23)$$

Now define  $\vec{\kappa} \equiv k(\hat{z} - \hat{r})$  such that  $\kappa = 2k \sin \theta/2$ . The exponential term becomes

$$e^{i\vec{\kappa} \cdot \vec{r}_0} = e^{i\kappa r_0 \cos \theta_0}.$$

Furthermore, the form of the potential  $V$  is known. Since the scattering for the low- $Z$  target happens at low temperatures, it is possible to use the Fermi-Thomas approximation for screening [24]. This modifies the Maxwell equation

$$\nabla^2 V(r) = -\frac{\rho}{\epsilon_0}$$

to

$$(\nabla^2 - b^2)V(r) = -\frac{Q}{\epsilon_0}\delta(r),$$

where  $\rho$  is the charge density,  $b$  is some screening constant,  $\epsilon_0$  is the permittivity of free space, and  $Q$  is the charge of the nucleus (in this case, the atomic number  $Z$ ).

The result is

$$V(r) = \frac{Q}{4\pi\epsilon_0} \frac{e^{-br}}{r}.$$

Then the quantum scattering equation (Eq. (2.23)) becomes

$$f(\theta) \propto \int e^{i\kappa r_0 \cos(\theta_0)} e^{-br_0} r_0 \sin(\theta_0) dr_0 d\theta_0 d\phi_0,$$

where the constant terms have been left out since  $|f(\theta)|^2$  is normalized anyway. Here it is seen that there does exist some  $\theta$  dependence in  $f(\theta)$  (by virtue of  $\kappa$ ). The

integral over  $\phi_0$  is trivial, and the integral over  $\theta_0$  can be done via  $u$  substitution, with  $u = \cos \theta_0$ . This leaves

$$f(\theta) \propto \frac{1}{\kappa} \int_0^\infty e^{-bro} \sin(\kappa r_0) dr_0,$$

which has the solution

$$f(\theta) \propto \frac{1}{b^2 + \kappa^2}.$$

For classical Rutherford scattering,  $b \rightarrow 0$ . Recalling that  $\kappa = 2k \sin \theta/2$  yields the final Rutherford scattering distribution:

$$\begin{aligned} |f(\theta)|^2 &\propto \frac{1}{\sin^4 \frac{\theta}{2}} = \frac{1}{(\sin^2 \frac{\theta}{2})^2} = \frac{1}{\left(\frac{1}{2} [1 - \cos^2(2 \cdot \frac{\theta}{2})]\right)^2}, \\ |f(\theta)|^2 &\propto \frac{1}{(1 - \cos^2 \theta)^2}. \end{aligned} \quad (2.24)$$

Only the tail of the distribution function in Eq. (2.24) should be used since it blows up at  $\theta = 0$ . This may seem like a contradiction since the Born series was truncated at the weak potential term (the first nontrivial term), and hence the incoming muons should not scatter much at all! In fact, the muons are not scattering much at all for each individual atom they encounter. Over the entire absorber, however, some muons have a net scattering angle which is small (and therefore should not be approximated by the Rutherford tail) whereas others have a large net scattering angle (and are well represented by Eq. (2.24)). Many weak potentials can still induce a relatively large scattering angle.

### 2.3 Energy Straggling in G4beamline

G4beamline uses the in-house straggling model implemented in GEANT4 based on [20]. GEANT4 considers the absorber a “thick absorber” when the following conditions are met:

$$|\Delta E| > \kappa T_c \quad \text{and} \quad T_{max} \leq 2T_c, \quad (2.25)$$

where  $\Delta E$  is the energy loss,  $\kappa$  the Vavilov limit parameter,  $T_c$  the kinetic energy cut of  $\delta$ -electrons, and  $T_{max}$  the maximum transferable kinetic energy between the incoming particle and target electron. (These symbols can also be found in the Definition of Terms at the beginning of this document.)

For thick absorbers, the energy loss is sampled according to a simple Gaussian distribution with average equal to the Bethe-Bloch energy loss (Eq. (2.5)) and a standard deviation according to Bohr's variance (Eq. (2.1)).

If these conditions are not met, a “thin absorber” algorithm is called. Here, atoms are assumed to have only two energy levels with binding energies  $E_1$  and  $E_2$ . The interacting muon can then lose energy via excitation, yielding an energy loss of  $E_1$  or  $E_2$ , or lose energy via  $\delta$  ray production, yielding an energy loss according to  $g(E) \propto 1/E^2$ , or (more likely) some combination or weighted average of the two.  $g(E)$  may then be normalized:

$$\int_{E_0}^{T_{up}} g(E) dE = 1 \rightarrow g(E) = \frac{E_0 T_{up}}{T_{up} - E_0} \frac{1}{E^2}, \quad (2.26)$$

where  $E_0$  is the ionization energy of the atom in question and  $T_{up}$  is some kinetic energy cutoff (either the production threshold for delta rays or the maximum transferable energy, whichever is smaller).

The probability of obtaining any one of these energy losses is given by the macroscopic cross section,  $\Sigma_i$ , where  $i = 1, 2, 3$ . For excitation ( $i = 1, 2$ ), the cross section has a form similar to the deterministic Bethe-Bloch equation (Eq. (2.5)):

$$\Sigma_i = C \frac{f_i}{E_i} \frac{\ln(2m_e c^2 (\beta\gamma)^2 / E_i)}{\ln(2m_e c^2 (\beta\gamma)^2 / I)} (1 - r). \quad (2.27)$$

Here,  $C$  and  $r = 0.55$  are model parameters with  $r$  describing the relative contribution of excitation to ionization,  $f_i$  are the relative oscillator strengths of the energy levels of  $E_i$ ,  $I$  is the average ionization energy, and the other symbols have their usual

meaning. For continuous energy loss, the cross section is given by

$$\Sigma_3 = C \frac{T_{up} - E_0}{T_{up} E_0 \ln(T_{up}/E_0)} r. \quad (2.28)$$

The oscillator strengths are relative to one another and hence should satisfy

$$f_1 + f_2 = 1. \quad (2.29)$$

The next constraint comes from [25] and states that all the energy levels should be weighted and added logarithmically to the total ionization energy:

$$f_1 \ln E_1 + f_2 \ln E_2 = \ln I. \quad (2.30)$$

Moreover,  $f_1$  and  $f_2$  can be thought of as representing the relative number of loosely and tightly bound electrons. Using the first constraint, it is easy to see that the absolute number of loosely bound electrons is  $Z \cdot f_1$  and the absolute number of tightly bound electrons is  $Z \cdot f_2$  (since  $Z \cdot f_1 + Z \cdot f_2 = Z$ ). For modeling purposes, GEANT4 has placed empirical initial conditions on these parameters:

$$f_2 = 0 \quad \text{for } Z = 1, \quad (2.31)$$

$$f_2 = 2/Z \quad \text{for } Z \geq 2, \quad (2.32)$$

$$E_2 = 10 \text{ eV} \cdot Z^2, \quad (2.33)$$

$$E_0 = 10 \text{ eV}. \quad (2.34)$$

From these,  $f_1$  and  $E_1$  can be found from Eqns. 2.29 and 2.30 given a particular muon through a particular material (from which  $Z$ ,  $I$ ,  $\beta$ , and the like are taken).

Finally, an energy loss for a thin absorber can be sampled. For the contribution due to excitation, two numbers  $n_1$  and  $n_2$  are sampled randomly from a Poisson distribution. These numbers represent the relative contributions of the energy levels of  $E_1$  and  $E_2$ , respectively:

$$\epsilon_{exc} = n_1 E_1 + n_2 E_2.$$

The contribution due to ionization can be found by inverting the cumulative distribution function of  $g(E)$  (see Eq. (2.26)):

$$G(E) = \int_{E_0}^E g(E)dE \rightarrow E = \frac{E_0}{1 - u \frac{T_{up} - E_0}{T_{up}}},$$

where  $u$  is uniformly randomly selected from  $[0, 1]$ . However, this treatment so far has only been executed for a single ionization. For an absorber of length  $L$ , the number of ionizations  $n_3$  is again sampled from a Poisson distribution. Then the total energy loss for thin absorbers is

$$\epsilon = n_1 E_1 + n_2 E_2 + \sum_{j=1}^{n_3} \frac{E_0}{1 - u_j \frac{T_{up} - E_0}{T_{up}}} \quad (2.35)$$

It should be noted that [20] does make a brief mention of a width correction algorithm. This algorithm allegedly decreases the dependence of the results on kinetic energy cuts and step sizes and works for any thickness of material. However, the section in the manual is less than a page long and purely conceptual without any mathematics or data on which to elaborate. The width correction algorithm is relevant to this work in order to make a fair comparison and understand why this work and G4beamline disagree in some places.

Finally, the GEANT4 straggling routine can be summarized as such:

1. Determine if the absorber is “thick” via Eq. (2.25).
2. If the absorber is thick, use Gaussian distribution with mean  $\mu = \langle dE/dx \rangle$  (from Eq. (2.5)) and standard deviation from Eq. (2.1).
3. If the absorber is “thin,” use Eq. (2.35).
  - Select  $n_1$ ,  $n_2$ , and  $n_3$  from a Poisson distribution.
  - Select  $u_j$  from a uniform distribution on  $[0, 1]$  (where  $j = 1 \dots n_3$ ).

- Find  $E_2$ ,  $f_2$ , and  $E_0$  from Eq. (2.31).
  - Find  $E_1$  from Eqns. 2.29 and 2.30.
4. Apply width correction algorithm.

## 2.4 Multiple Scattering in G4beamline

The G4beamline scattering model in [19] uses the GEANT4 Urbán model [20] and parameterizes according to experimental data and Lewis theory [26]. For this section, the scattering distribution is  $g(u)$ , where  $u = \cos \theta$  and  $\theta$  is the scattering angle.

Based on the models available, it can be inferred that the function responsible for the sampling of the angular distribution,  $g(u)$ , is based on both the Goudsmit-Saunderson treatment of scattering [27] and Rutherford scattering. One fundamental result from Goudsmit and Saunderson is that for small angles, the scattering distribution is Gaussian. Recall that Rutherford scattering was derived in Section 2.2 and resulted in Eq. (2.24). It should be noted that the shape of  $g(u)$  was chosen empirically, and is

$$g(u) = q_g [p_g g_1(u) + (1 - p_g) g_2(u)] + (1 - q_g) g_3(u), \quad (2.36)$$

where  $0 \leq p_g, q_g \leq 1$  and

$$\begin{aligned} g_1(u) &= C_1 e^{-a(1-u)} & -1 \leq u_0 \leq u \leq 1 \\ g_2(u) &= C_2 \frac{1}{(b_r - u)^{d_r}} & -1 \leq u \leq u_0 \leq 1 \\ g_3(u) &= C_3 & -1 \leq u \leq 1 \end{aligned}$$

are normalized over  $[-1, 1]$ , where  $C_i$  are normalization constants and  $a$ ,  $b_r$ ,  $d_r$ , and  $u_0$  are empirical parameters. All of these parameters are discussed in this section, and can be found in Table 2.1.

Table 2.1. The nine parameters of the scattering distribution used by G4beamline (see Eq. (2.36)).

Parameter	Physical Meaning	Found Via	Eq.
$C_1, C_2,$ and $C_3$	Normalization constants	Normalization	$N/A$
$a$	Related to Gaussian-like	Relating the Gaussian-like behavior of $g_1(u)$ to	2.37
	$\sigma$	Highland-like theory [28]	
$u_0$	The boundary between the Gaussian-like $g_1(u)$ and the Rutherford-like $g_2(u)$	empirical parameterization	2.39
$d_r$	The Rutherford-like exponent in $g_2(u)$	empirical parameterization	2.40
$p_g$	Relative contribution of the Gaussian-like $g_1(u)$ to the Rutherford-like $g_2(u)$	Demanding continuity	2.43
$b_r$	Relative $u$ offset of the Rutherford-like $g_2(u)$	Demanding smoothness	2.44
$q_g$	The relative contribution of the varying functions $g_1(u)$ and $g_2(u)$ to the constant function $g_3(u)$	Demanding that $g$ gives the same mean value as Lewis theory	2.45

Observe that for small angles,  $g(u)$  is nearly Gaussian since  $\exp(1-u) = \exp(1-\cos\theta) \approx \exp(\theta^2/2)$ . For large angles,  $g(u)$  resembles the Rutherford dependence of Eq. (2.24) for  $b_r \approx 1$  and  $d_r$  close to 2. Moreover, at small  $q_g$  the shape of  $g(u)$  is nearly constant since the constant function  $g_3(u)$  dominates.

While Eq. (2.36) is the main point of this section, it would be incomplete without detailing the nine parameters mentioned. The  $C_i$  (with  $i = 1, 2, 3$ ) are normalization constants.  $a$ ,  $u_0$ , and  $d_r$  are chosen based on theoretical and experimental data and are a bit more interesting. Finally,  $p_g$ ,  $q_g$ , and  $b_r$  can be found using constraints.

### *Finding parameter $a$*

Observe from Eq. (2.36) that  $a$  appears only in  $g_1(u)$ . Further observe from Eq. (2.36) that  $g_1(u)$  is valid only for  $u$  close to 1. Since  $u = \cos\theta$  (where  $\theta$  is the scattering angle),  $g_1(u)$  must be the part of  $g(u)$  that determines small angle scattering.

It has already been noted that  $g_1(u)$  is approximately Gaussian for  $u$  close to 1. Highland [28] provided an estimate for the width of the (approximate) Gaussian scattering distribution. Let the width of this Gaussian distribution be  $\theta_0$ . Lynch and Dahl [29] gave corrections to Highland's form of  $\theta_0$  in 1991. If  $\theta_0$  truly is the width of the Gaussian scattering distribution, then it follows that

$$g_1(u) \propto \exp\left(-\frac{\theta^2}{2\theta_0^2}\right) \approx \exp\left(\frac{1}{2} \cdot \frac{1-\cos\theta}{1-\cos\theta_0}\right),$$

where  $\propto$  means “approximately proportional to.” Recall from Eq. (2.36) that

$$g_1(u) \propto \exp(-a(1-u)).$$

Then it is reasonable to choose  $a$  as

$$a = \frac{0.5}{1 - \cos\theta_0}, \quad (2.37)$$

so that

$$\exp(-a(1-u)) = \exp\left(\frac{1}{2} \cdot \frac{1-\cos\theta}{1-\cos\theta_0}\right).$$

For heavy charged particles (such as muons), the model for  $\theta_0$  has been modified even more from Lynch and Dahl by GEANT4 [20]. Its form is now chosen by GEANT4 [20] as

$$\theta_0 = \frac{13.6\text{MeV}}{\beta cp} z_{ch} \sqrt{\frac{t}{X_0} \left[ 1 + 0.105 \ln\left(\frac{t}{X_0}\right) + 0.0035 \left(\ln\left(\frac{t}{X_0}\right)\right)^2 \right]} \left(1 - \frac{0.24}{Z(Z+1)}\right). \quad (2.38)$$

### *Finding parameter $u_0$*

Observe from Eq. (2.36) that the parameter  $u_0$  is the boundary between the Gaussian-like  $g_1(u)$  and the Rutherford-like  $g_2(u)$ . GEANT4 [20] has chosen  $u_0$  as

$$u_0 = 1 - \frac{3}{a}. \quad (2.39)$$

It is assumed that this parameter has been chosen as such based on empirical results, but no formal explanation is given. While GEANT4 [20] does not elaborate on this parameterization, validation in Section 5.2 shows that this choice is reasonable.

### *Finding parameter $d_r$*

Observe from Eq. (2.36) that the parameter  $d_r$  is the Rutherford-like exponent. Note that a classical Rutherford distribution would have  $d_r = 2$ . For heavy particles such as muons, the parameter  $d_r$  has been chosen by GEANT4 [20] as

$$d_r = 2.40 - 0.027Z^{\frac{2}{3}}. \quad (2.40)$$

It is assumed that this parameter has been chosen as such based on empirical results, but no formal explanation is given. While GEANT4 [20] does not elaborate on this parameterization, validation in Section 5.2 shows that this choice is reasonable.

### *Finding parameter $p_g$*

Now  $p_g$  is found using constraints on the scattering distribution  $g(u)$ . Observe from Eq. (2.36) that the parameter  $p_g$  is the relative contribution of the Gaussian-like  $g_1(u)$  to the Rutherford-like  $g_2(u)$ . It is reasonable to demand that  $g(u)$  be continuous and smooth on  $[-1, 1]$ . Taking continuity and smoothness at  $u = u_0$  yields the following constraints:

$$p_g g_1(u_0) = (1 - p_g) g_2(u_0), \quad (2.41)$$

$$a \cdot p_g g_1(u_0) = (1 - p_g) g_2(u_0) \cdot \frac{d_r}{b_r - u_0}. \quad (2.42)$$

From Eq. (2.41), it is easy to see that

$$p_g = \frac{g_2(u_0)}{g_1(u_0) + g_2(u_0)}. \quad (2.43)$$

### *Finding parameter $b_r$*

Observe from Eq. (2.36) that the parameter  $b_r$  is the relative  $u$  offset of the Rutherford-like distribution. For a classical Rutherford distribution,  $b_r = 1$ . From Eq. (2.42),

$$a = \frac{d_r}{b_r - u_0}.$$

Rearranging this yields

$$b_r = \frac{a}{d_r} + u_0. \quad (2.44)$$

### *Finding parameter $q_g$*

Lastly,  $q_g$  is found by knowing that  $g(u)$  must give the same mean value as Lewis theory. Observe from Eq. (2.36) that the parameter  $q_g$  is the relative contribution of the varying functions  $g_1(u)$  and  $g_2(u)$  to the constant function  $g_3(u)$ . GEANT4 [20] shows that

$$q_g = \frac{\left(1 - \frac{\lambda_{10} - \lambda_{11}}{\lambda_{10}}\right)^{\frac{t}{\lambda_{10} - \lambda_{11}}}}{p_g \langle u \rangle_1 + (1 - p_g) \langle u \rangle_2}, \quad (2.45)$$

where  $\lambda_{10}$  is the value of the first transport free mean path at the beginning of the step,  $\lambda_{11}$  is this value at the end of the step,  $t$  is the true path length, and  $\langle u \rangle_i$  is the mean value of  $u$  computed from the distribution  $g_i(u)$ .

### *Summary*

In summary, the scattering model used by G4beamline is based on the Geant4 model, which includes Lewis theory. The full form of the scattering equation is given by Eq. (2.36). This model has nine parameters which are summarized in Table 2.1. As can be seen in the G4beamline validation documents [19], this model works quite well. G4beamline sets a precedent to use theory in conjunction with empirical parameters—a philosophy that this work also uses. Moreover, as is seen in the next chapter, this work employs the piecewise Gaussian-like and Rutherford-like distribution in its scattering algorithm.

## CHAPTER 3

### STOCHASTIC PROCESSES IN COSY INFINITY

In this chapter, the new algorithms implemented into COSY Infinity in the framework of this work are elaborated upon. First, energy straggling via Landau theory is detailed, including novel corrections. Next, the multiple scattering algorithm (which resembles the G4beamline algorithm discussed in Section 2.4) and its implementation are discussed. Finally, the transverse displacement and temporal displacement algorithms are shown.

#### 3.1 Energy Straggling in COSY

For energy loss, COSY uses the Bethe-Bloch equation (Eq. (2.5)) to find the mean energy loss. This can be done in the transfer map paradigm since average energy loss is a deterministic effect. However, this work is concerned with simulating realistic stochastic fluctuations about the average energy loss. For this reason, this work has implemented Landau theory [22] to describe the straggling distribution. Landau theory is discussed in detail in Section 2.1.2.

Due to its long tail, the average of the Landau distribution is undefined. This is clearly nonphysical. Recall from Eq. (B.8) that the universal Landau parameter is

$$\lambda = \frac{\epsilon - \langle \epsilon \rangle}{\xi} - (1 - C_{Euler}) - \beta^2 - \ln(\xi/T_{max}),$$

where  $\epsilon$  is the energy loss,  $C_{Euler}$  is the Euler constant ( $\approx 0.577$ ),  $\beta = v/c$  is the velocity in units of  $c$ , and  $T_{max}$  is the maximum transferable energy from an incident muon to an electron at rest. However, this means that fluctuations about the mean energy loss ( $\epsilon - \langle \epsilon \rangle$ ) are also divergent given enough samples. This can be seen as

follows:

$$\begin{aligned}\langle \lambda \rangle &\rightarrow \infty \\ \left\langle \frac{\epsilon - \langle \epsilon \rangle}{\xi} - (1 - C_{Euler}) - \beta^2 - \ln(\xi/T_{max}) \right\rangle &\rightarrow \infty \\ \left\langle \frac{\epsilon - \langle \epsilon \rangle}{\xi} \right\rangle &\rightarrow \infty \\ \langle (\epsilon - \langle \epsilon \rangle) \rangle &\rightarrow \infty.\end{aligned}$$

The possibility of divergence results in a sensitivity to step size since smaller steps effectively produce a large sample size. In order to combat this, an artificial cutoff is given to  $\lambda$  such that the average Landau  $\epsilon$  is equal to the average Bethe-Bloch energy loss  $\langle \epsilon \rangle$ . That is, it is required that

$$\begin{aligned}\langle \lambda \rangle &= \left\langle \frac{\epsilon - \langle \epsilon \rangle}{\xi} \right\rangle - (1 - C_{Euler}) - \beta^2 - \ln(\xi/T_{max}) \\ &= -(1 - C_{Euler}) - \beta^2 - \ln(\xi/T_{max}).\end{aligned}$$

If the cutoff is  $\lambda_{max}$ , then  $\langle \lambda \rangle$  can be calculated by the definition of an average over the range  $[0, \lambda_{max}]$ :

$$\langle \lambda \rangle = \frac{\int_0^{\lambda_{max}} \lambda * f(\lambda) d\lambda}{\int_0^{\lambda_{max}} f(\lambda) d\lambda}.$$

The task then is to numerically find  $\lambda_{max}$  such that it satisfies

$$\frac{\int_0^{\lambda_{max}} \lambda * f(\lambda) d\lambda}{\int_0^{\lambda_{max}} f(\lambda) d\lambda} = -(1 - C_{Euler}) - \beta^2 - \ln(\xi/T_{max}).$$

GEANT version 3.21 [30] suggests the following form for  $\lambda_{max}$ :

$$\lambda_{max} = 0.60715 + 1.1934 \langle \lambda \rangle + (0.67794 + 0.052382 \langle \lambda \rangle) \exp[0.94753 + 0.74442 \langle \lambda \rangle)] \quad (3.1)$$

(note that GEANT4 does not have a section on the Landau cutoff since the Urbán straggling model<sup>6</sup> is used instead). However, a plot of required cutoffs ( $\lambda_{max}$ ) vs.

---

<sup>6</sup>Note that the Urbán straggling model should not be confused with the Urbán multiple scattering model.

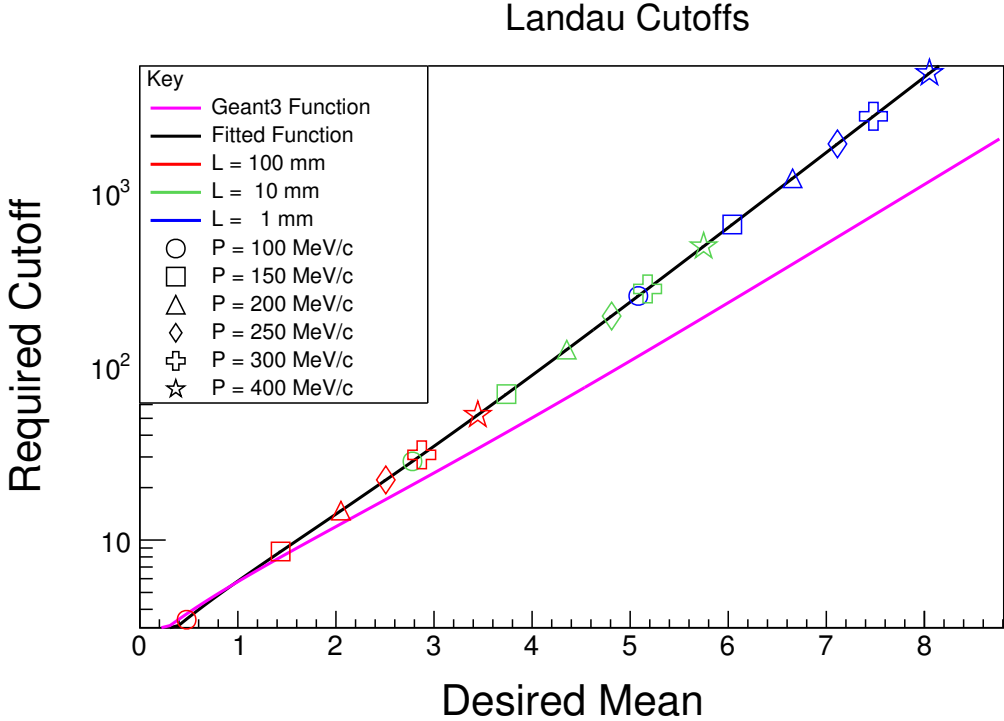


Figure 3.1.  $\lambda_{max}$  vs.  $\langle \lambda \rangle$  over a variety of liquid hydrogen absorber lengths and initial beam momenta. The pink line is the form given by GEANT3 (see Eq. (3.1)) and the black line is the fitted curve (see Eq. (3.2)). The data points are combinations of shapes and colors, as seen in the key. For example, since green means 10 mm and the square means 150 MeV/c, the green square data point represents the required cutoff for 150 MeV/c muons passing through 10 mm of liquid hydrogen. Liquid hydrogen was chosen in order to match the results in Section 5.1. However, other materials (such as lithium hydride) still fall within the desired  $\langle \lambda \rangle$  range of [0, 9].

desired means ( $\langle \lambda \rangle$ ) was produced independently in this work with muon ionization cooling parameters in mind. The form suggested by GEANT3 (see, e.g., Eq. (3.1)) was used to fit the plot in Figure 3.1. The determined form of the function is

$$\lambda_{max} = 0.517891 + 1.17765 \langle \lambda \rangle + (0.476074 + 0.00880733 \langle \lambda \rangle) \exp[1.15467 + 0.984008 \langle \lambda \rangle]. \quad (3.2)$$

Based on Eq. (B.8), it is possible to find  $\epsilon_{max}$ :

$$\epsilon_{max} = \xi [\lambda_{max} + (1 - C_{Euler}) + \beta^2 + \ln(\xi/T_{max})] + \langle \epsilon \rangle.$$

Therefore, during the energy loss sampling, if any energy loss  $\epsilon$  is selected which is greater than  $\epsilon_{max}$  it is discarded and the sampling is performed again. However, if the result has been discarded 100 times, the particle is assumed to have lost too much energy and is considered lost.

### 3.2 Multiple Scattering in COSY Infinity

Similar to ICOOL’s fifth model of scattering, the Rutherford model (see Section 2.2), COSY utilizes a piecewise distribution function which is Gaussian at small angles (as Goudsmit and Saunderson suggested [27]) and Rutherford-like at large angles. This Rutherford-like tail is derived at length in Appendix C, with a review of the relevant particle physics symbols and methods in Appendix D. The result is the (differential) Mott scattering cross section:

$$\frac{d\sigma}{d\Omega} \propto \frac{1 + \frac{(\beta\gamma)^2}{2}(1 + \cos\theta)}{(1 - \cos\theta)^2}, \quad (3.3)$$

where  $d\sigma/d\Omega$  is the differential scattering cross section,  $\beta$  is the velocity in units of  $c$ ,  $\gamma = 1/\sqrt{1 - \beta^2}$ , and  $\theta$  is the scattering angle. Observe that for the non-relativistic limit  $\beta \rightarrow 0$  the cross section does indeed approach a Rutherford distribution (Eq. (2.24)). The practical implementation of this cross section into the probability distribution function is discussed in Section 3.2.1.

**3.2.1 Implementation.** Now that the forms of the Gaussian and Rutherford-like scattering cross sections have been obtained, implementation of these cross sections is discussed. In this work, when a particle passes through matter, the change in angle of this particle is selected from a probability distribution. For  $u = \cos\theta$ , this distribution should be Gaussian-like at small angles [27] and follow the Mott cross section at large angles. Based on a Gaussian-like cross section for small angles and

the cross section in Eq. (3.3), the distribution has been chosen as

$$g(u) = \begin{cases} e^{-a(1-u)} & u_0 \leq u \\ \zeta \frac{1 + \frac{1}{2}(\beta\gamma)^2(1+u-b_c)}{(1-u+b_c)^2} & u \leq u_0 \end{cases}, \quad (3.4)$$

where  $u_0$  is the cutoff between the Gaussian-like distribution and the Mott distribution,  $\zeta$  is the amplitude of the Mott distribution, and  $b_c$  is the relative  $u$  shift of the Mott distribution. The parameter  $a$  is an empirical parameter, based on Highland theory [28], and can be found in Eq. (2.37). Eq. (2.37) is reproduced here for convenience:

$$a = \frac{0.5}{1 - \cos \theta_0},$$

where  $\theta_0$  has the form [28]

$$\theta_0 = \frac{E_s}{p\beta} \sqrt{\frac{L}{X_0}}.$$

However, this definition has been extended in this work to include empirical corrections based on GEANT4's [20] treatment of  $\theta_0$  (see Eq. (2.38)):

$$\theta_0 = \frac{13.6 \text{ eV}}{\beta p} \sqrt{\frac{L}{X_0} \left[ 1 + h_1 \ln \frac{L}{X_0} + h_2 \left( \ln \frac{L}{X_0} \right)^2 \right]}. \quad (3.5)$$

The Highland correction terms have been chosen novelly in this work as  $h_1 = 0.12$  and  $h_2 = 0.006$ . This was done by fitting the curve given by Eq. (3.4) to match the MuScat results [31], the results of which can be found in Section 5.2. It is important to note that these correction terms are tunable for future data based on muons traversing higher  $Z$  material.

$u_0$  is the point at which the Gaussian term meets the Mott tail. This has been chosen empirically as

$$u_0 = 1 - \frac{4.5}{a}. \quad (3.6)$$

This parameter was fitted alongside the Highland correction terms to match the experimental results in [31].

$\zeta$  and  $b_c$  are the angular scattering distribution's amplitude and offset for the tail. These are found by demanding continuity and smoothness at  $u_0$ :

$$e^{-a(1-u_0)} = \zeta \frac{1 + \frac{1}{2}(\beta\gamma)^2(1+u_0-b_c)}{(1-u_0+b_c)^2},$$

$$ae^{-a(1-u_0)} = \zeta \frac{1 + \frac{1}{2}(\beta\gamma)^2(1+u_0-b_c)}{(1-u_0+b_c)^2} \left( \frac{2}{1-u_0+b_c} + \frac{(\beta\gamma)^2}{2+(\beta\gamma)^2(1+u_0-b_c)} \right).$$

Then

$$a = \frac{2}{1-u_0+b_c} + \frac{(\beta\gamma)^2}{2+(\beta\gamma)^2(1+u_0-b_c)}.$$

Solving this for  $(u_0 - b_c)$  yields a quadratic with the solution

$$b_c = u_0 + \frac{A_2 + \sqrt{A_2^2 - 4A_1A_3}}{2A_1}, \quad (3.7)$$

with

$$A_1 = -a(\beta\gamma)^2,$$

$$A_2 = -(\beta\gamma)^2 - 2a,$$

$$A_3 = (\beta\gamma)^2(a-3) + 2a - 4.$$

The continuity condition for  $g(u_0)$  yields the expression for  $\zeta$ :

$$\zeta = \frac{e^{-a(1-u_0)}(1-u_0+b_c)^2}{1 + \frac{1}{2}(\beta\gamma)^2(1+u_0-b)}. \quad (3.8)$$

Now that the distribution function has a concrete form, it is implemented by inverting the cumulative distribution function (CDF). Let  $G(u)$  be the integral of  $g(u)$ . Then the variable  $G$  is uniformly sampled over the region  $[0, G_{max}]$ . If  $G \geq G(u_0) \equiv G_0$  then the Gaussian part of the distribution is used to generate  $u$  (i.e.,  $G(u \geq u_0)$ ). Otherwise, the tail of the CDF is used. Figure 3.2 shows  $G(u)$  for

### Scattering Cumulative Distribution Function

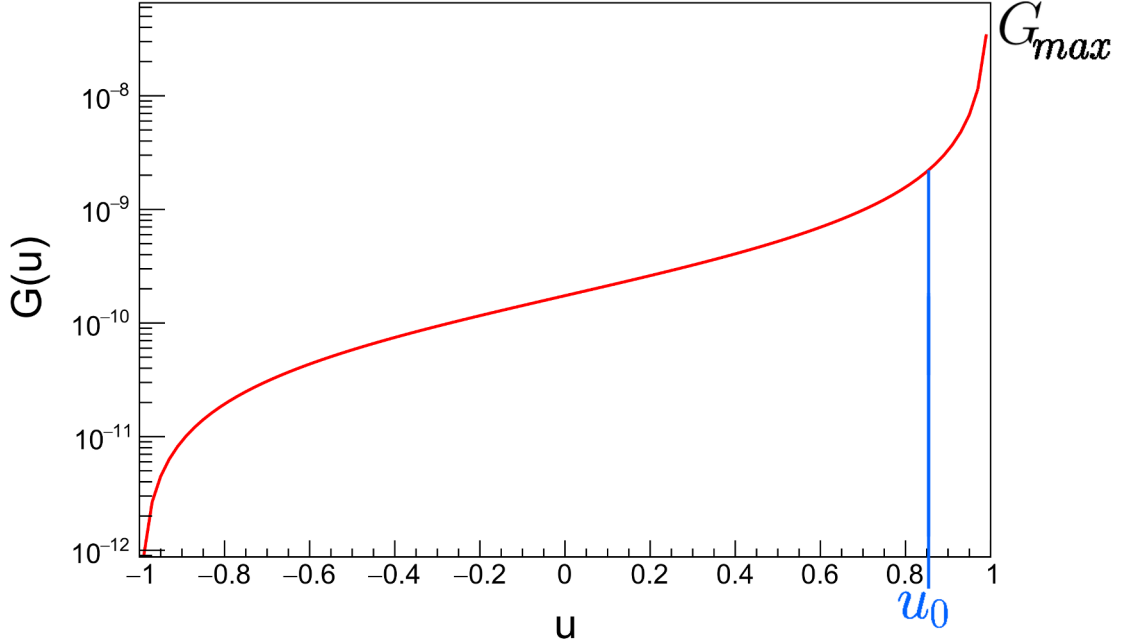


Figure 3.2. Example of the cumulative angular distribution function for muons with momenta of 200 MeV/c passing through 100 mm of liquid hydrogen. Note that the  $y$  axis is log scaled due to the very sharp peak. Furthermore, note that  $u_0$  is greatly exaggerated, since its actual value for these parameters is 0.99987.

$L = 100$  mm,  $p = 200$  MeV/c, and a radiation length  $X_0 = 8.66$  m (to simulate a liquid hydrogen target).<sup>7</sup>

However, since this is a piecewise function, the CDF is inverted in pieces. The tail of the CDF is found first:

$$G(u \leq u_0) = \int_{-1}^u \zeta \frac{1 + \frac{1}{2}(\beta\gamma)^2(1 + u' - b_c)}{(1 - u' + b_c)^2} du'.$$

---

<sup>7</sup>The value of 8.66 m as the radiation length of liquid hydrogen was chosen so that it matches the value found in the ICOOL source files. This differs from the radiation length of liquid hydrogen found in the PDG website [16], which is 8.904 m.

This integral may be solved by substituting  $v = 1 - u' + b_c$  and simply splitting the numerator into separate parts:

$$\begin{aligned} G(u \leq u_0) &= -\zeta\left(1 + \frac{1}{2}(\beta\gamma)^2(1 - b_c)\right) \int_{2+b_c}^{1-u+b_c} v^{-2} dv - \\ &\quad \zeta \frac{(\beta\gamma)^2}{2} \int_{2+b_c}^{1-u+b_c} (v^{-2} - v^{-1} + b_c v^{-2}) dv, \\ G(u \leq u_0) &= \zeta(1 + (\beta\gamma)^2) \left( \frac{1}{1 - u + b_c} - \frac{1}{2 + b_c} \right) + \zeta \frac{(\beta\gamma)^2}{2} \ln \left( \frac{1 - u + b_c}{2 + b_c} \right). \end{aligned} \quad (3.9)$$

The goal is to solve Eq. (3.9) for  $u(G)$ . However, using direct inversion is extremely difficult and involves special functions. Therefore, it is more prudent to generate  $u$  via bisection method (see Figure 3.3). In this method, the true  $G$  is sampled uniformly on the range  $[0, G_{max}]$ , where  $G_{max} \equiv G(1)$ . Explicitly,  $G_{max}$  is

$$\begin{aligned} G_{max} \equiv G(1) &= \int_{-1}^{u_0} \zeta \frac{1 + \frac{1}{2}(\beta\gamma)^2(1 + u - b_c)}{(1 - u + b_c)^2} du + \int_{u_0}^1 e^{-a(1-u)} du, \\ &= G_0 + \frac{1}{a} - \frac{e^{-a(1-u_0)}}{a}. \end{aligned}$$

If  $G < G_0$ , then the tail is sampled. A trial  $u$  called  $\bar{u}$  (as in “average”) is selected from some range which is known to contain the actual  $u$ . The range is described as  $[u_{min}, u_{max}]$ , and  $\bar{u} = (u_{min} + u_{max})/2$ .

Initially, the range is chosen as  $u_{min} = -1$  and  $u_{max} = u_0$  (since that is the largest range on which  $G(u \leq u_0)$  is valid and hence  $u$  is guaranteed to be in this range).  $\bar{G} \equiv G(\bar{u})$  is found using Eq. (3.9), and then the routine is subject to the following conditions:

- |   |   |
|---|---|
| If $\bar{G} \in [G - \delta G, G + \delta G]$ | then $u = \bar{u}$ , return value.                    |
| If $\bar{G} < G - \delta G$                   | then $u_{min} = \bar{u}$ , rerun with new $u_{min}$ . |
| If $\bar{G} > G + \delta G$                   | then $u_{max} = \bar{u}$ , rerun with new $u_{max}$ . |

### Scattering Cumulative Distribution Function

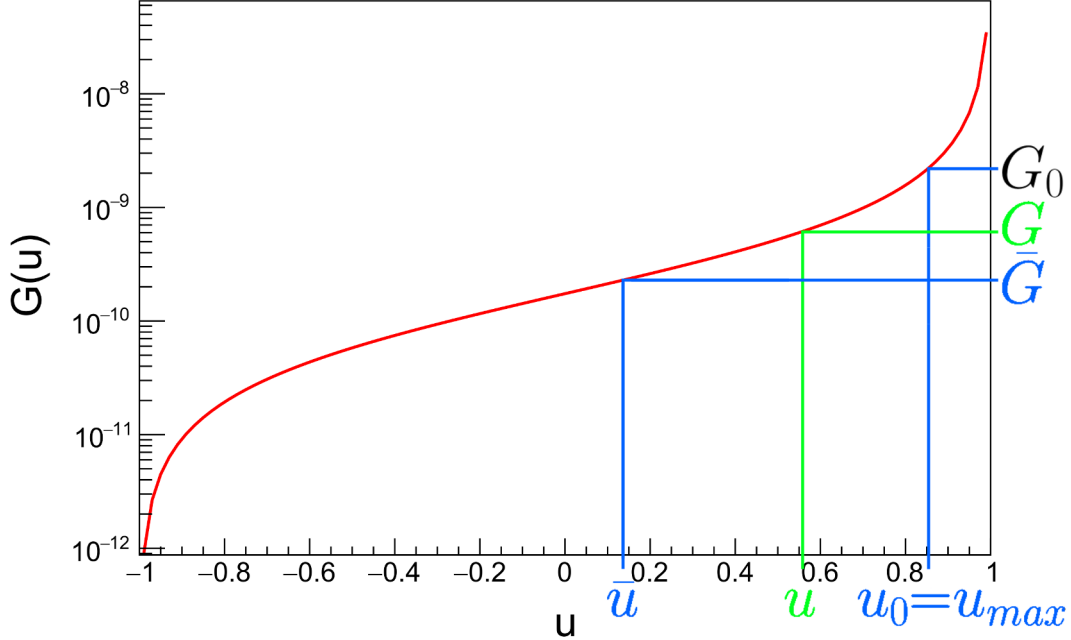


Figure 3.3. Example of the first iteration of the algorithm to obtain the true  $u$  (in green). The true  $G$  is chosen uniformly from  $G \in [0, G_{max}]$ . If  $G < G_0$ , then the tail is sampled via bisection method. In this case, since  $\bar{G} < G$ ,  $\bar{u}$  is the new  $u_{min}$  and  $\bar{u}$  is calculated again.

$\delta G$  is a precision, and has been chosen for this work as  $\delta G = 10^{-8}$ . However, it is conceded that in the future  $\delta G$  should be a percentage of  $G_{max}$  rather than an absolute number.

For the peak,  $u_0 \leq u$  and so the CDF becomes

$$G(u_0 \leq u) = \int_{-1}^{u_0} g(u)du + \int_{u_0}^u e^{-a(1-u)}du.$$

The first term is simply  $G_0$ , the cumulative distribution function at  $u_0$ . The second term is easily integrable and yields

$$G(u_0 \leq u) = G_0 + \frac{e^{-a(1-u)} - e^{-a(1-u_0)}}{a}. \quad (3.10)$$

The inversion of this function is quite straightforward, and is

$$u(G_0 \leq G) = 1 + \frac{1}{a} \ln [a(G - G_0) + e^{-a(1-u_0)}]. \quad (3.11)$$

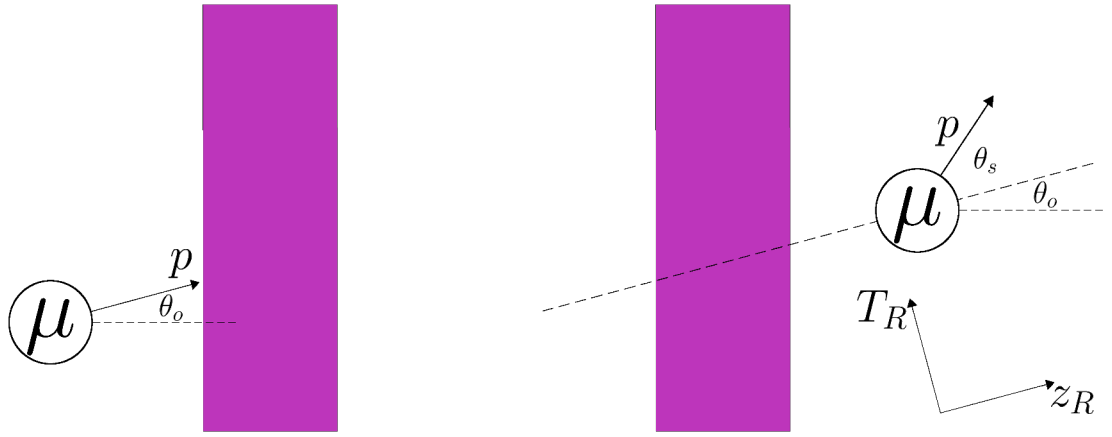


Figure 3.4. Example of a muon entering an absorber (purple) with some nonzero initial angle  $\theta_o$ . The muon then scatters an angle  $\theta_s$  with respect to its initial momentum  $\vec{p}$ . The scattering distribution  $g(u)$  assumes a straight, on-axis particle ( $x = y = p_x = p_y = 0$ ) before scattering, and so is in the rotated frame represented by  $T_R, z_R$ .

Therefore, if  $G \in [0, G_{max}]$  is greater than or equal to  $G_0$ , then it is simply inserted into Eq. (3.11) and the true  $u$  is obtained.

It is a subtle yet important point to note that the Mott cross section (Eq. (3.3)), upon which the probability distribution function  $g(u)$  in Eq. (3.4) is based, assumes an on-axis straight line trajectory. An on-axis trajectory is equivalent to saying that  $p_z = p$  and  $x = y = p_x = p_y = 0$ . For particles that are not on-axis, the reference frame both before and after scattering is rotated such that  $p = p_z$ . A particle that is not on-axis is exemplified in Figure 3.4. Here, the muon has some angle  $\theta_o$  before entering the medium. The lab frame has transverse and longitudinal position axes  $T$  and  $z$  and the rotated frame has corresponding transverse and longitudinal position axes  $T_R$  and  $z_R$ .

To reiterate, prior to scattering, in the rotated frame the rotated longitudinal momentum is the total momentum ( $p_{z,R} = p$ ) and the rotated transverse momentum

is zero ( $p_{T,R} = 0$ ). After scattering,  $g(u)$  yields the scattered angle  $\theta_s$ . The rotated longitudinal momentum is no longer necessarily equal to the total momentum, but rather  $p_{z,R} = p \cos \theta_s$ . Similarly, the rotated transverse momentum is not necessarily zero but instead  $p_{T,R} = \sqrt{p^2 - p_{z,R}^2}$ . Note that since energy straggling has already been accounted for, the total momentum  $p$  stays constant throughout the scattering process and regardless of reference frame.

Due to cylindrical symmetry, the transverse momentum in the rotated frame  $p_{T,R}$  must be distributed uniformly into the transverse  $x$  and  $y$  momenta. The constraint upon the transverse momentum in any frame is

$$p_T^2 = p_x^2 + p_y^2.$$

Therefore, the variable  $\phi$  is selected uniformly from  $[0, 2\pi]$ . The  $x$  and  $y$  momenta in the rotated frame are

$$p_{x,R} = P_{T,R} \cos \phi \cdot \text{sgn}(\phi - \pi),$$

$$p_{y,R} = P_{T,R} \sin \phi,$$

where  $\text{sgn}$  is the sign function defined by

$$\text{sgn}(x) = \begin{cases} -1 & \text{for } x < 0 \\ 0 & \text{for } x = 0 \\ 1 & \text{for } x > 0 \end{cases}.$$

The rotated  $x$  and  $y$  momenta ( $p_{x,R}$  and  $p_{y,R}$ ) are subsequently transformed into the lab frame.

To summarize, the angular distribution used by COSY Infinity is based on a piecewise function which is Gaussian for small angles [27] and has a Mott tail for large angles. This distribution is represented by  $g(u)$  in Eq. (3.4), where  $u \equiv \cos \theta$ .  $g(u)$  has four parameters:  $a$ , an empirical parameter that is based on Highland theory [28]

and is dependent on some critical angle  $\theta_0$ , defined in Eq. (3.5);  $u_0$ , the empirical cutoff angle that distinguishes which angles are Gaussian and which are not, found by Eq. (3.6);  $b_c$ , a parameter derivable from smoothness of  $g$  at  $u_0$ , which represents the offset of the Mott tail, found in Eq. (3.7); and  $\zeta$ , a parameter derivable from continuity of  $g$  at  $u_0$  which represents the amplitude of the Mott tail, found in Eq. (3.8). From  $g(u)$ , its antiderivative  $G(u)$  may be found and a particular  $G$  may be picked from the range  $[0, G_{max}]$ . If  $G < G_0 \equiv G(u_0)$ , then  $u$  comes from the Mott tail and a bisection method is used to find  $u$ . If  $G_0 \leq G$  then  $u$  comes from the Gaussian peak and  $G(u)$  may be inverted to find  $u(G)$ . This scattered angle must then be rotated into the lab frame and the additional transverse momentum must be uniformly distributed into  $p_x$  and  $p_y$ .

### 3.3 Transverse Displacement in COSY Infinity

Due to multiple scattering events, when a particle traverses matter, a direct correlation between the particle transverse position and scattered angle is not always clear. Two identical particles with identical initial conditions may end up with identical scattered angles but different transverse positions (see Figure 3.5). This is because these two particles may take different paths through the absorber. While both of these paths may lead to a similar final angle with respect to the  $z$  axis, the positions are likely different due to their trajectories.

For this reason, transverse corrections have been implemented in COSY. Due to a lack of experimental data at the time, COSY was compared to G4beamline across several initial momenta and absorber lengths. The result was

$$x = x_o + x_D + \text{Gaus}(\theta_{diff} * L/2, \theta_c/(2\sqrt{3})), \quad (3.12)$$

where  $x_o$  is the original  $x$  position,  $x_D = L * P_{x,o}/P_{z,o}$  is the deterministic gain in  $x$ , and  $\text{Gaus}(\mu, \sigma)$  is a randomly selected number from a Gaussian distribution with mean  $\mu$

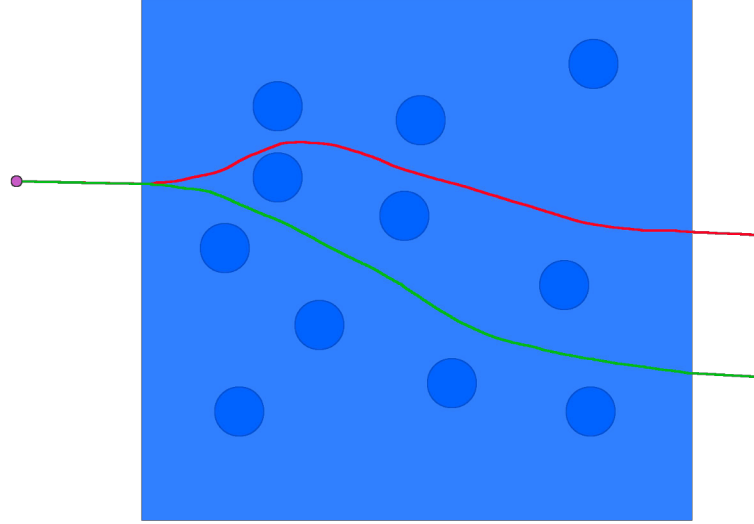


Figure 3.5. Two examples of true paths which a particle might take when traversing a medium. Note that both the red and green paths have the same final scattered angle but different transverse positions.

and standard deviation  $\sigma$ . The forms of  $\mu$  and  $\sigma$  were selected based on a combination of the Particle Data Group [16] and Fernow and Gallardo [32]. Note that the average  $\mu = \theta_{diff} * L/2$  represents the transverse displacement that would have occurred if all of the angular scattering had happened at the point  $L/2$ .  $\theta_{diff} = \theta_{final} - \theta_o$  is the amount of deflection which occurred due to scattering and  $\theta_c = 13.6 \text{ eV}/\beta p \cdot \sqrt{1/X_0}$  is the coefficient from Highland theory [28].

The fitting of these parameters is discussed next. As previously mentioned, the data for the fits were generated by G4beamline [19]. Here, a particular example of a simulation of  $10^6$  particles passing through 1 cm of liquid hydrogen is shown. The initial beam distribution was a pencil beam of momentum  $200 \text{ MeV}/c$ . A plot of the histogram of  $(x, p_x)$  phase space can be seen in Figure 3.6. It can be seen in Figure 3.7 that the cross section for a given transverse momentum results in a nearly-Gaussian  $x$  histogram. It can also be inferred from the figure that the mean and standard deviation of the Gaussian fit vary depending on which  $p_x$  is chosen. For example,

higher values of  $p_x$  appear to have both a larger mean and standard deviation. While this trend is conceptual, it aids in the understanding of the form of Eq. (3.12).

The phase space portrait in Figure 3.8 shows that the distribution is only locally Gaussian. However, fitting in the range of  $p = 100\text{--}400 \text{ MeV}/c$ ,  $L = 1\text{--}100 \text{ mm}$  has shown that this is a good approximation for the majority of particles (see Section 5.1).

An example of the success of this implementation can be seen in Figure 3.9, where  $10^6$  muons of momentum  $250 \text{ MeV}/c$  were simulated through 100 mm of liquid hydrogen. The simulation was carried out in both COSY and ICOOL [18] with good agreement.

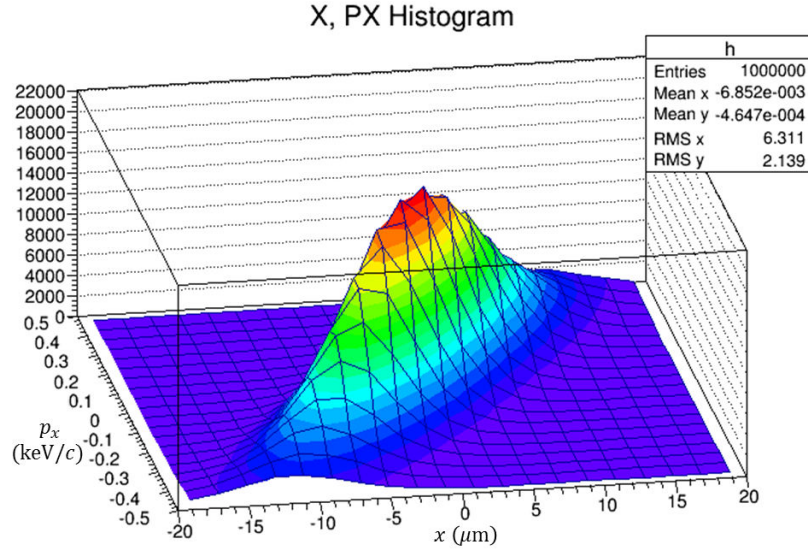


Figure 3.6. 2D histogram of  $(x, p_x)$  phase space for  $10^6$  muons of momentum  $200 \text{ MeV}/c$  passing through 1 cm of liquid hydrogen.

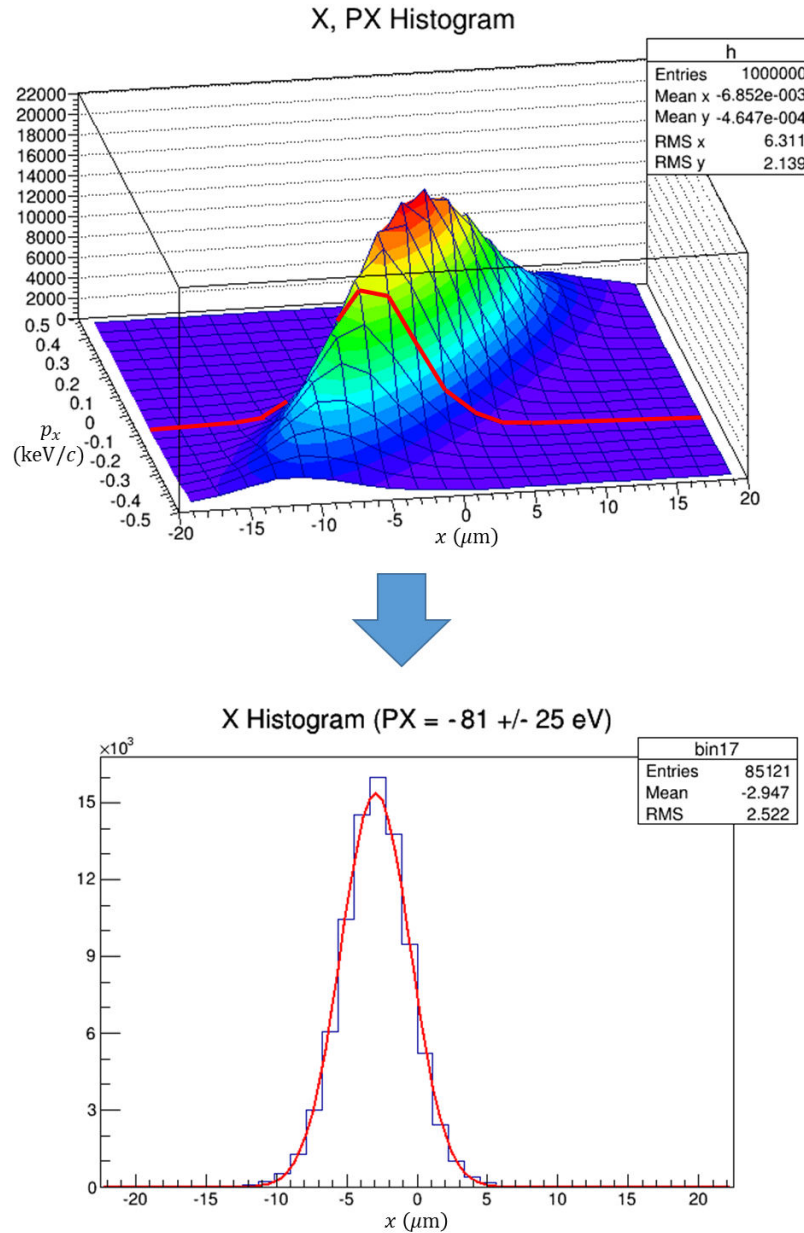


Figure 3.7. Cross section of Figure 3.6 at  $p_x = (-0.081 \pm 0.025)$  keV/c. The resulting  $x$  histogram is fit (in red) with a Gaussian.

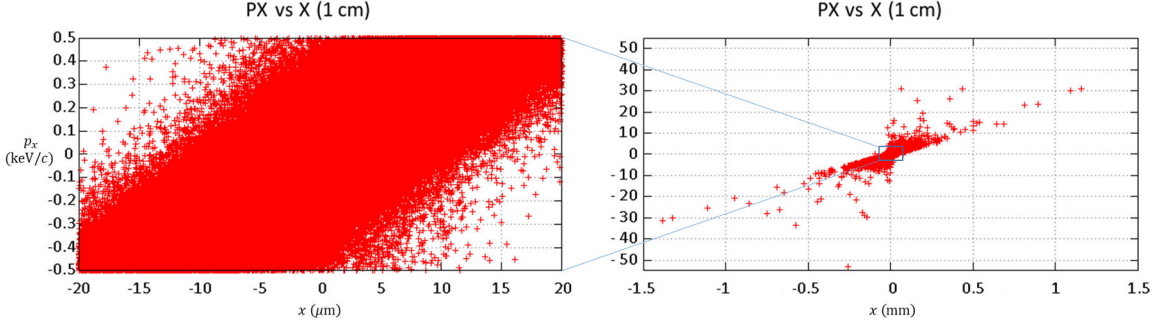


Figure 3.8. Phase space portrait of Figure 3.6. The bulk in Figure 3.6 (left) is approximately Gaussian. The extremities in Figure 3.6 (right) are not approximately Gaussian.

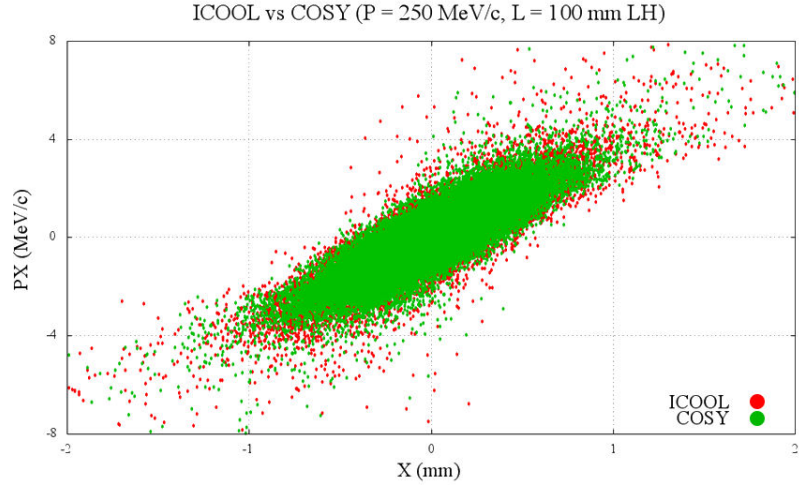


Figure 3.9. Sample simulation results for the implementation of the transverse coordinate correction algorithm.

### 3.4 Temporal Displacement in COSY Infinity

The time-of-flight (ToF) is the amount of time it takes for a particle to traverse an absorber. The deterministic ToF is the average time it takes for a particle to traverse an absorber and is correlated to the average energy loss. For the ToF in COSY, both the deterministic and stochastic processes are handled in the same routine. To first order, the particle decelerates at some average rate through an absorber of length

*L.* If  $a$  is the constant acceleration then

$$v_f = v_o + a\Delta t,$$

or

$$a = \frac{v_f - v_o}{\Delta t}.$$

At the same time,  $v_f^2 = v_o^2 + 2aL$ , and so

$$a = \frac{v_f^2 - v_o^2}{2L}.$$

Then  $\Delta t$  becomes

$$\Delta t = \frac{(v_f - v_o)2L}{v_f^2 - v_o^2} = \frac{2L}{v_f + v_o}.$$

Given  $\beta = pc/E$  and  $v = \beta c$ , then

$$\Delta t = 2L / \left( \frac{p_f c}{E_f} + \frac{p_o c}{E_o} \right). \quad (3.13)$$

However, COSY does not have a time variable, but rather a variable  $\ell$  that is described as the time-of-flight in units of length. In COSY [4], this is defined as

$$\ell = \frac{-(t - t_0)v_0\gamma}{1 + \gamma},$$

where the subscript 0 signifies the reference particle. Let the time before a step be denoted  $t_1$  and the time after a step denoted  $t_2$ . Then to find  $\ell_2$  given  $\ell_1$  and  $\Delta t$  from Eq. (3.13), observe that

$$\begin{aligned} \ell_1 &= \frac{(t_{01} - t_1)v_{01}\gamma_1}{1 + \gamma_1} = (t_{01} - t_1)A_1 \\ \ell_2 &= \frac{(t_{02} - t_2)v_{02}\gamma_2}{1 + \gamma_2} = (t_{02} - t_2)A_2, \end{aligned} \quad (3.14)$$

where

$$A_n \equiv v_{0n}\gamma_n/(1 + \gamma_n) \quad \text{for } n = 1, 2 \quad (3.15)$$

and the subscript 0 again denotes the reference particle. Then

$$\begin{aligned}
\ell_2 - \ell_1 &= (t_{02} - t_2) A_2 - (t_{01} - t_1) A_1 \\
&= [(t_{02} - t_{01}) + t_{01}] - [(t_2 - t_1) + t_1] A_2 - (t_{01} - t_1) A_1 \\
&= (\Delta t_0 - \Delta t) A_2 + (t_{01} - t_1) A_2 - (t_{01} - t_1) A_2 \\
&= (\Delta t_0 - \Delta t) A_2 + (t_{01} - t_1)(A_2 - A_1).
\end{aligned}$$

Eq. (3.14) says that  $t_{01} - t_1 = \ell_1/A_1$ . Moving  $\ell_1$  to the right hand side,

$$\begin{aligned}
\ell_2 &= (\Delta t_0 - \Delta t) A_2 + \frac{\ell_1}{A_1}(A_2 - A_1) + \ell_1 \\
&= (\Delta t_0 - \Delta t) A_2 + \ell_1 \left( \frac{A_2 - A_1}{A_1} + \frac{A_1}{A_1} \right) \\
&= (\Delta t_0 - \Delta t) A_2 + \ell_1 \frac{A_2}{A_1}.
\end{aligned}$$

Substituting for  $A_n$  via Eq. (3.15) yields the final result

$$\ell_2 = \frac{(\Delta t_0 - \Delta t)v_{02}\gamma_2}{1 + \gamma_2} + \ell_1 \frac{v_{02}\gamma_2(1 + \gamma_1)}{v_{01}\gamma_1(1 + \gamma_2)}. \quad (3.16)$$

Using Eq. (3.16),  $\Delta t$  from Eq. (3.13) can be directly input into the new COSY variable for time-of-flight in units of length. Figure 3.10 shows the simulation results for a beam of  $10^6$  muons of momentum 172 MeV/c passing through 109 mm of liquid hydrogen, which were the parameters of the MuScat experiment [31]. The COSY results are shown alongside those from ICOOL [18]. Note that the agreement is quite good. ICOOL displays a thicker bulk at around 0.430 ns, but it is approximately 1 ps in width—about 0.2% of the average time-of-flight.

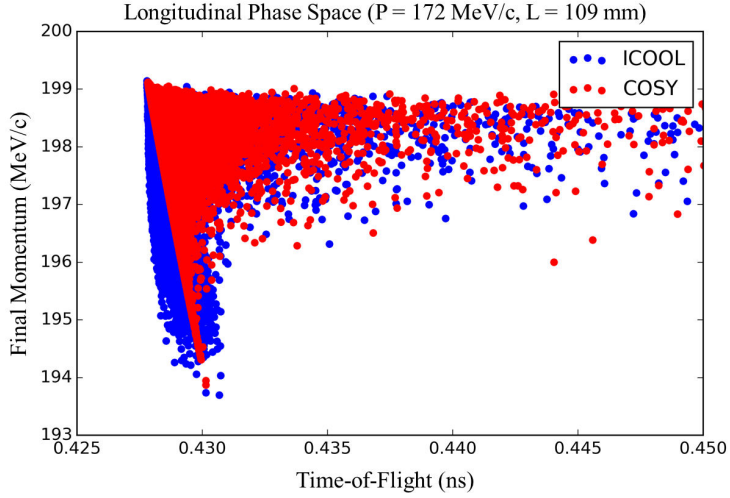


Figure 3.10. Sample simulation results for the implementation of the temporal displacement algorithm discussed in this section.

In conclusion, the two primary stochastic effects, energy straggling and multiple scattering, were discussed at length, resulting in Eqs. (2.9) and (3.3). The secondary stochastic effects were temporal and transverse displacement, which correspond respectively to energy straggling and multiple scattering. These secondary effects were also elaborated upon, resulting in Eqs. (3.16) and (3.12). The success of these theoretical equations will be discussed in the next section.

## CHAPTER 4

### SOFTWARE IMPLEMENTATION

This chapter discusses in detail the organization and internal structure of the code that is the implementation of the novel algorithms discussed in Chapter 3. For reference, a reproduction of the code itself may be found in Appendix G. First, the user input is discussed. Next, the *cosy.fox* level of the code is examined. Finally, the structure of the FORTRAN code is briefly considered. Figure 4.1 is referenced during these discussions.

In addition to the user's input file, COSY also uses a *cosy.fox* file. This file contains a plethora of global variables, functions, and routines which the user can access. However, *cosy.fox* can also be used to hide most of the complicated machinery from the user. For example, for this study the routine in *cosy.fox* transforms the COSY coordinates  $(x, a, y, b, \ell, d)$  into absolute coordinates  $(x, p_x, y, p_y, t, E)$ ,<sup>8</sup> and then relays the information to the FORTRAN code. Both the user file and the *cosy.fox* file are written in COSYScript, the programming language of COSY.

#### 4.1 User Input

As with the deterministic absorber routine previously present in COSY, WA, the user must first call the procedure

```
BBC <Z> <A> <ρ> <I> <δ> <C> ;
```

This stores the material parameters in a global array. The arguments are the nuclear charge  $Z$ , the atomic mass  $A$ , the density of the material  $\rho$ , the ionization energy  $I$ , the density correction  $\delta$ , and the shell correction  $C$ . Next, the user must either generate a distribution of particles or read a distribution of particles from a file. Using

---

<sup>8</sup>Recall from Eq. (1.1) that  $x$  and  $y$  are the transverse coordinates;  $a = p_x/p_0$  the  $x$  angle;  $b = p_y/p_0$  the  $y$  angle;  $\ell = -(t - t_0)v_0\gamma/(1 + \gamma)$  the time-of-flight in units of length;  $\delta = (K - K_0)/K_0$  the relative energy;  $E$  the total energy;  $K$  the kinetic energy; and the subscript 0 denotes the coordinate of the reference particle.

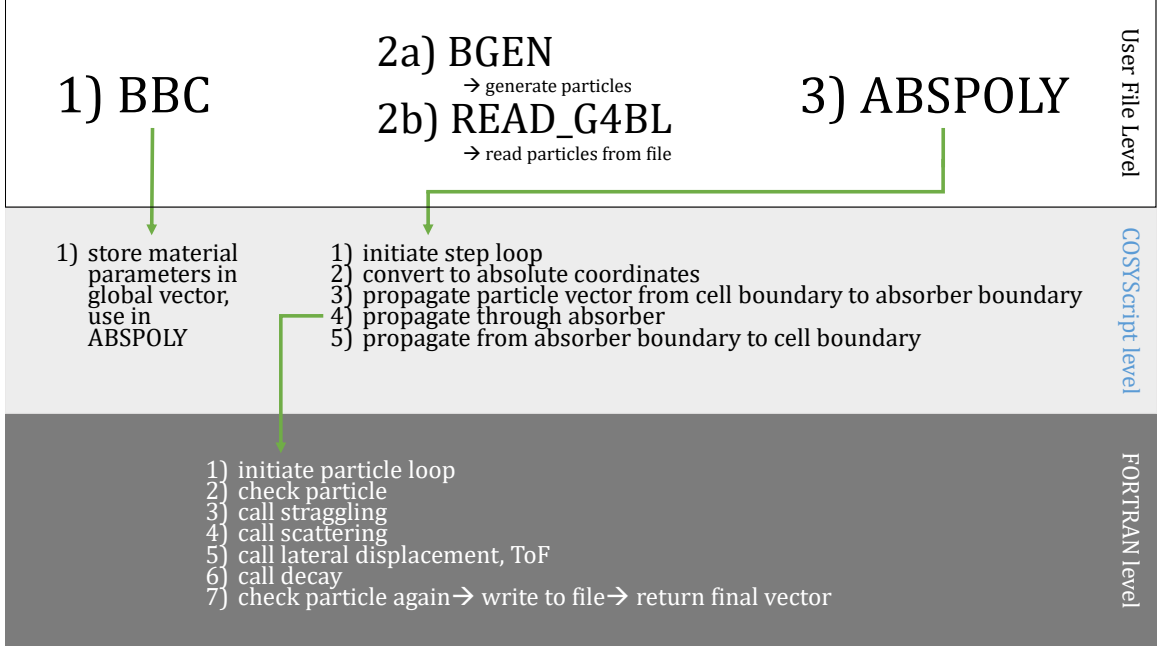


Figure 4.1. A flowchart for the structure of the new COSY routines implemented in this work.

**BGEN**  $\langle n \rangle \langle V \rangle \langle \mu_x \rangle \langle \sigma_x \rangle \langle \mu_{p_x} \rangle \langle \sigma_{p_x} \rangle \langle \mu_y \rangle \langle \sigma_y \rangle \langle \mu_{p_y} \rangle \langle \sigma_{p_y} \rangle \langle \mu_t \rangle \langle \sigma_t \rangle \langle \mu_{p_z} \rangle \langle \sigma_{p_z} \rangle ;$

the user can generate a Gaussian beam of  $n$  particles into a 2D ( $n \times 6$ ) vector  $V$ .

Note that in COSY, a 2D vector is a vector of vectors and is not the same data class as an array. Alternatively, the user may use

**READ\_G4BL**  $\langle \text{file} \rangle \langle n \rangle \langle V \rangle ;$

to read an ASCII-formatted G4beamline [19] file of  $n$  particles and store it into a 2D vector  $V$ . Finally, the user can call

**ABSPOLY**  $\langle S_1 \rangle \langle S_2 \rangle \langle n \rangle \langle L \rangle \langle A \rangle \langle V \rangle \langle X_0 \rangle \langle S_n \rangle \langle L_c \rangle \langle O \rangle ;$

where  $S_1$ <sup>9</sup> is an  $n^{th}$  order polynomial describing the entrance surface,  $S_2$  is an  $n^{th}$  order polynomial describing the exit surface,  $L$  is the on-axis length of the absorber,  $A$  is the circular aperture,  $V$  is the 2D input and output particle vector,  $X_0$  is the radiation

---

<sup>9</sup>For a full description of the entrance and exit polynomials  $S_1$  and  $S_2$ , please see the COSY beam physics manual [4], page 33.

length of the material,  $S_n$  is the number of steps inside the absorber,  $L_c$  is the length of the absorber cell (such that the longest part of the absorber is contained within  $L_C$ ), and  $O$  is the output unit number (e.g. “12” to save the results in `fort.12`). A depiction of some of the parameters can be found in Figure 4.2.

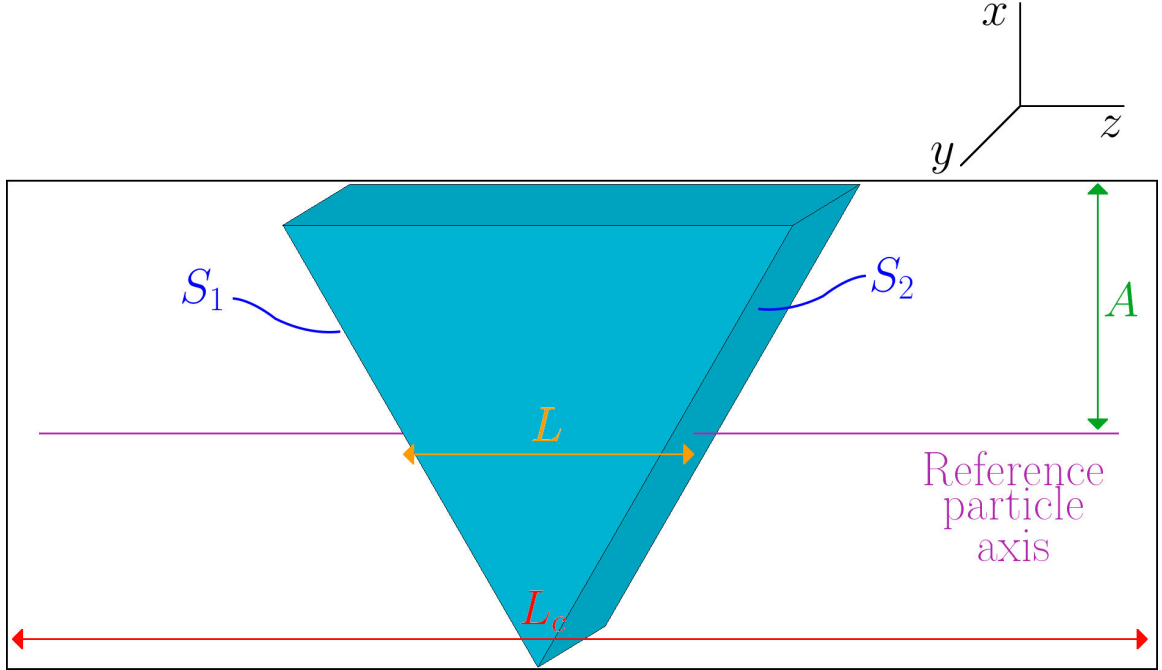


Figure 4.2. Cartoon example of some of the ABSPOLY parameters.

## 4.2 COSYScript Level

As previously mentioned, the `ABSPOLY` routine is defined in the external file `cosy.fox`. Here, if the user desires iteration through the absorber, the step loop over  $S_n$  (the input of number of steps inside the absorber) is initialized. Next, input 2D vector  $V$  is converted from coordinates relative to the reference particle to absolute coordinates. The particle vector is then propagated from the cell boundary (whose width is defined by  $L_c$ ) to the absorber boundary (whose on-axis width is defined by  $L$ ). If  $L_c < L$  then no such propagation occurs since the particles are already at the absorber boundary. When the particles are at the absorber boundary, the 2D particle vector  $V$  is passed on to the FORTRAN level of the code, where propagation through

the absorber takes place. The routine linking the COSYScript and FORTRAN levels is **STOABS** and is discussed in Section 4.3. After the 2D particle vector  $V$  is returned,  $V$  is propagated to the end of the cell and returned to the user.

### 4.3 FORTRAN Level

Except for the propagation of particles through the absorber, the processes found in Section 4.2 are much faster in COSYScript than in FORTRAN. This is because processes like coordinate conversion, propagation through a vacuum, etc. are deterministic and can, therefore, be handled by transfer maps.

The routine

```
STOABS <V> <m> <L> <MP> <X0> <O> <A> <n> ;
```

takes input parameters from the COSYScript level and returns the input 2D particle vector  $V$ . Here,  $m$  is the particle mass (taken from the reference particle),  $L$  is an array containing the  $n$ -path lengths for each particle,  $MP$  is an array containing the material parameters (taken from the global array *BETHEBLOCHC* set up by the routine **BBC**),  $X_0$  is the radiation length of the material,  $O$  is the output unit number,  $A$  is the aperture, and  $n$  is the number of particles.

Once the FORTRAN level has this information, a loop over  $n$  particles is started. Each particle is checked at the beginning of each loop for the following flags: particle stopped, particle hit aperture, particle missed absorber, drift. If either the particle was stopped ( $E \leq m$ ) or the particle hit the aperture ( $x^2 + y^2 \geq A^2$ ) then the particle is terminated. If the particle missed the absorber completely then the drift flag is turned on. If the drift flag is on then the particle is simply propagated without the stochastic processes called.

Provided that the particle has not been flagged, the particle is subject to energy straggling and then multiple scattering. After these two routines, the lateral

displacement and time-of-flight corrections are called. It should be noted that the order matters for energy straggling and multiple scattering. The order does not matter for lateral displacement and time-of-flight provided that both straggling and scattering have already occurred. Finally, decay can be called. Note that for this work, decay has been turned off completely, and so this step is skipped.

Finally, the particle is checked again. If the output unit number  $O$  is not equal to zero, then the particles are written to a file. Lastly, the 2D particle vector  $V$  is returned to the COSYScript level.

#### 4.4 Summary

Figure 4.1 displays the conceptual process of operating the implemented routines. First, the user defines the material parameters in **BBC**, which stores these parameters as global variables at the COSYScript level. Next, the user creates a 2D vector of particles, either by generating a Gaussian beam via **BGEN** or reading particles from a G4beamline file via **READ\_G4BL**. Finally, the user calls the **ABSPOLY** routine. **ABSPOLY** converts the COSY coordinates to and from absolute coordinates and calls the FORTRAN routine to step through the absorber. At the FORTRAN level, each particle is subjected to the energy straggling, multiple scattering, transverse displacement, and time-of-flight algorithms described in Chapter 3. These particles are returned to the user at the end of the propagation.

## CHAPTER 5

## RESULTS

In this chapter, the new COSY routines are benchmarked against both ICOOL and G4beamline for pencil beams. Recall that a pencil beam is a beam with an RMS of zero for all transverse coordinates. Pencil beams are used in order to simulate a plethora of possible paths and energy losses for a particular initial condition. Both validation against past experiments and studies of current muon ionization cooling channel (MICE) are shown. Since both ICOOL and G4beamline have automatic variable stepping, their maximum step sizes are left as default unless explicitly stated otherwise.

### **5.1 Benchmark Against Other Codes**

This section briefly discusses the comparison of the new COSY routines with those of two other codes, ICOOL [18] and G4beamline [19]. Refer to Figures 5.1–5.12 (12 figures, each with three subplots) mentioned here. The benchmarking was done over both the typical momentum range of cooling channels (100, 200, 300, and 400 MeV/ $c$ ) and various absorber lengths (1, 10, and 100 mm). These simulations were performed using a pencil beam of  $5 \times 10^4$  muons with the aforementioned momenta through liquid hydrogen. Note that for the transverse position and transverse momentum histograms, the absolute value of the coordinate is plotted. Therefore, the mean is not zero. For COSY, the step size was the entire absorber length. For G4beamline in the case of a 1 mm absorber, the maximum step size was limited to 0.1 mm. This was done because of the heavy dependence of the transverse position on step size for short absorbers in G4beamline.

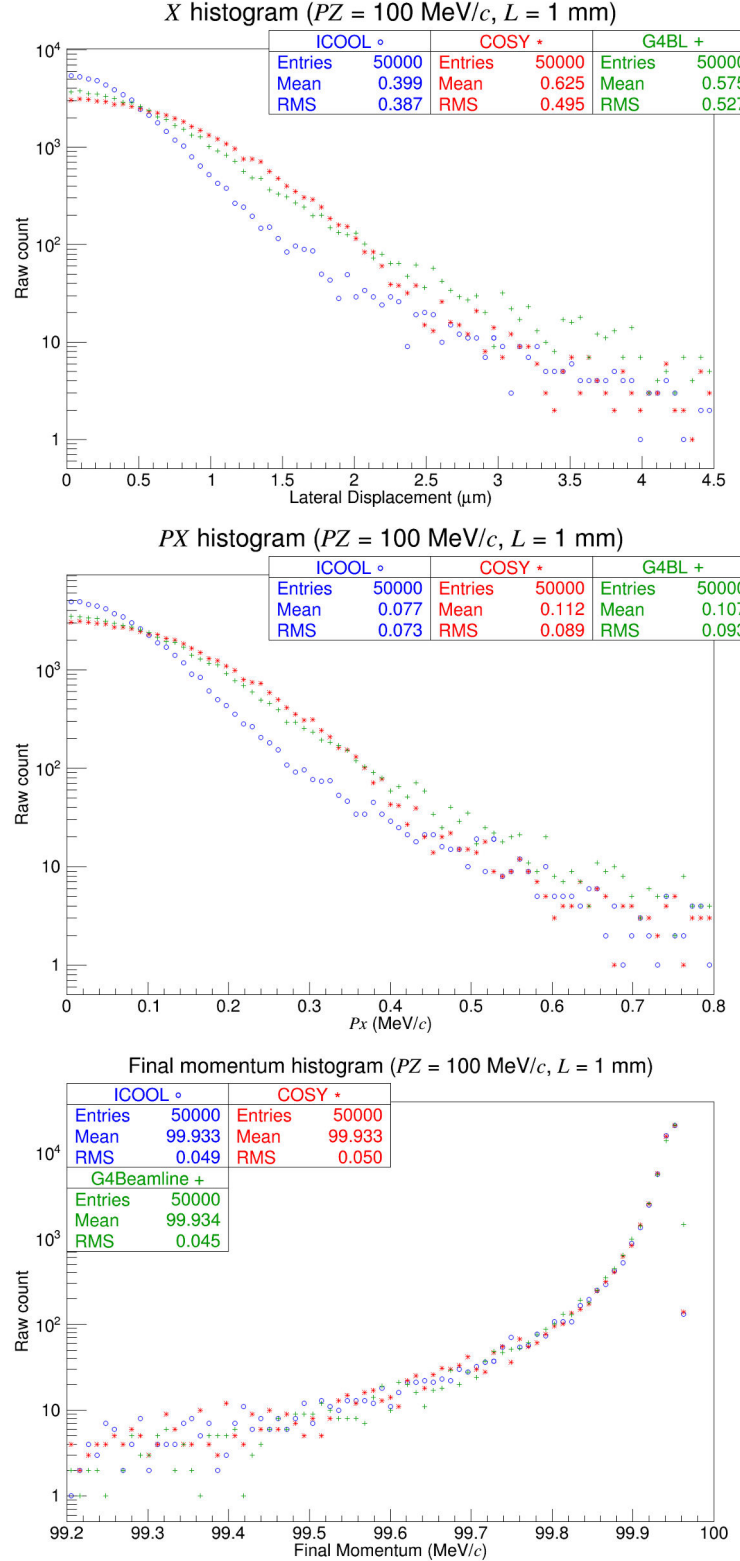


Figure 5.1. Muons of momentum  $100 \text{ MeV}/c$  through 1 mm liquid hydrogen. For the  $x$  and  $p_x$  histograms, COSY and G4beamline follow a Gaussian-like peak whereas ICOOL follows a Fano peak.

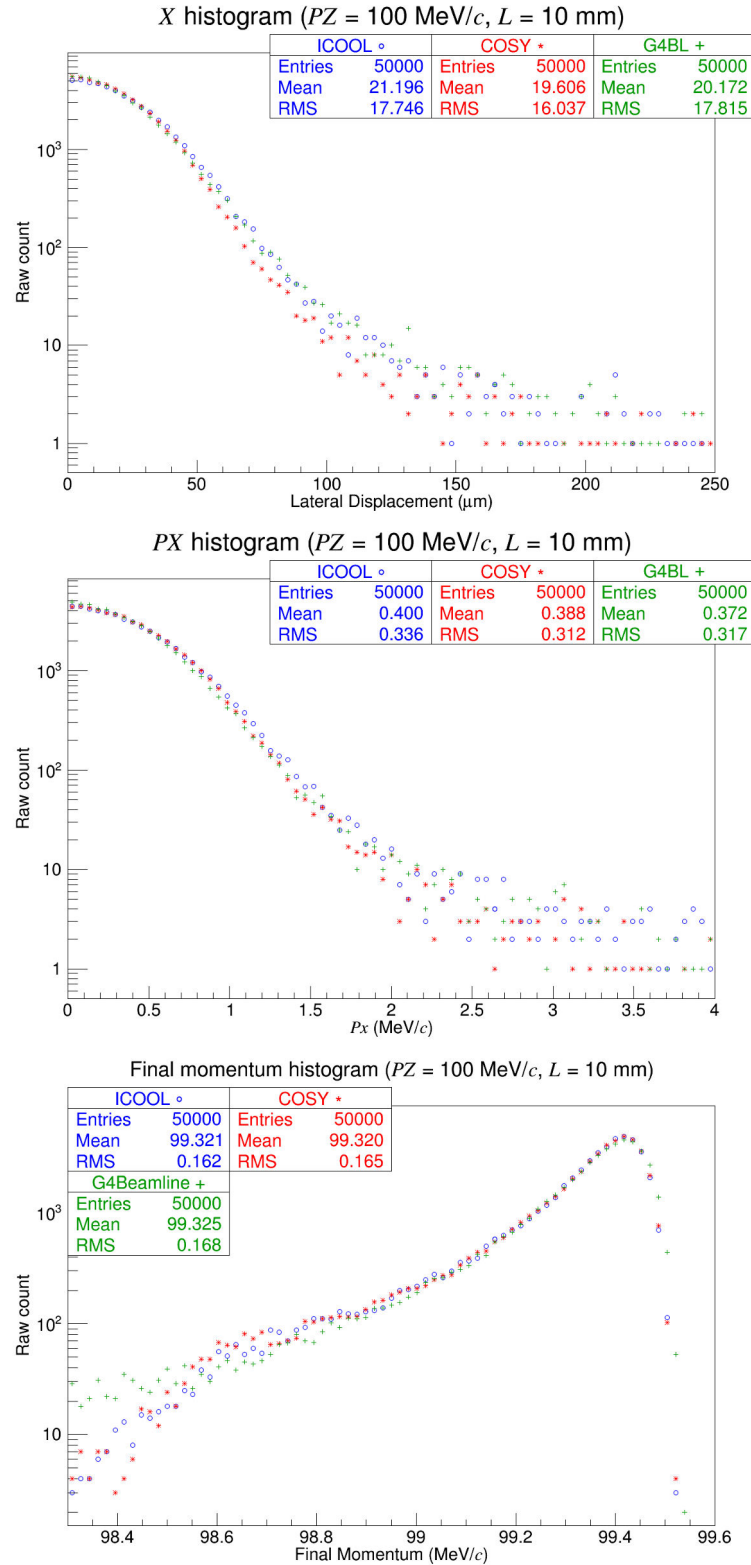


Figure 5.2. Muons of momentum  $100 \text{ MeV}/c$  through  $10 \text{ mm}$  liquid hydrogen.

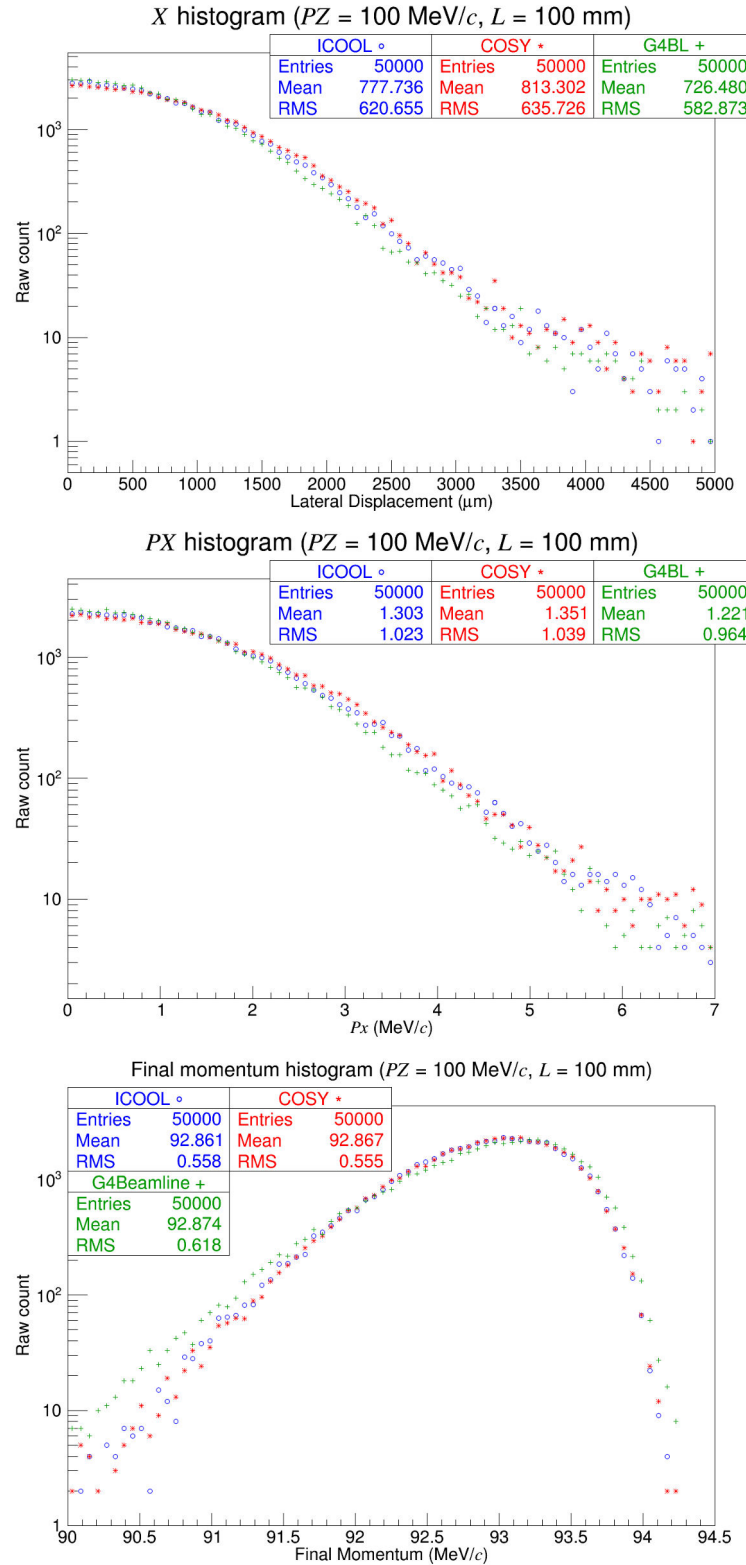


Figure 5.3. Muons of momentum  $100 \text{ MeV}/c$  through  $100 \text{ mm}$  liquid hydrogen.

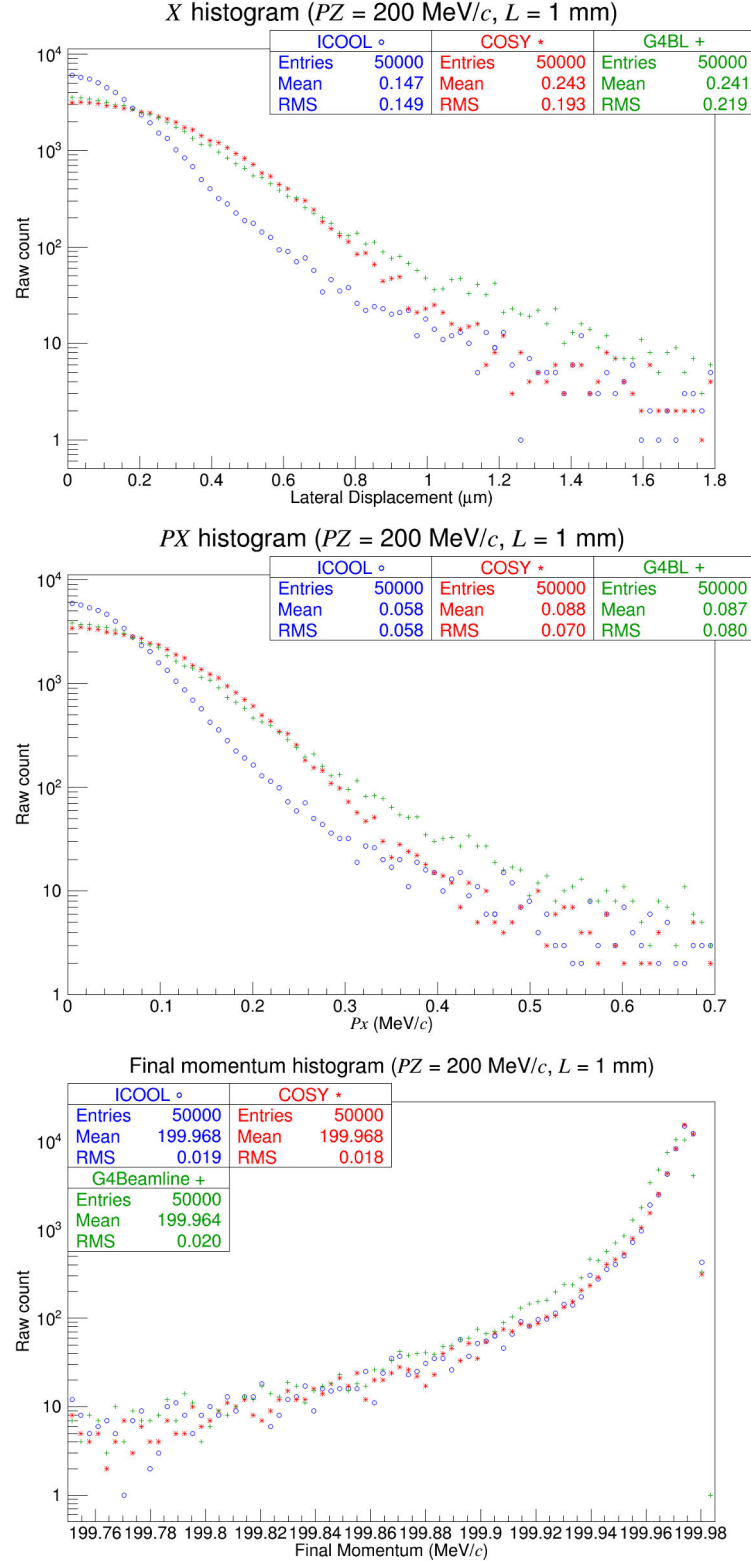


Figure 5.4. Muons of momentum  $100 \text{ MeV}/c$  through  $1 \text{ mm}$  liquid hydrogen. Observe that for the  $x$  and  $p_x$  histograms, COSY and G4beamline follow a Gaussian-like peak whereas ICOOL follows a Fano peak.

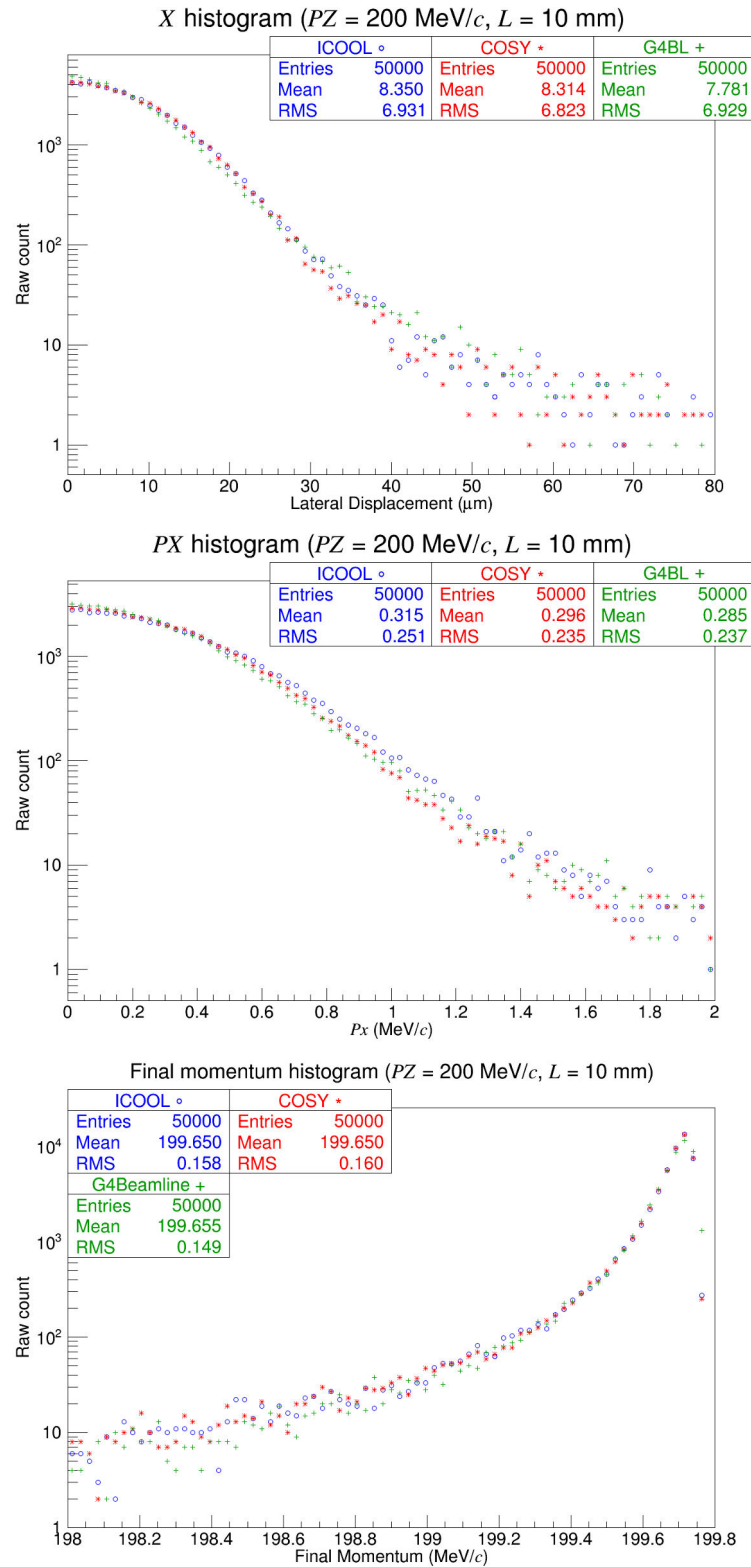


Figure 5.5. Muons of momentum  $200 \text{ MeV}/c$  through  $10 \text{ mm}$  liquid hydrogen.

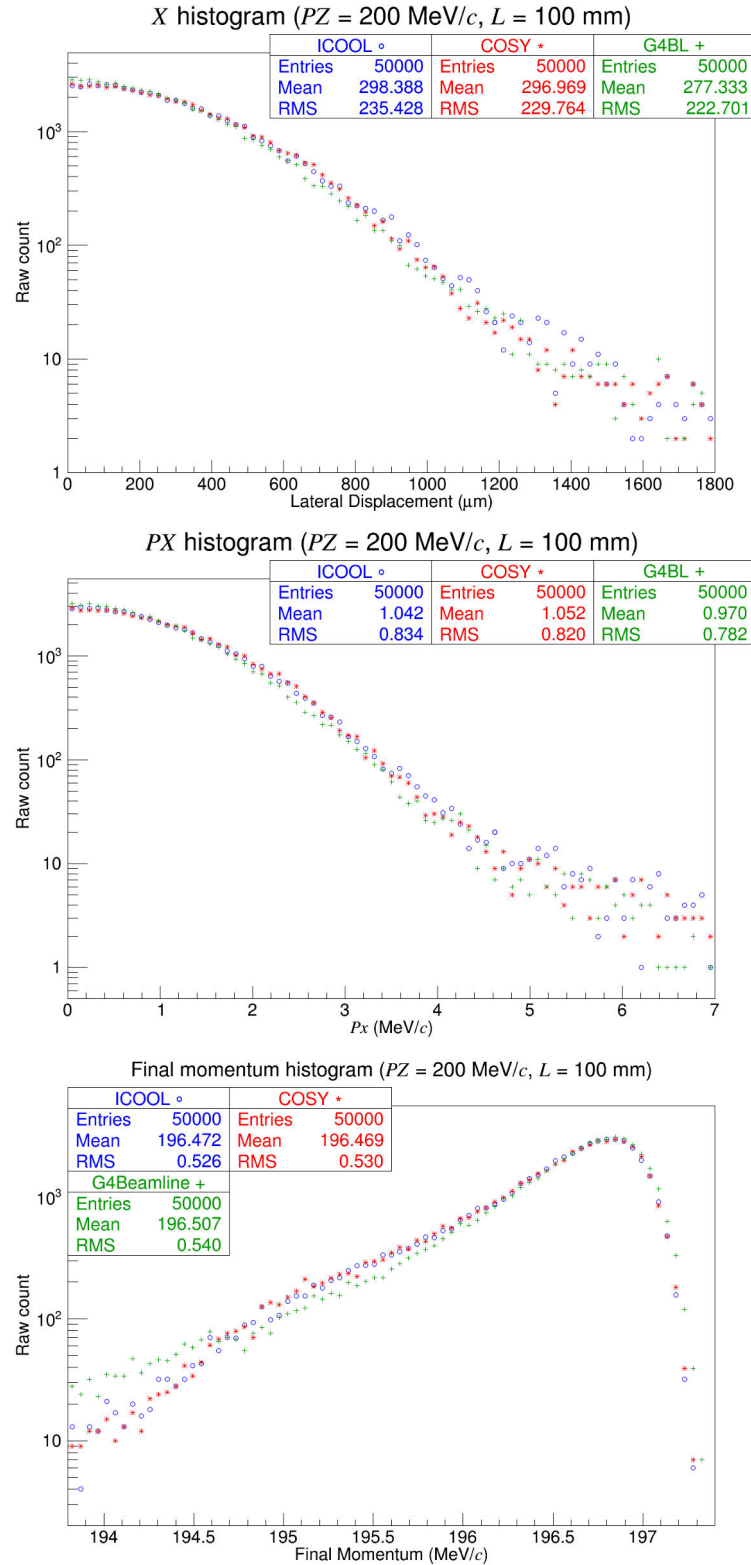


Figure 5.6. Muons of momentum  $200 \text{ MeV}/c$  through  $100 \text{ mm}$  liquid hydrogen.

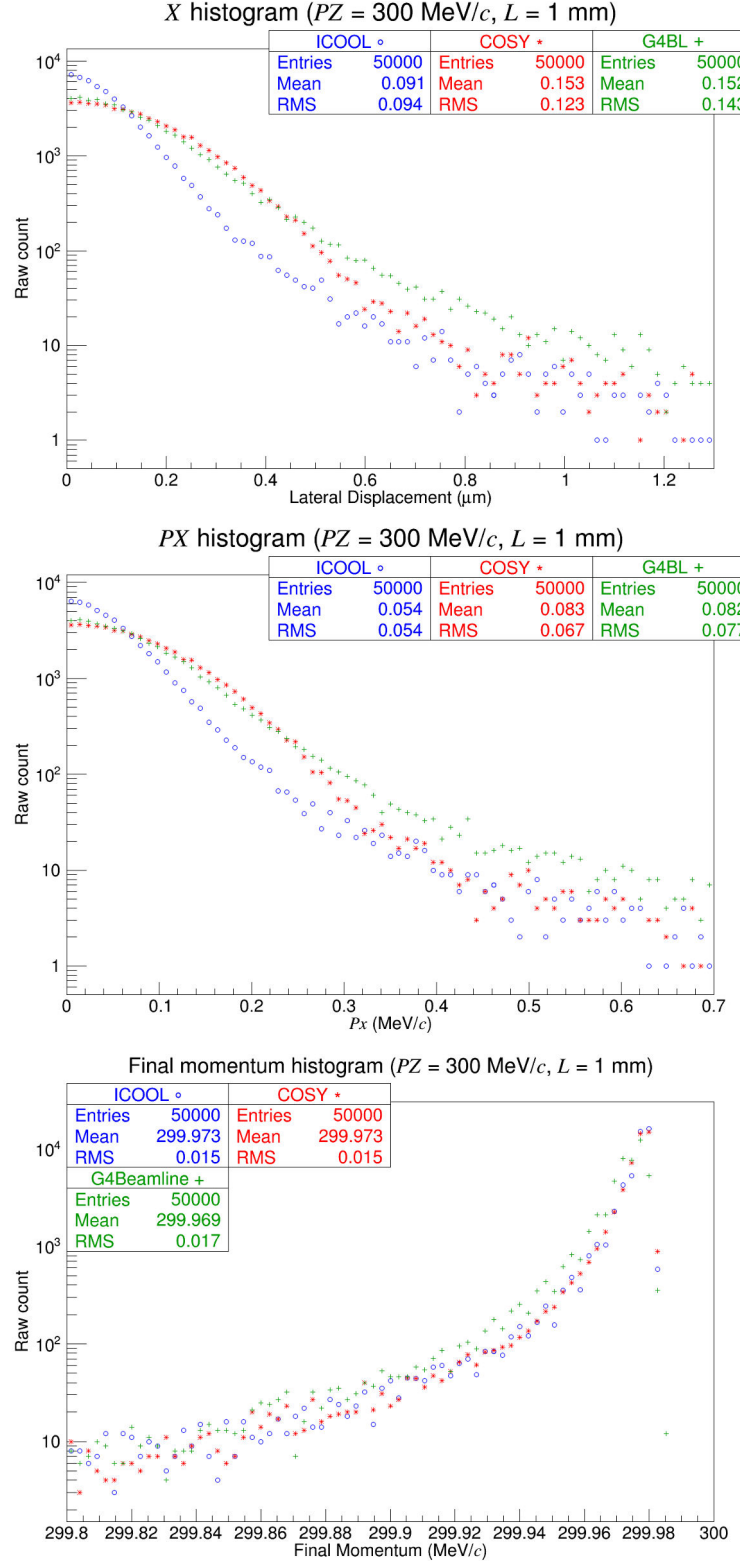


Figure 5.7. Muons of momentum 100 MeV/ $c$  through 1 mm liquid hydrogen. Observe that for the  $x$  and  $p_x$  histograms, COSY and G4beamline follow a Gaussian-like peak whereas ICOOL follows a Fano peak.

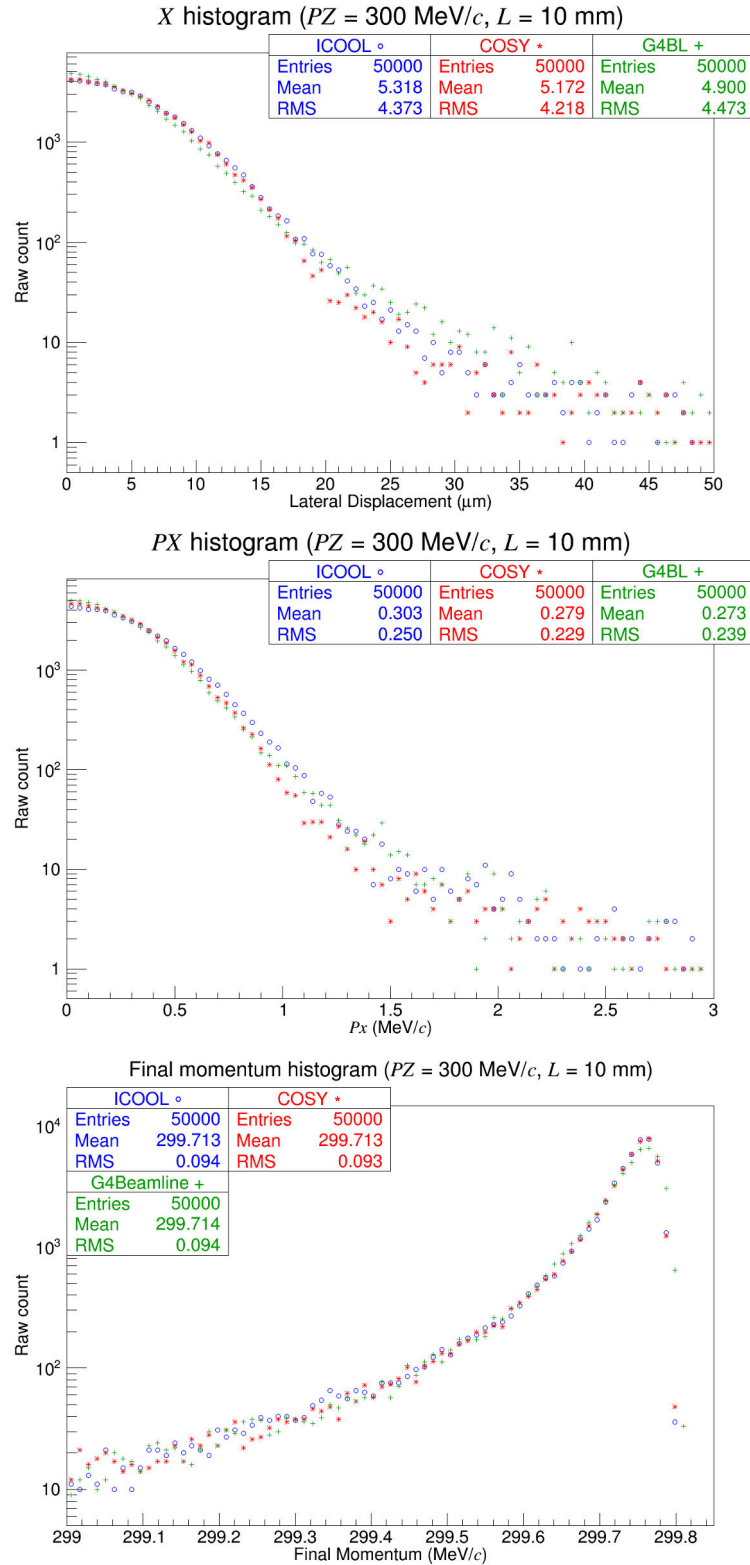


Figure 5.8. Muons of momentum  $300 \text{ MeV}/c$  through  $10 \text{ mm}$  liquid hydrogen.

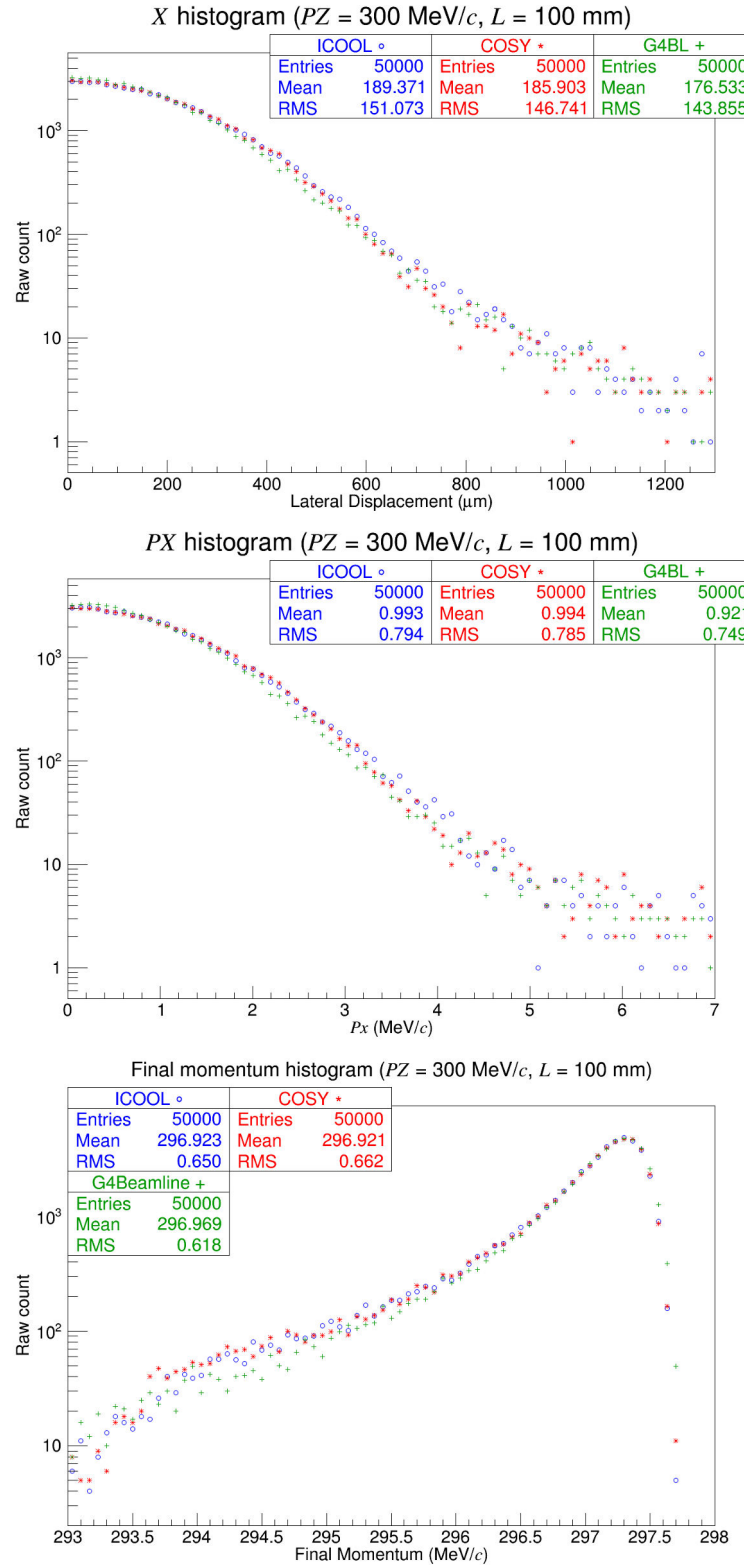


Figure 5.9. Muons of momentum  $300 \text{ MeV}/c$  through  $100 \text{ mm}$  liquid hydrogen.

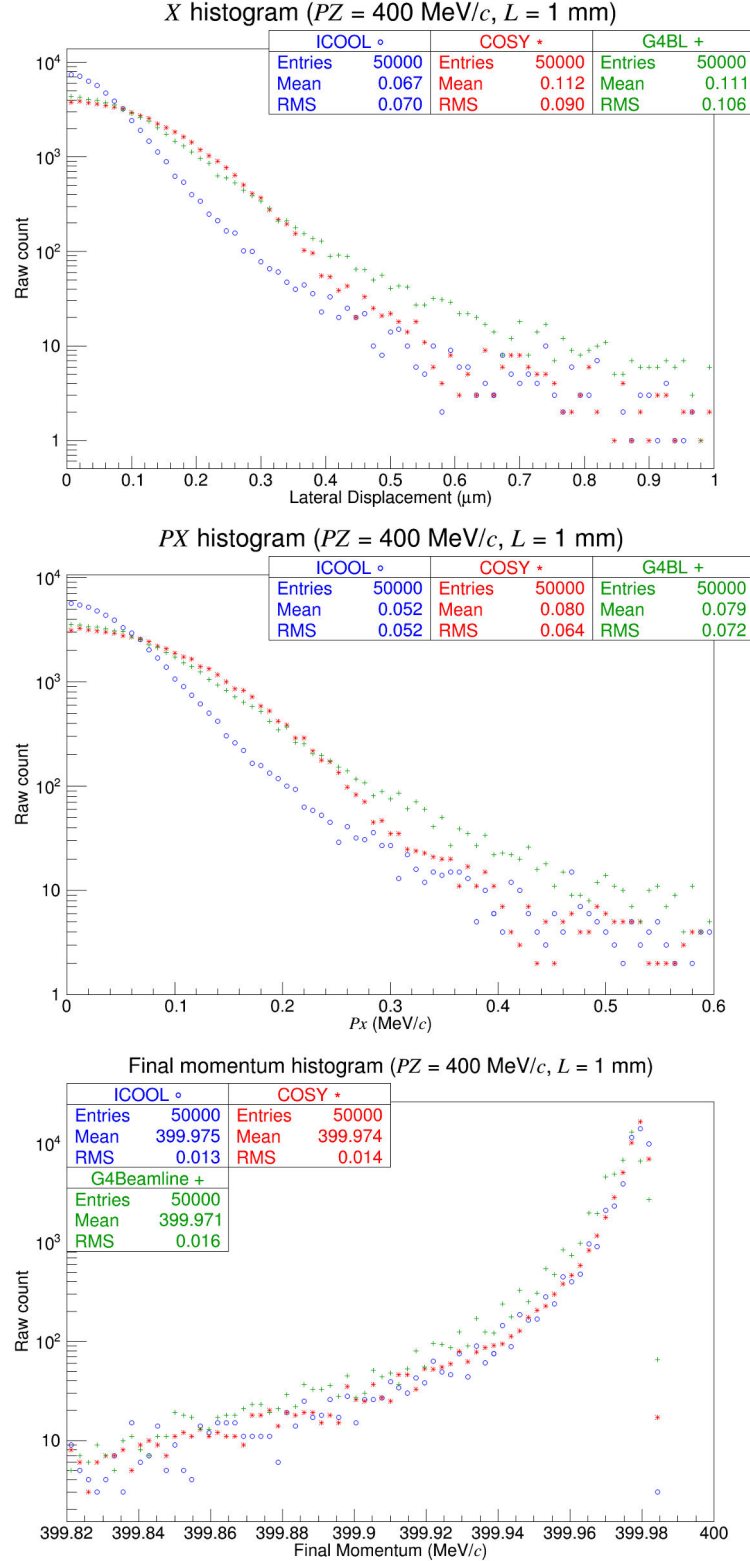


Figure 5.10. Muons of momentum  $100 \text{ MeV}/c$  through 1 mm liquid hydrogen. Observe that for the  $x$  and  $p_x$  histograms, COSY and G4beamline follow a Gaussian-like peak whereas ICOOL follows a Fano peak.

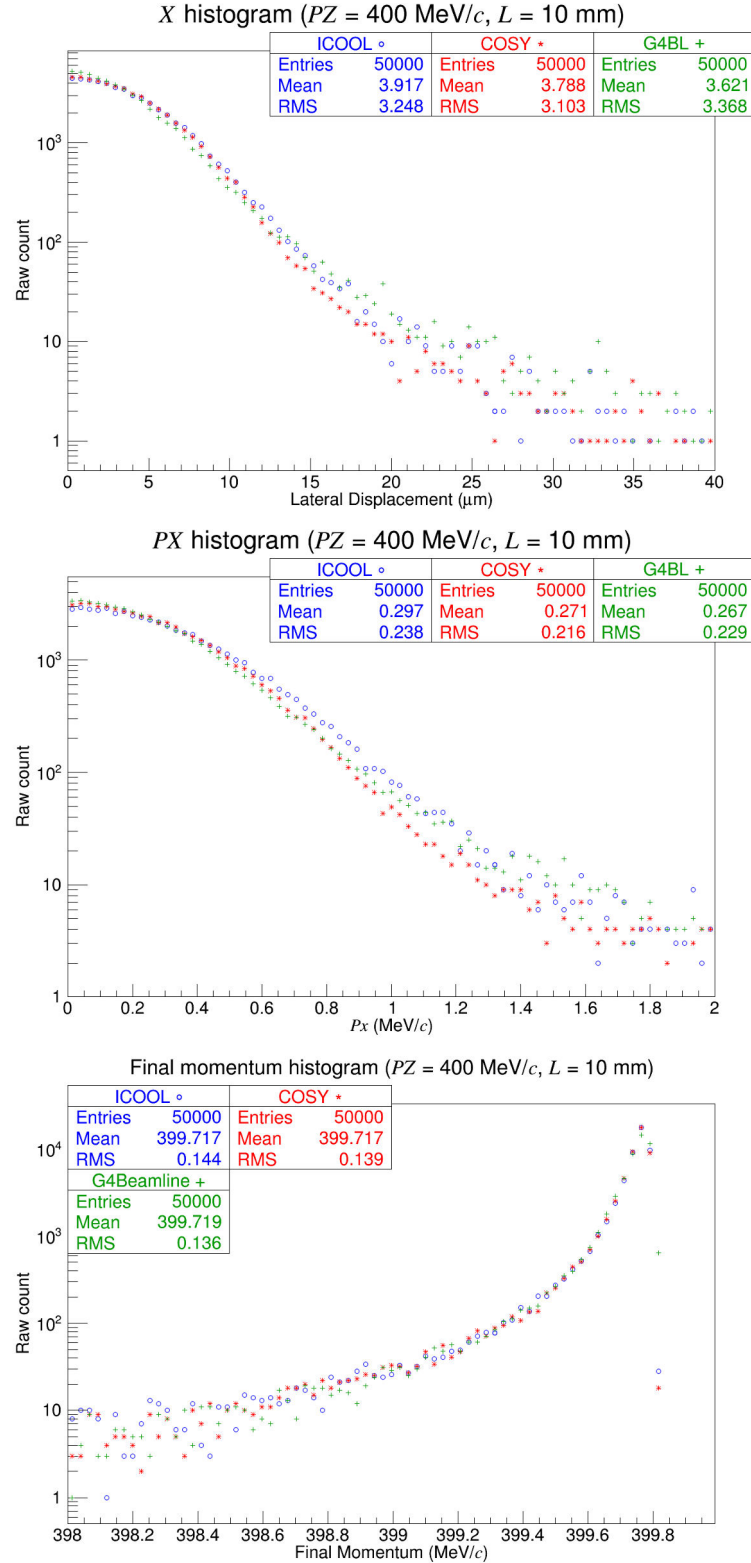


Figure 5.11. Muons of momentum  $400 \text{ MeV}/c$  through  $10 \text{ mm}$  liquid hydrogen.

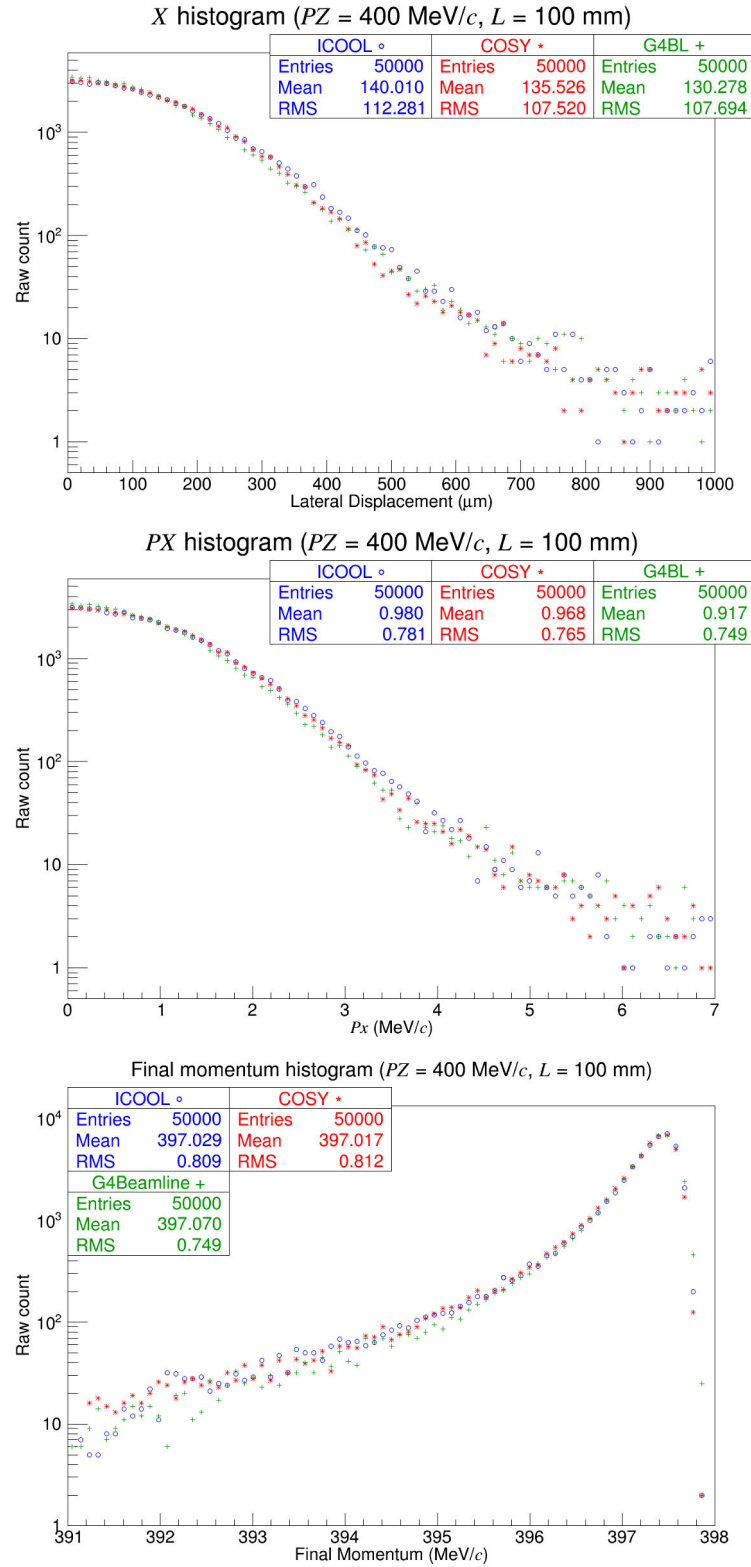


Figure 5.12. Muons of momentum  $400 \text{ MeV}/c$  through  $100 \text{ mm}$  liquid hydrogen.

For the 1 mm figures (Figures 5.1, 5.4, 5.7, and 5.10) there is much disagreement among the codes' transverse momentum distributions. Since the transverse momentum and transverse position coordinates are related, there is also disagreement among the transverse position distributions. This is likely because the default ICOOL scattering model uses a Fano peak with a Rutherford tail whereas both COSY and G4beamline use a Gaussian peak. It can be seen in, e.g., Figure 5.1 that COSY, like G4beamline, uses the Gaussian model for the peak but, like ICOOL, then switches to a Rutherford tail.

For the 10 mm figures (Figures 5.2, 5.5, 5.8, and 5.11), both  $x$  and  $p_x$  distributions agree well. For COSY, the tail of the distribution falls off slightly faster after approximately 1 MeV/ $c$ .

For the final momentum plots, ICOOL and COSY agree quite well. This is not surprising since both codes use Landau theory to describe the energy loss distribution. G4beamline occasionally disagrees, which is expected since G4beamline uses a different model. An example of this can be seen in Figure 5.4. However, given the scale of the horizontal axis this disagreement is much smaller than it initially appears.

## 5.2 Validation

The new COSY routines were also compared to the Muon Scattering Experiment [31], often referred to as MuScat. This experiment measured the scattering of a beam of collimated muons through seven materials. To emulate this, pencil beams with momentum  $P = 172$  MeV/ $c$  were created in COSY, G4beamline, and ICOOL. The pencil beam consisted of  $5 \times 10^6$  particles and was propagated through 109 mm of liquid hydrogen, 159 mm of liquid hydrogen, and 3.73 mm of beryllium. Liquid hydrogen was chosen to represent muons through long absorbers of low- $Z$  materials.

Beryllium, on the other hand, was chosen to represent muons through much thinner and denser media. COSY took a single step through the absorbers while G4BL took a step size of 1 mm. The data points were normalized to the total probability (via Simpson's rule). The probability per radian was then found by dividing the probability of the data point by its angle. The results are shown below.

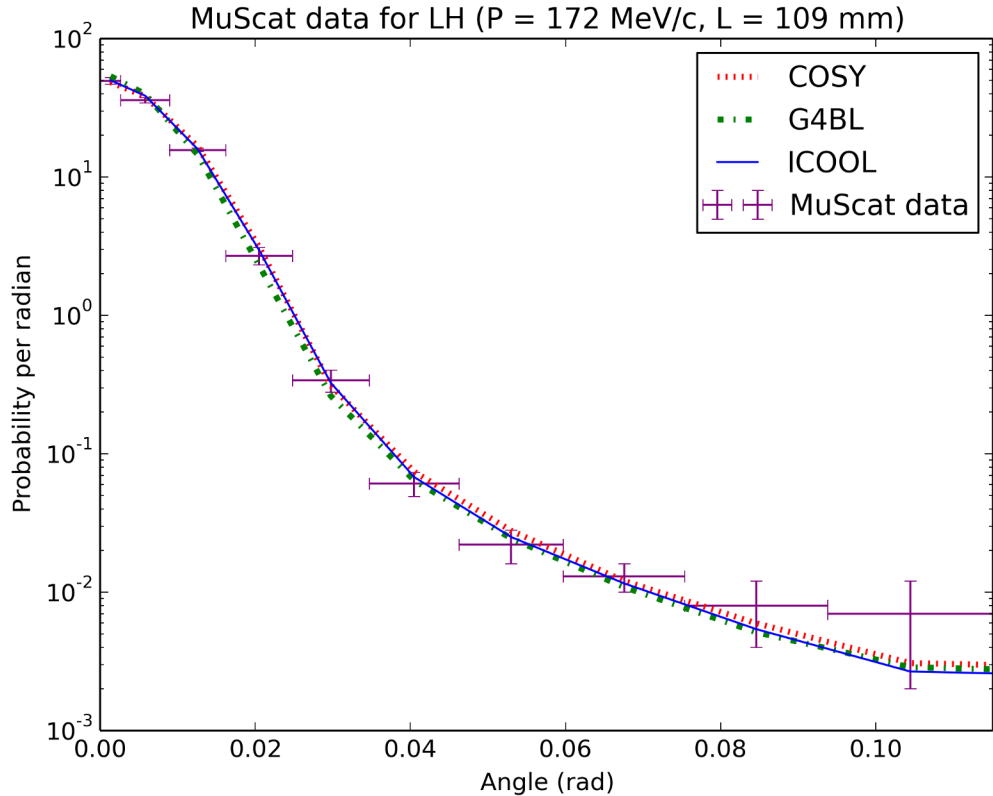


Figure 5.13. MuScat angular scattering results for 109 mm of liquid hydrogen compared against COSY (red), G4BL (green), and ICOOL (blue).

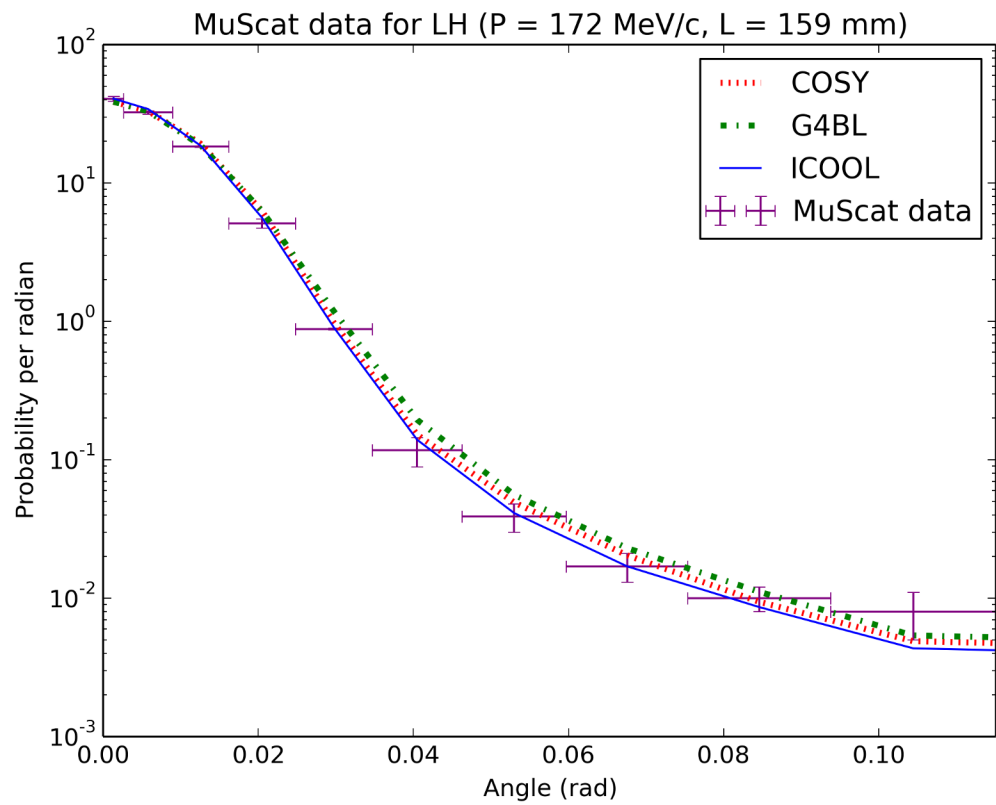


Figure 5.14. MuScat angular scattering results for 159 mm of liquid hydrogen compared against COSY (red), G4BL (green), and ICOOL (blue).

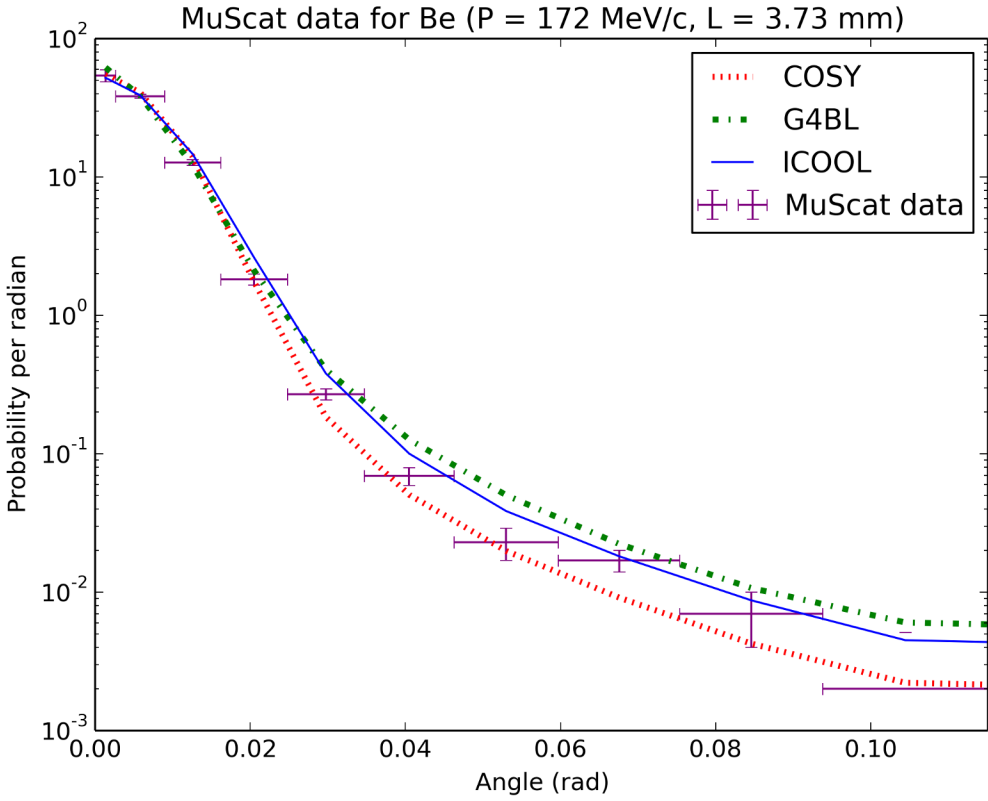


Figure 5.15. MuScat angular scattering results for 3.73 mm of beryllium compared against COSY (red), G4BL (green), and ICOOL (blue).

In the liquid hydrogen cases, COSY appears to match both G4beamline and ICOOL very well, as well as the MuScat data points. ICOOL appears to have a sharper peak than either COSY or G4beamline, which can be more easily seen in the 159 mm liquid hydrogen case than in the 109 mm case. In the case of beryllium, COSY matches the MuScat points slightly better than G4beamline and ICOOL, particularly for the two data points between 0.04 and 0.06 radians.

### 5.3 The Muon Ionization Cooling Experiment

This section introduces the Muon Ionization Cooling Experiment (MICE, [33]), a practical application for the new absorber routines in COSY. The results of the

MICE simulations in ICOOL, G4beamline, and COSY are examined, showing good agreement.

**5.3.1 Introduction to MICE.** The Muon Ionization Cooling Experiment (MICE) [33]) is an experiment currently in progress at the Rutherford Appleton Laboratory in Oxfordshire, U.K. Its goal is to show a proof-of-principle demonstration of muon ionization cooling. The MICE Step IV configuration is explored in this work. The Step IV cell includes 12 magnetic coils positioned symmetrically around a flat absorber. Figure 5.16 shows a schematic of this lattice with 350 mm of liquid hydrogen as the absorber.

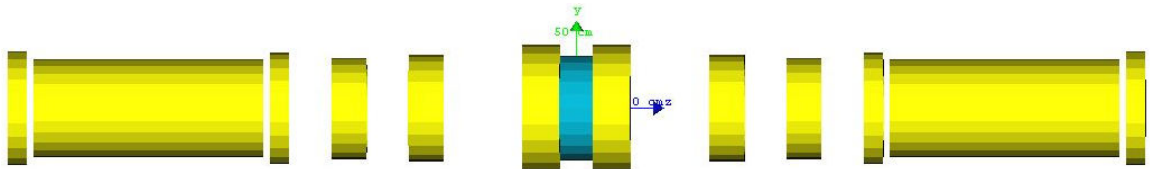


Figure 5.16. MICE Step IV cell. Magnetic coils are shown in yellow and the absorber is shown in blue. The green and blue axes are the  $y$  and  $z$  axes, here drawn to scale as 500 mm each. The aperture (invisible for display purposes) is 300 mm. Image rendered via G4beamline [19].

**5.3.2 Results of the MICE Simulation.**  $10^6$  muons were simulated through the cell in Figure 5.16. The coil parameters may be found in Table 5.1. The absorber was a 350 mm cylindrical block<sup>10</sup> of liquid hydrogen centered at  $z = 0$ . The aperture was set to 300 mm. Note that other materials such as safety windows were not accounted for in this simulation. The decay process was disabled in all simulation codes. The beam started at  $-2.45105$  m and ended at 2.450 m. The initial distribution was Gaussian with parameters summarized in Table 5.2.

---

<sup>10</sup>The cylindrical block geometry is an approximation. It should be noted that a real absorber has a more complicated geometry since it is shaped with curved windows. However, since we are using the same simple geometry in each code, the comparison is valid.

Table 5.1. MICE Step IV coil parameters corresponding to Figure 5.16. Here, the coils are in the so-called “flip” mode, where the coil currents downstream have the opposite sign of the coils upstream.

Name	$z$ position mm	Length mm	Inner radius mm	Outer radius mm	Current density A/mm <sup>2</sup>
End2	±3200.28	110.642	258	325.783	±126
Center	±2450.275	1314.3	258	280.125	±148
End1	±1700.29	110.642	258	318.905	±133
Match2	±1300.29	199.492	258	288.925	±132
Match1	±860.645	201.268	258	304.165	±133
Focus	±202.2	213.3	267.6	361.9	±104

Table 5.2. MICE Step IV initial distribution Gaussian parameters.

Parameter	Mean	Standard deviation
$x$ (mm)	0	32
$y$ (mm)	0	32
$z$ (mm)	0	0
$p_x$ (MeV/c)	0	20
$p_y$ (MeV/c)	0	20
$p_z$ (MeV/c)	200	30

While the selection of order and step size is detailed in the next section, it was found that a 5th order simulation was sufficient for COSY. Through the coil-only portion of the simulation, 50 steps were taken on each side of the absorber (or roughly a step size of 46 mm both upstream and downstream). The particles were tracked through the succession of transfer maps corresponding to individual steps. It was noted that for the coil-only section, a single transfer map was not sufficient even at the 9th order. This is due to the relatively large phase space volume of the beam and the complexity of the magnetic field. Through the absorber-coil region ( $-350/2$  mm to  $350/2$  mm), it was found that a 1st order map with 5 steps was sufficient. This is due to the transverse phase space of the beam passing through a focal point and the magnetic field passing through the point of symmetry.

Compounding the map without propagating the beam also gave poor results. When one takes the composition of two  $n^{th}$  order transfer maps, a transfer map of order  $n \times n$  is the result. For example, the first step in the MICE simulation would yield a 5th order transfer map. Taking the second step would give a new transfer map of order  $5 \times 5 = 25$ . However, since COSY is operating in the 5th order mode, the new transfer map would not be 25th order, but rather it would be truncated to a 5th order map. For this reason, the particles were propagated through the momentary transfer map after each step in the simulation.

The magnetic field in G4beamline was created using the `coil` and `solenoid` commands. The field was then exported to a file using the `printfield` command to a file. The field map file was read by both G4beamline (which used the `fieldmap` command) and ICOOL (which used the `GRID` command operating in `G43D` mode).

The results of the simulation represented by Figure 5.16 can be seen in Figures 5.17 through 5.19. It can be seen that all three codes agree to within 1%.

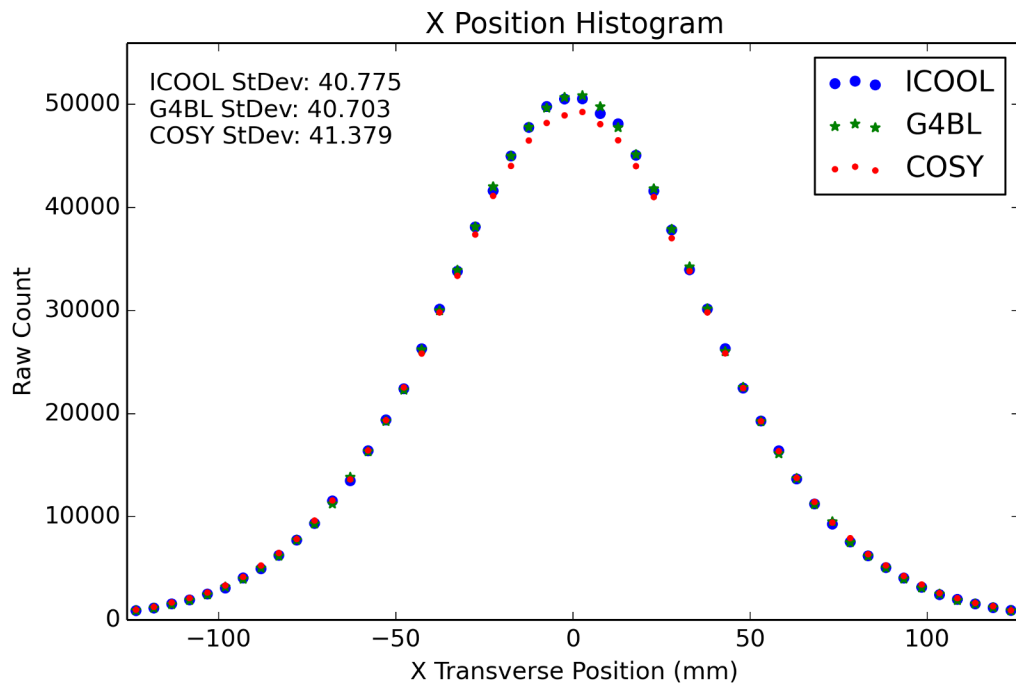


Figure 5.17. MICE Step IV  $x$  position results for 350 mm of liquid hydrogen.

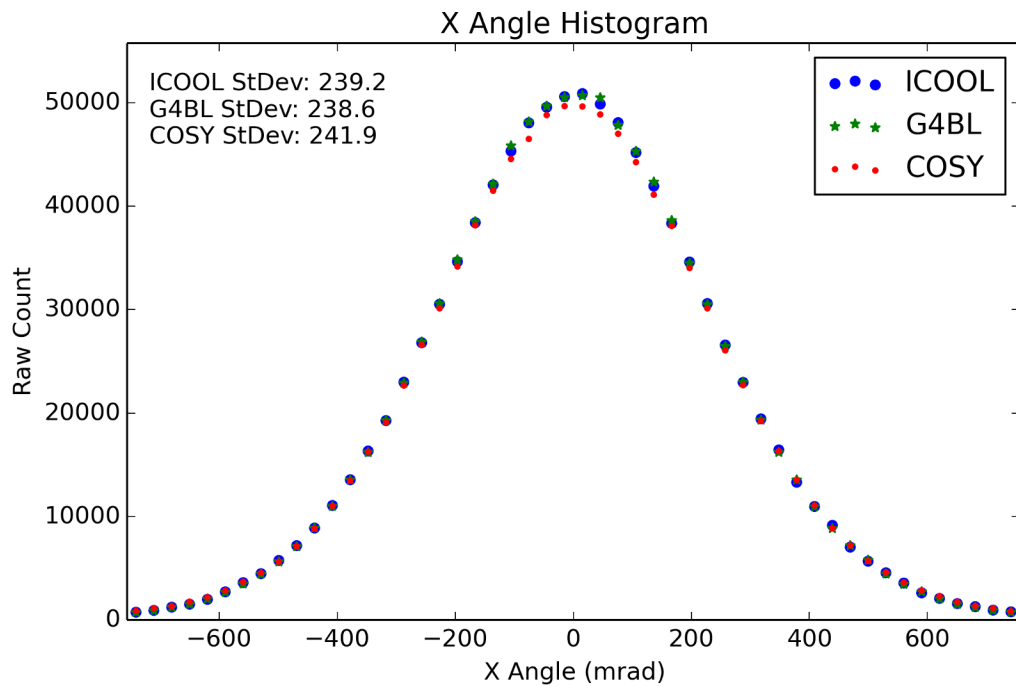


Figure 5.18. MICE Step IV  $x$  angle results for 350 mm of liquid hydrogen.

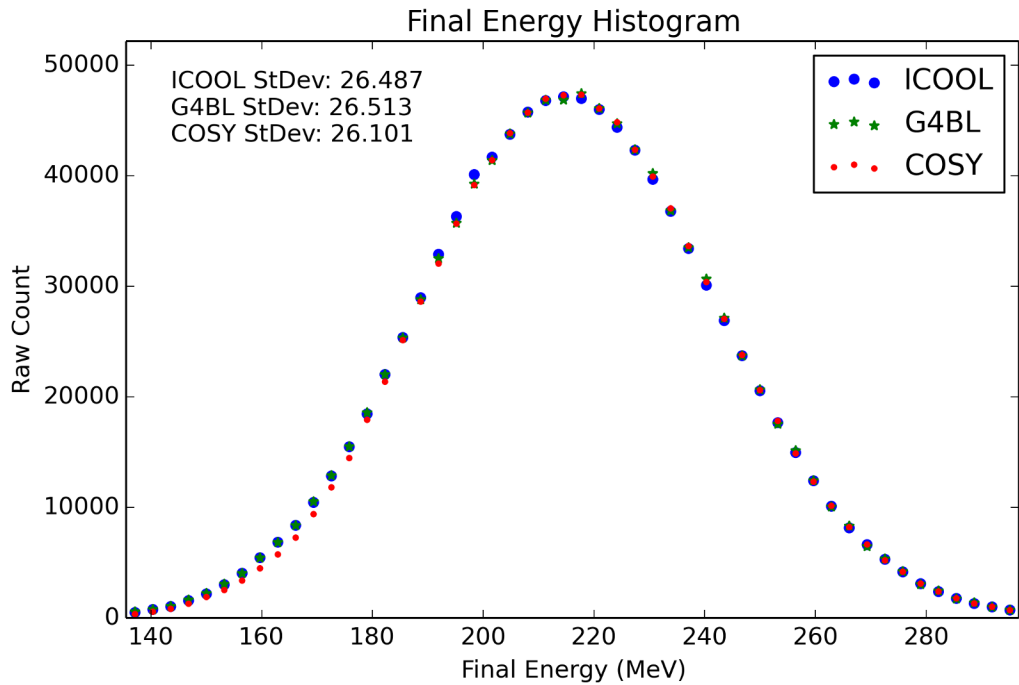


Figure 5.19. MICE Step IV final energy results for 350 mm of liquid hydrogen.

The runtimes of ICOOL, G4beamline, and COSY are listed in Table 5.3. To reiterate, COSY was run at 5th order with 50 steps before the absorber, 5 steps at 1st order inside the absorber, and 50 steps at 5th order after the absorber. Note that the initialization time for G4beamline to create the field maps was 33 seconds. The time it took to create a text file for ICOOL input was 11 seconds. Since G4beamline only has to create the field map once, the initialization time is added to neither the ICOOL nor G4beamline run times in Table 5.3. COSY did not have any initialization time.

As a second test, the MICE configuration in Figure 5.16 was simulated using 65 mm of lithium hydride. Lithium hydride is an attractive material because, unlike liquid hydrogen, it does not require cryogenic conditions, but still maintains a low  $Z$  value. It can be seen from Figures 5.20, 5.21, and 5.22 that 65 mm of lithium hydride has a similar effect on the beam as 350 mm of liquid hydrogen.

Table 5.3. Run times for the MICE Step IV simulation for liquid hydrogen. Note that the G4beamline initialization time was not added to the run time values. G4BL (coils) represents the simulation in G4beamline when the `coil` parameter was used. G4BL (field map) represents the simulation when G4beamline (like ICOOL) read the field map from a file.

Number of particles:	$10^6$	$10^5$	$10^4$	$10^3$
COSY:	367	31	6	4
G4BL (coils):	3973	392	40	6
G4BL (field map):	662	75	15	9
ICOOL (field map):	1091	117	19	9

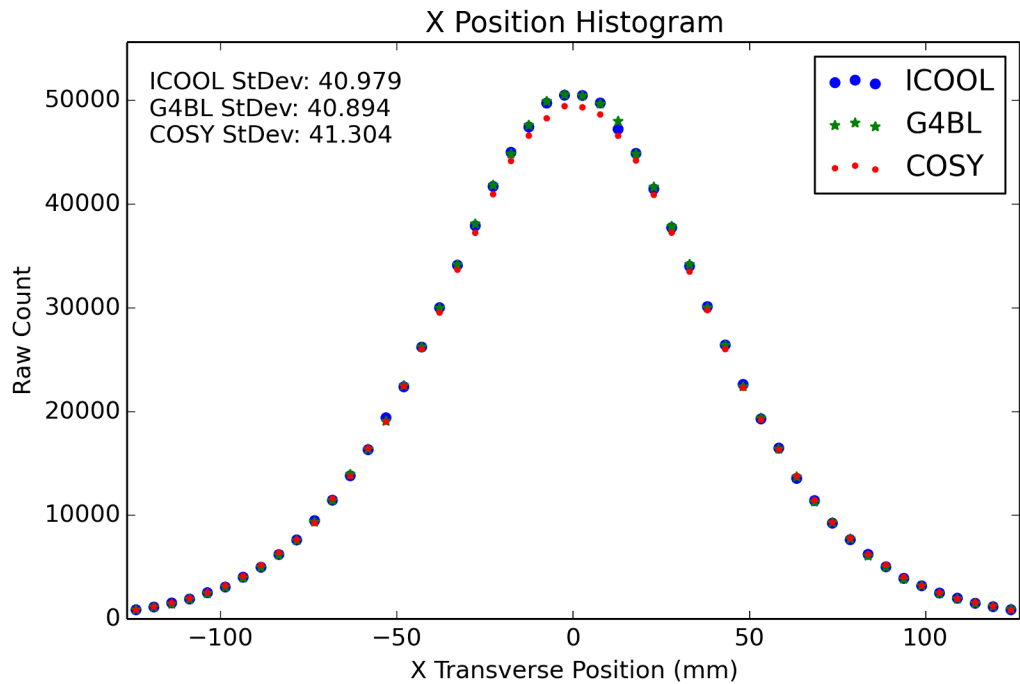


Figure 5.20. MICE Step IV  $x$  position results for 65 mm of lithium hydride.

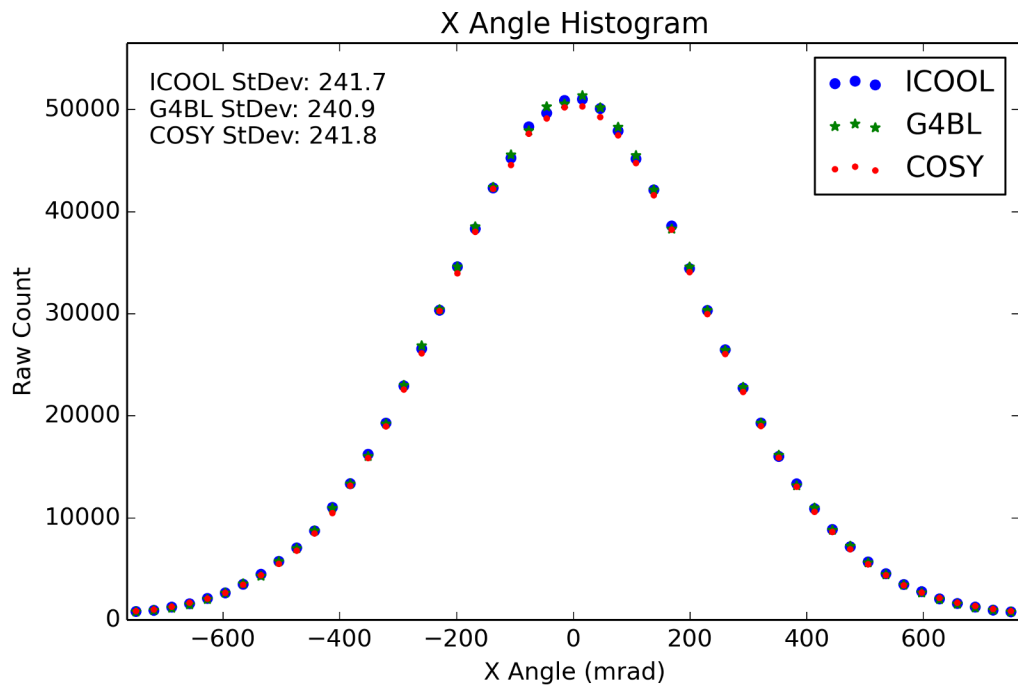


Figure 5.21. MICE Step IV  $x$  angle results for 65 mm of lithium hydride.

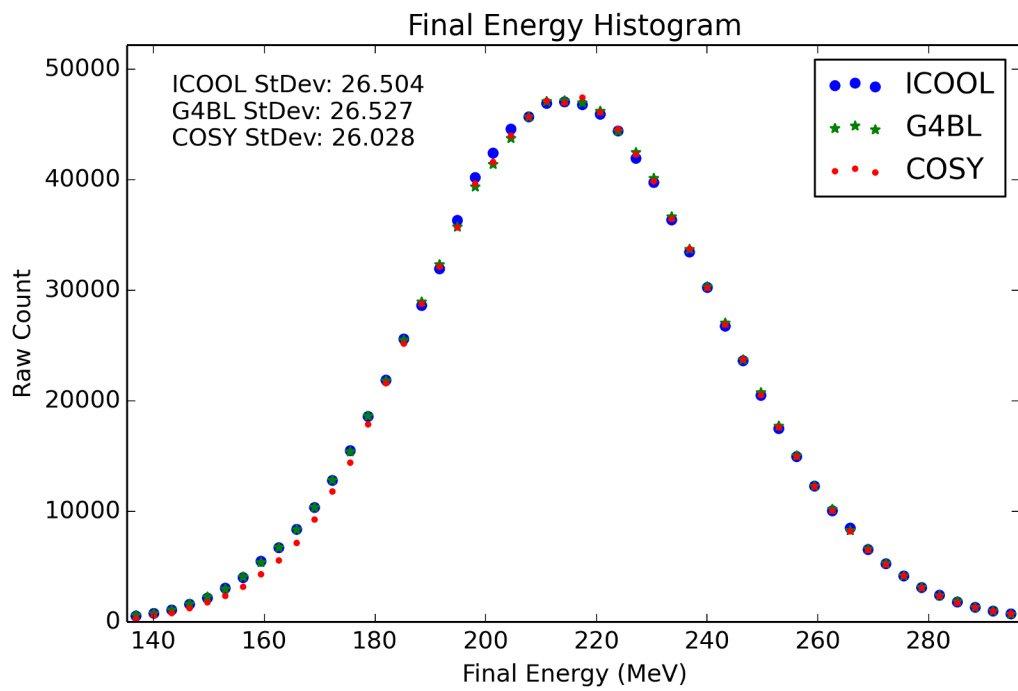


Figure 5.22. MICE Step IV final energy results for 65 mm of lithium hydride.

Table 5.4. First order step size dependence for the absorber-coil section of the MICE Step IV lattice for  $10^5$  muons passing through 350 mm of liquid hydrogen. The transmission was very nearly 100% for all three codes regardless of circumstances. The energy for COSY does not change much with respect to order since the energy loss algorithm does not use a transfer map approach.

	ICOOL (field map)	G4BL (field map)	COSY		
			1 step	5 steps	10 steps
$\sigma_x$ (mm):	50.5	50.4	50.3	50.6	50.7
$\sigma_{\theta_x}$ (mrad):	201.9	201.4	205.7	200.5	199.9
$\sigma_E$ (MeV):	26.7	26.7	26.6	26.6	26.6
Computational time (s):	19	25	4	5	8

**5.3.3 Step Size Effects.** Several step sizes were tested in COSY to ensure optimal efficiency. The results are discussed here.

For the absorber-coil section of the MICE liquid hydrogen lattice ( $-350/2$  mm to  $350/2$  mm), it was found that 5 steps were sufficient to approximate the superposition of the absorber and coils. To study this step size dependence,  $10^5$  particles from the initial distribution found in Table 5.2 were propagated through the 350 mm liquid hydrogen flat absorber. This simulation took the surrounding magnetic fields into account. Table 5.4 shows the effect of changing the step size for the absorber-coil section only.

The discrepancy of COSY w.r.t. G4beamline is  $<1\%$  for all components. Results of the absorber-coil simulation can be seen in Figures 5.23-5.25. There is good agreement between ICOOL, G4beamline, and COSY.

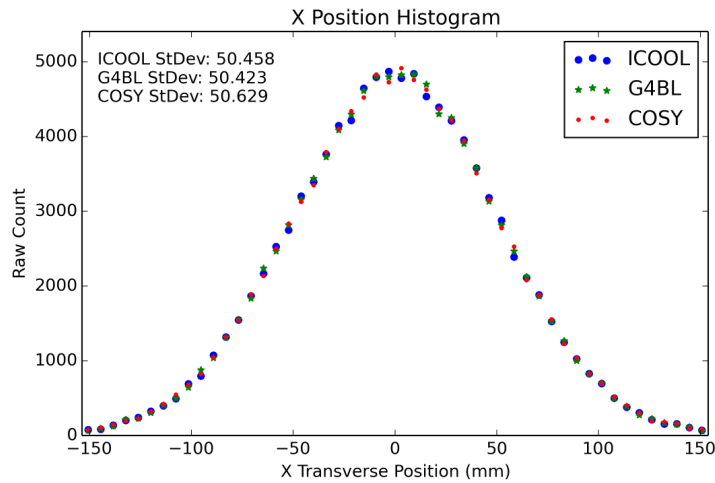


Figure 5.23. Absorber-coil simulation results for  $x$  with  $10^5$  muons and a 5 step propagation.

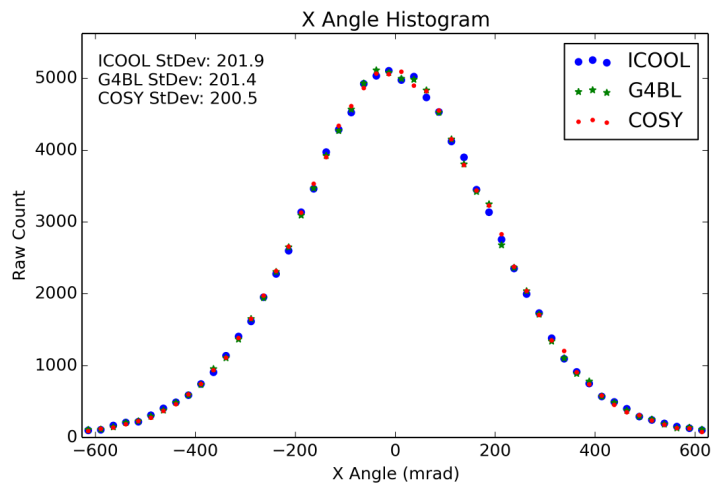


Figure 5.24. Absorber-coil simulation results for  $\theta_x$  with  $10^5$  muons and a 5 step propagation.

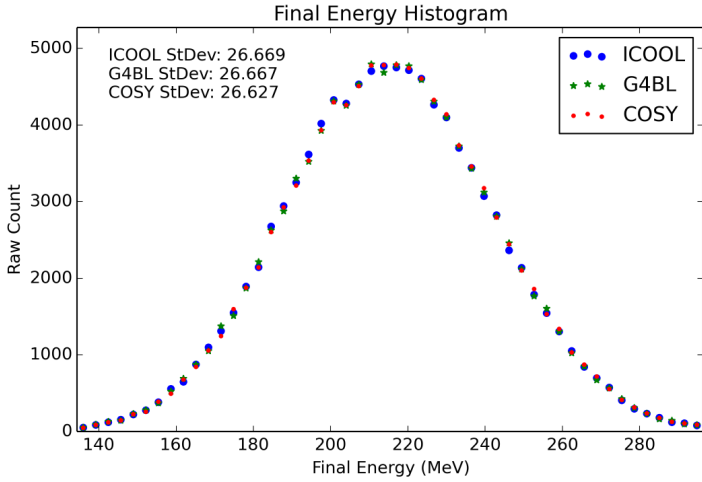


Figure 5.25. Absorber-coil simulation results for the final energy with  $10^5$  muons and a 5 step propagation.

For both the upstream and downstream sections, the entire MICE cell was simulated ( $-2.45105$  m to  $2.450$  m). It was found that COSY operated sufficiently well at order 5 and with 50 steps in the simulation.

To study this step size dependence,  $10^5$  particles from the initial distribution found in Table 5.2 were propagated through the MICE cell. Table 5.5 shows the effect of changing the step size.

For most COSY cases, the discrepancy w.r.t. G4beamline is on the order of 1%. 5th order at 50 steps was selected as “best” because of the increased agreement with both ICOOL and G4beamline when compared to both 3@50 and 5@30 (particularly for the transmission). Moreover, 5@50 gives similar results as 7@100 but with drastically decreased computational time.

Results of the step size study for 5@50 can be seen in Figures 5.26 and 5.27. There is good agreement between ICOOL, G4beamline, and COSY.

Table 5.5. Step size dependence for the MICE Step IV lattice for  $10^5$  muons. The notation for COSY is [order]@[number of steps].

	ICOOL (field map)	G4BL (field map)	COSY [order]@[number of steps]				
			3@50	5@30	5@50	5@100	7@100
$\sigma_x$ (mm):	40.7	40.7	42.5	41.2	41.4	41.4	41.0
$\sigma_{\theta_x}$ (mrad):	240.2	240.2	248.3	239.8	242.1	243.8	241.8
% transmission:	98.5	98.5	99.6	96.8	97.7	98.6	97.9
Comp. time (s):	114	82	12	21	25	43	132

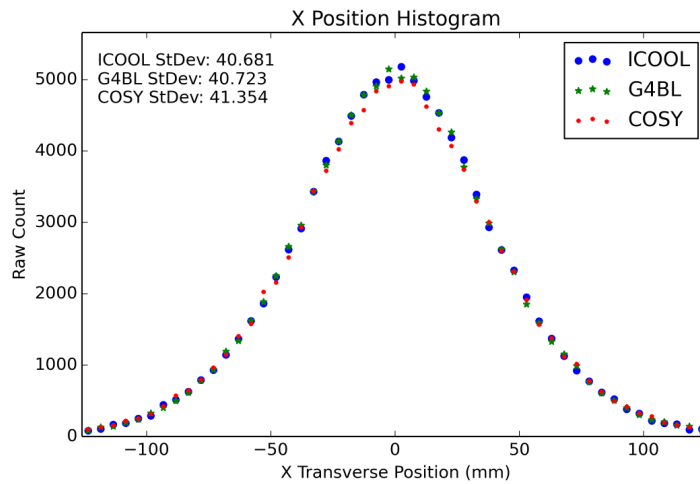


Figure 5.26. MICE simulation results for  $x$  with  $10^5$  muons at 5th order and 50 steps.

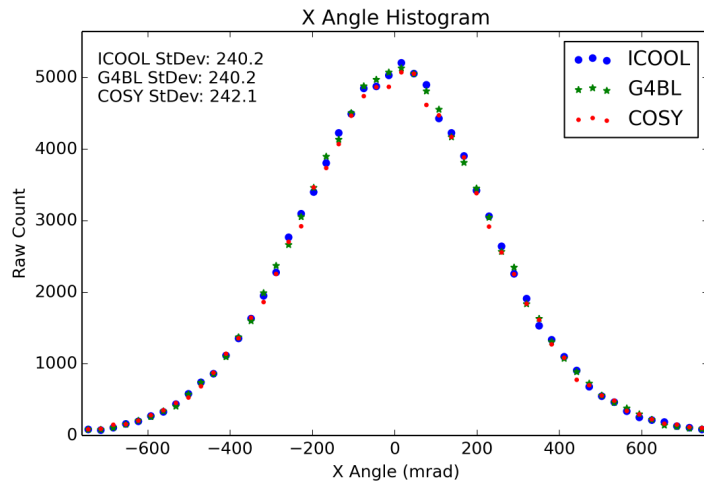


Figure 5.27. MICE simulation results for  $\theta_x$  with  $10^5$  muons at 5th order and 50 steps.

#### 5.4 Summary

In summary, new simulation tools for muon ionization cooling have been added to COSY Infinity for particle-by-particle propagation. The energy straggling, multiple scattering, transverse position, and time-of-flight models were developed from first principles. The algorithms implemented have been modified via empirical fit to MuScat [31] while keeping a reasonable agreement with G4beamline. Fitted with this new software, COSY has simulated one of the current muon ionization cooling efforts, MICE Step IV [33], yielding agreement within 1% of both ICOOL and G4beamline. The code developed in this work is accurate, fast, and user-friendly.

APPENDIX A  
DERIVATION OF TRANSVERSE EMITTANCE

The following is a derivation of Eq. (1.2). First, it is assumed that the beam is an on-axis Gaussian beam. Explicitly, this is to say that the distribution of transverse coordinates is Gaussian and that  $(\langle x \rangle, \langle \theta \rangle) = (0, 0)$ . Recall that emittance is a measure of phase space volume. To measure this volume, it is necessary to use a bivariate Gaussian distribution.

In general, a multivariate Gaussian distribution has the form

$$f_n(X) = \frac{1}{(2\pi)^{n/2}|\mathcal{A}|^{1/2}} \exp\left(-\frac{1}{2}(X - \mu)^T \mathcal{A}^{-1}(X - \mu)\right),$$

where  $X = (x_1, \dots, x_n)$  is a column vector of independent variables,  $\mathcal{A} \in S_{++}^n$  is the covariance matrix, and  $\mu = (\mu_1, \dots, \mu_n)$  is a column vector of average values (which are all zero for this derivation) [34].  $S_{++}^n$  is the space of symmetric positive definite  $n \times n$  matrices. The covariance matrix  $\mathcal{A}$  is a matrix that describes the covariance between variables. That is,  $\mathcal{A}$  describes how much two given variables change with one another.

As an example, consider the univariate Gaussian distribution. The only variable is  $x$  and it changes with itself as  $\langle x \cdot x \rangle = \sigma^2$ . Then

$$X = x, \quad \mathcal{A} = \sigma^2,$$

and

$$\begin{aligned} f_1(X) &= \frac{1}{(2\pi)^{1/2}\sigma} \exp\left(-\frac{1}{2}x \frac{1}{\sigma^2}x\right) \\ &= \frac{1}{\sqrt{2\pi}\sigma} \exp\left(-\frac{x^2}{2\sigma^2}\right). \end{aligned}$$

For the transverse emittance, there are two variables,  $x$  and  $\theta$ . They change with themselves as their respective  $\sigma^2$  and with one another as  $\langle x\theta \rangle$ , and so

$$X = (x, \theta) \quad \mathcal{A} = \begin{pmatrix} \sigma_x^2 & \langle x\theta \rangle \\ \langle x\theta \rangle & \sigma_\theta^2 \end{pmatrix}.$$

The distribution is

$$f_2(X) = \frac{1}{2\pi\sqrt{\sigma_x^2\sigma_\theta^2 - \langle x\theta \rangle^2}} \exp\left(-\frac{x^2\sigma_\theta^2 - 2x\theta\langle x\theta \rangle + \theta^2\sigma_x^2}{2(\sigma_x^2\sigma_\theta^2 - \langle x\theta \rangle^2)}\right).$$

Since the boundary of this function is undefined, it is conventional to use a metric called the Mahalanobis distance [35]. This is a measure of how far some point is away from the center of a multivariate distribution. For a bivariate Gaussian distribution, it is

$$\text{distance} = \frac{1}{2}(X - \mu)^T \mathcal{A}^{-1}(X - \mu) = \frac{x^2\sigma_\theta^2 - 2x\theta\langle x\theta \rangle + \theta^2\sigma_x^2}{2(\sigma_x^2\sigma_\theta^2 - \langle x\theta \rangle^2)}.$$

As it pertains to emittance, the boundary of interest is all  $x$  and  $\theta$  combinations which are unit distance from the central peak. Then

$$1 = \frac{x^2\sigma_\theta^2 - 2x\theta\langle x\theta \rangle + \theta^2\sigma_x^2}{2(\sigma_x^2\sigma_\theta^2 - \langle x\theta \rangle^2)}.$$

Now it is apparent that this equation represents an ellipse in  $x - \theta$  phase space:

$$1 = Ax^2 + 2Bx\theta + C\theta^2, \quad (\text{A.1})$$

with

$$A = \sigma_\theta^2/D,$$

$$B = -\langle x\theta \rangle /D,$$

$$C = \sigma_x^2/D,$$

$$D = 2(\sigma_x^2\sigma_\theta^2 - \langle x\theta \rangle^2).$$

Indeed, an ellipse is exactly what one would expect. Observe from Figure A.1 that the projection of equal heights from a bivariate Gaussian onto the  $x - \theta$  plane is an ellipse. This ellipse can get bigger or smaller depending on the Mahalanobis distance chosen, with the extrema being 0 and  $\infty$ .

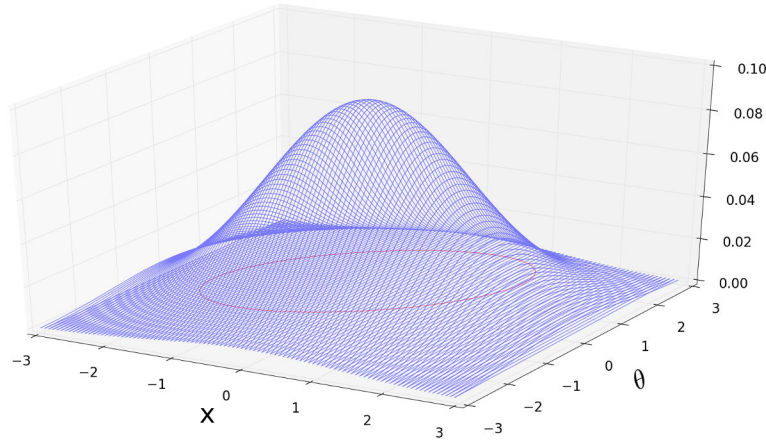


Figure A.1. Sample scatterplot of a bivariate Gaussian (blue). The ellipse (red) is a projection of points of equal heights onto the  $x - \theta$  plane.

The area of this ellipse is the emittance (the volume of phase space) that is desired. For an untilted ellipse, this area is equal to  $\pi$  times the length of the major axis ( $a$ ) times the length of the minor axis ( $b$ ), or  $\text{Area} = \pi ab$ . The goal, then, is to apply a transformation of coordinates to the (potentially) tilted ellipse. This transformation to a new coordinate system  $(x', \theta')$  is a simple rotation such that the major and minor axes of the ellipse are coincident with the  $x'$  and  $\theta'$  axes. Then it is much easier to find the major and minor axis lengths.

Note that Eq. (A.1) can also be represented by

$$1 = \begin{pmatrix} x & \theta \end{pmatrix} \mathcal{B} \begin{pmatrix} x \\ \theta \end{pmatrix}$$

where

$$\mathcal{B} = \begin{pmatrix} A & B \\ B & C \end{pmatrix}.$$

This is a useful representation, since the “normal” form (with the ellipse aligned to the  $x'$  and  $\theta'$  axes) is desired:

$$1 = A'x'^2 + C'\theta'^2, \quad (\text{A.2})$$

or equivalently

$$1 = \begin{pmatrix} & \\ x' & \theta' \end{pmatrix} \mathcal{B}' \begin{pmatrix} x' \\ \theta' \end{pmatrix}$$

with

$$\mathcal{B}' = \begin{pmatrix} A' & 0 \\ 0 & C' \end{pmatrix}.$$

The goal, then, is to diagonalize  $\mathcal{B}$ . The diagonalization may be done via finding the eigenvalues and eigenvectors or by introducing some angle that relates  $x'$  and  $\theta'$  to  $x$  and  $\theta$ . Regardless, the result is

$$\begin{aligned} A' &= \frac{1}{2} \left( A + C + \sqrt{A^2 - 2AC + C^2 + 4B^2} \right) \\ C' &= \frac{1}{2} \left( A + C - \sqrt{A^2 - 2AC + C^2 + 4B^2} \right). \end{aligned}$$

In accordance with Eq. (A.2), the major and minor axis lengths are given by  $1/2\sqrt{A'}$  and  $1/2\sqrt{C'}^{11}$ . Then the area of the ellipse in question is

$$\text{Area} = \pi \frac{1}{2\sqrt{A'}} \frac{1}{2\sqrt{C'}} = \pi \sqrt{\sigma_x^2 \sigma_\theta^2 - \langle x\theta \rangle^2}.$$

For the emittance, the  $\pi$  term is usually absorbed into the units (e.g. millimeter pi radians), and so the emittance is simply

$$\epsilon = \sqrt{\sigma_x^2 \sigma_\theta^2 - \langle x\theta \rangle^2}. \quad (\text{A.3})$$

<sup>11</sup>It may help to recall that the normal form equation for an ellipse may also be represented by  $\frac{x^2}{a^2} + \frac{y^2}{b^2} = 1$ , where  $a$  and  $b$  are the major or minor axis half-lengths.

## APPENDIX B

## DERIVATION OF THE LANDAU ENERGY LOSS DISTRIBUTION

Landau [22] begins the derivation by stipulating that this theory assumes fast particles (“so that the usual ionisation theory may be applied,” here taken as particles whose energy is in the Bethe regime in Figure 1.11). Moreover, the thickness of the absorber should be small enough, so that the energy loss is small compared to the initial energy. Landau defines the weight function  $w(E, u)$  as the probability per unit length of an energy loss  $u$  given the instantaneous total energy  $E$ . For the aforementioned constraints, the weight function may be written simply as  $w(u)$  (since  $E$  is now a constant instead of a variable). Another way of describing this constraint is that the total energy of the particle is roughly constant while traversing the medium.

Let  $f(L, \epsilon)$  be the desired distribution function for the energy loss. This means that the particle loses an amount of energy between  $\epsilon$  and  $\epsilon + d\epsilon$  while traversing an absorber of length  $L$ . Then on one hand

$$\text{change in } f \text{ per unit length} = \frac{\partial f(L, \epsilon)}{\partial L}.$$

On the other hand, the change in  $f$  may also be expressed as the difference of two functions: one at a length  $L$  with possible energy losses between  $\epsilon$  and  $\epsilon + d\epsilon$  and another at length  $L$  and with possible energy losses between  $\epsilon - u$  and  $\epsilon + d\epsilon - u$ , with  $u$  accounting for the infinitesimal change in length. Then

$$\text{change in } f \text{ per unit length} = \left[ \int_0^\infty w(u)f(L, \epsilon - u)du \right] - f(L, \epsilon).$$

Often referred to as the integral transport equation, the two previous definitions of the change in  $f$  per unit length may be combined as

$$\frac{\partial f(L, \epsilon)}{\partial L} = \left[ \int_0^\infty w(u)f(L, \epsilon - u)du \right] - f(L, \epsilon). \quad (\text{B.1})$$

Since  $L$  and  $\epsilon$  are independent and implicit variables, this allows for a Laplace transformation. Take the transformed function with respect to  $\epsilon$  as

$$\phi(p, L) = \int_0^\infty e^{-p\epsilon} f(\epsilon)d\epsilon.$$

(Note that  $p$  is a dummy variable and not the momentum.) Then the inverse transformation gives

$$f(L, \epsilon) = \frac{1}{2\pi i} \int_{K-i\infty}^{K+i\infty} \phi(p, L) e^{p\epsilon} dp, \quad (\text{B.2})$$

where  $K > 0$  is a real constant small enough so that the integral is just to the right of the imaginary axis. This is done in order to avoid a potential singularity at the origin.  $f(L, \epsilon)$  is the desired distribution function, and so is useful later. However, without the form of  $\phi$  it is not useful. The goal then is to find a closed form of  $\phi$ .

Multiplying both sides of Eq. (B.1) by  $e^{-p\epsilon}$  and integrating with respect to  $d\epsilon$  yields

$$\int_0^\infty \frac{\partial f}{\partial L} e^{-p\epsilon} d\epsilon = \int_0^\infty \left[ \int_0^\infty w(u) f(L, \epsilon - u) du \right] e^{-p\epsilon} d\epsilon - \int_0^\infty f(L, \epsilon) e^{-p\epsilon} d\epsilon.$$

On the left side, the operations of partial derivative and integration are commutable, and are therefore switched. On the right side, the first term has commutable integrations and so the order is switched. For the second term, note that the weight function  $w(u)$  is normalized. Consequently, multiplying the second term by the integral of  $w(u)$  over all  $u$  changes nothing. Dropping the implicit  $L$  for now,

$$\begin{aligned} \frac{\partial}{\partial L} \int_0^\infty e^{-p\epsilon} f(\epsilon) d\epsilon &= \int_0^\infty \left[ \int_0^\infty e^{-p\epsilon} f(\epsilon - u) d\epsilon \right] w(u) du - \\ &\quad \int_0^\infty \left[ \int_0^\infty e^{-p\epsilon} f(\epsilon) d\epsilon \right] w(u) du. \end{aligned}$$

The term of the left side and the second term on the right side may be substituted for  $\phi$  directly, while the first term on the right side may be shifted by  $-u$ , resulting in

$$\frac{\partial}{\partial L} \phi(p, L) = \int_0^\infty \left[ \int_{-u}^\infty e^{-p(\epsilon+u)} f(\epsilon) d\epsilon \right] w(u) du - \int_0^\infty \phi(p, L) w(u) du.$$

Now recall that  $f(\epsilon)$  is the desired function for energy loss. Therefore,  $f(\epsilon < 0) = 0$  (i.e., the particle cannot gain energy while traversing a medium), and so

$$\begin{aligned}\frac{\partial}{\partial L} \phi(p, L) &= \int_0^\infty e^{-pu} \left[ \int_0^\infty e^{-p\epsilon} f(\epsilon) d\epsilon \right] w(u) du - \phi(p, L) \int_0^\infty w(u) du \\ &= \phi(p, L) \int_0^\infty w(u) (e^{-pu} - 1) du.\end{aligned}$$

This differential equation is a first-order, undriven normal linear ODE (ordinary differential equation) [36]. Let prime (') denote a partial derivative with respect to  $L$ . Then the strategy to solve this ODE is to define a function  $h(L)$  as

$$h(L) = - \int_0^\infty w(u) (e^{-pu} - 1) du$$

and its antiderivative as

$$H(L) = \int h(L) dL = L \int_0^\infty w(u) (1 - e^{-pu}) du.$$

Then

$$\phi' + \phi \cdot h(L) = 0. \quad (\text{B.3})$$

Since  $(e^{H(L)})' = e^{H(L)} \cdot H'(L) = e^{H(L)} \cdot h(L)$ , it is useful to multiply both sides of the ODE in Eq. (B.3) by  $e^{H(L)}$ , resulting in

$$\phi' \cdot e^{H(L)} + \phi \cdot h(L) \cdot e^{H(L)} = 0,$$

$$(\phi \cdot e^{H(L)})' = 0.$$

Integrating both sides yields

$$\begin{aligned}\phi \cdot e^{H(L)} &= K_1, \\ \phi &= K_1 e^{-H(L)}, \\ \phi(p, L) &= K_1 \exp \left[ -L \int_0^\infty w(u) (1 - e^{-pu}) du \right].\end{aligned}$$

This solution may be put to use if the initial conditions are provided. The first observation is that for  $L = 0$ , the only possible energy loss is zero. Mathematically,

this means that  $f(0, \epsilon) = \delta(\epsilon)$ ; that is, the probability of energy loss is 100% for an energy loss of zero and 0% for all other energy losses. Then the boundary condition on  $\phi$  is

$$\begin{aligned}\phi(p, 0) &= \int_0^\infty \delta(\epsilon) e^{-p\epsilon} d\epsilon \\ \phi(p, 0) &= e^{p \cdot 0} \\ \phi(p, 0) &= 1 = K_1 \exp[0].\end{aligned}$$

Then

$$\phi(p, L) = \exp \left[ -L \int_0^\infty w(u)(1 - e^{-pu}) du \right].$$

Now using Eq. (B.2), the energy loss distribution function  $f$  in terms of  $w(u)$

is

$$f(L, \epsilon) = \frac{1}{2\pi i} \int_{K-i\infty}^{K+i\infty} \exp \left[ p\epsilon - L \int_0^\infty w(u)(1 - e^{-pu}) du \right] dp. \quad (\text{B.4})$$

In principle, this is the general solution to the energy loss profile for a particle traversing some medium. In practice, the only things inhibiting implementation are an algorithm to generate a number from this distribution (which is discussed in Chapter 3) and the function  $w(u)$ . Once  $w(u)$  is obtained, the integral may be found using numerical integration.

Livingston and Bethe [37] derived the form of  $w(u)$  in 1937, and it is

$$w(u) = \frac{\xi}{L} \frac{1}{u^2},$$

where

$$\xi = \frac{2\pi r_e^2 m_e N_A Z \rho L}{\beta^2 A} \quad (\text{B.5})$$

is in units of energy. Here,  $r_e$  is the classical electron radius,  $m_e$  the electron mass,  $N_A$  Avogadro's number,  $Z$  the nuclear charge,  $\rho$  the density of the material,  $L$  the length of the material,  $A$  the nuclear mass, and  $\beta = v/c$  the velocity in units of  $c$ .

Now the form of the integral of  $w(u)(1 - e^{-pu})$  may be seen in Figure B.1. It can be seen that the most important values of  $p$  are those where  $pu \ll 1$  and  $1 \ll pu$ . This is true since  $pu = 1$  vanishes and values around  $pu = 1$  do not significantly contribute to the integral (since both  $pu \rightarrow 0$  and  $pu \rightarrow \infty$  are divergent).

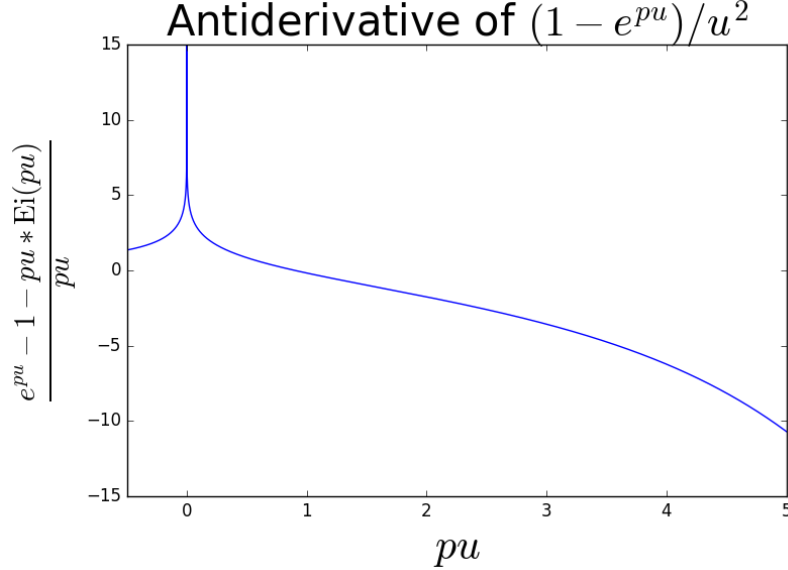


Figure B.1. Plot of  $\int w(u)(1 - e^{-pu}) du$  for various  $pu$ . On the vertical axis is the antiderivative of  $w(u)(1 - e^{-pu})$ , with  $Ei(x) = \int_1^\infty \frac{e^{xt}}{t} dt$  representing the exponential integral.

Since  $u \rightarrow 0$  approaches a singularity, let  $u_{min}$  be the minimum possible energy loss. Now consider a certain energy  $u_1$  such that  $u_{min} \ll u_1$  and  $pu_1 \ll 1$ . Then the integral in the exponent of Eq. (B.4) has the form

$$L \int_{u_{min}}^\infty w(u)(1 - e^{-pu}) du = \xi \left( \int_{u_{min}}^{u_1} \frac{1 - e^{-pu}}{u^2} du + \int_{u_1}^\infty \frac{1 - e^{-pu}}{u^2} du \right).$$

Since the first integral is over the small values, it is possible to write  $1 - e^{pu} \approx 1 - (1 - pu) = pu$ . Then

$$\begin{aligned} \frac{L}{\xi} \int_{u_{min}}^\infty w(u)(1 - e^{-pu}) du &= \int_{u_{min}}^{u_1} \frac{pu}{u^2} du + \int_{u_1}^\infty \frac{1 - e^{-pu}}{u^2} du \\ &= p \int_{u_{min}}^{u_1} \frac{1}{u} du + \int_{u_1}^\infty \frac{1 - e^{-pu}}{u^2} du \\ &= p \ln \frac{u_1}{u_{min}} + \int_{u_1}^\infty \frac{1 - e^{-pu}}{u^2} du. \end{aligned}$$

For the second term, integration by parts gives

$$\frac{L}{\xi} \int_{u_{min}}^{\infty} w(u)(1 - e^{-pu}) du = p \ln \frac{u_1}{u_{min}} + \frac{1 - e^{-pu_1}}{u_1} + p \int_{u_1}^{\infty} \frac{e^{-pu}}{u} du.$$

Recalling that  $u_1$  was chosen such that  $pu_1 \ll 1$ , the exponential in the second term may be approximated as  $e^{-pu_1} \approx 1 - pu_1$ . Then

$$\frac{L}{\xi} \int_0^{\infty} w(u)(1 - e^{-pu}) du = p \ln \frac{u_1}{u_{min}} + p + p \int_{u_1}^{\infty} \frac{e^{-pu}}{u} du. \quad (\text{B.6})$$

The final integral may be evaluated by introducing a new variable,  $\kappa = pu$ :

$$\begin{aligned} \frac{L}{\xi} \int_{u_1}^{\infty} \frac{e^{-pu}}{u} du &= \int_{pu_1}^{\infty} \frac{e^{-\kappa}}{\kappa} d\kappa \\ &= \int_{pu_1}^{\infty} \frac{e^{-\kappa}}{\kappa} d\kappa + \int_{pu_1}^1 \frac{d\kappa}{\kappa} - \int_{pu_1}^1 \frac{d\kappa}{\kappa} \\ &= \int_{pu_1}^1 \frac{e^{-\kappa}}{\kappa} d\kappa + \int_1^{\infty} \frac{e^{-\kappa}}{\kappa} d\kappa + \int_{pu_1}^1 \frac{d\kappa}{\kappa} - \int_{pu_1}^1 \frac{d\kappa}{\kappa} \\ &= \int_{pu_1}^1 \left( \frac{e^{-\kappa}}{\kappa} - \frac{1}{\kappa} \right) d\kappa + \int_1^{\infty} \frac{e^{-\kappa}}{\kappa} d\kappa + \int_{pu_1}^1 \frac{d\kappa}{\kappa} \\ &= \int_{pu_1}^1 \frac{d\kappa}{\kappa} + \left[ \int_{pu_1}^1 \frac{e^{-\kappa} - 1}{\kappa} d\kappa + \int_1^{\infty} \frac{e^{-\kappa}}{\kappa} d\kappa \right]. \end{aligned}$$

The first term is easily evaluated, and the second term in brackets is approximately<sup>12</sup> the negative of Euler's constant,  $-C_{Euler} \approx -0.577$ . Putting this back into Eq. (B.6) yields

$$\begin{aligned} \frac{L}{\xi} \int_{u_{min}}^{\infty} w(u)(1 - e^{-pu}) du &= p \ln \frac{u_1}{u_{min}} + p(1 - C_{Euler} - \ln pu_1) \\ &= p(1 - C_{Euler} - \ln pu_{min}). \end{aligned}$$

Now Eq. (B.4) may be rewritten as

$$\begin{aligned} f(L, \epsilon) &= \frac{1}{2\pi i} \int_{K-i\infty}^{K+i\infty} \exp \left[ p\epsilon - L \int_0^{\infty} w(u)(1 - e^{-pu}) du \right] dp \\ &= \frac{1}{2\pi i} \int_{K-i\infty}^{K+i\infty} \exp [p\epsilon - p\xi(1 - C_{Euler} - \ln pu_{min})] dp. \end{aligned}$$

---

<sup>12</sup>This expression would be exactly  $-C_{Euler}$  if  $pu_1 = 0$ .

If a unitless variable of integration is desired, then  $p \rightarrow p/\xi$ , and

$$\begin{aligned} f(\xi, \epsilon) &= \frac{1}{2\pi i} \int_{K-i\infty}^{K+i\infty} \exp \left[ p \frac{\epsilon}{\xi} - p \left( 1 - C_{Euler} - \ln \frac{pu_{min}}{\xi} \right) \right] dp \\ &= \frac{1}{2\pi i} \int_{K-i\infty}^{K+i\infty} \exp \left[ p \frac{\epsilon}{\xi} - p \left( 1 - C_{Euler} - \ln p - \ln \frac{u_{min}}{\xi} \right) \right] \frac{dp}{\xi} \\ &= \frac{1}{2\pi i \xi} \int_{K-i\infty}^{K+i\infty} \exp \left[ p \frac{\epsilon}{\xi} - p \left( 1 - C_{Euler} - \ln \frac{u_{min}}{\xi} \right) + p \ln p \right] dp, \end{aligned}$$

or simply

$$f(\lambda) = \frac{1}{2\pi i \xi} \int_{K-i\infty}^{K+i\infty} \exp [p \ln p + \lambda p] dp, \quad (\text{B.7})$$

where evidently

$$\lambda = \frac{\epsilon}{\xi} - 1 + C_{Euler} + \ln \frac{\xi}{u_{min}}.$$

However, typically the Landau function is evaluated for the desired *fluctuation about the mean energy loss*, not the energy loss itself. Because of this,  $\lambda$  must be shifted by the mean,  $\langle \epsilon \rangle$ . Furthermore, a relativistic correction of  $-\beta^2$  is added. Finally, it can be reasoned that for ionization to occur, the incident particle must transfer energy to at least one electron. Therefore,  $T_{max}$  (the maximum transferable energy to a single electron from Eq. (2.8)) is a good approximation of the order of magnitude. Hence  $u_{min}$  is replaced with  $T_{max}$ . This results in the final form of the Landau parameter:

$$\lambda \equiv \frac{\epsilon - \langle \epsilon \rangle}{\xi} - (1 - C_{Euler}) - \beta^2 - \ln(\xi/T_{max}). \quad (\text{B.8})$$

APPENDIX C  
DERIVATION OF IMPLEMENTED SCATTERING CROSS SECTION

Electron-muon scattering is a textbook scattering problem following Feynman rules [38]. Similar to both Section 2.1 and Section 2.2, either the collision time of the muon and electron is assumed to be very small compared to the electron orbital time or the electron is initially at rest. The longitudinal ( $z$ ) axis is aligned with the muon velocity such that  $v_x = v_y = 0$ . The reference frame is the lab frame. Please refer to the information in Appendix D for a review on symbols and methods.

To find the (differential) scattering cross section  $d\sigma/d\Omega$ , it is necessary to have both the scattering amplitude  $\mathcal{M}$  (sometimes also called the “matrix element,” although this is a little ambiguous) and the available phase space over which to integrate. However, [38] notes that the integration over the available phase space is a constant, and so only the scattering amplitude is of interest.

Recall that the desired cross section is the Rutherford-like tail of a Gaussian–Rutherford-like piecewise function. The multiplicative constants are ignored since only the forms of the individual Gaussian and Rutherford-like functions are desired. Then

$$\frac{d\sigma}{d\Omega} \propto |\mathcal{M}|^2.$$

To find the scattering amplitude  $\mathcal{M}$ , observe that Figure C.1 represents a muon-electron interaction via exchange of a virtual photon from the electron vertex  $\alpha$  to the muon vertex  $\beta$ . The fermion flow is the path which goes along the directions of the arrows. For example, the first fermion flow which is observed is the muon flow: a muon enters from the left, there is an interaction at the propagator vertex  $\beta$ , and a muon exits from the right. Each muon contributes its spinor. The outgoing muon and incoming muon are adjoints of one another (i.e. if the spinor of  $P_2$  is  $U(P_2)$  then the spinor of  $P_4$  is  $\bar{U}(P_4)$ ). The propagator vertex contributes a factor of  $-ieQ_\mu\gamma^\beta$ . Since matrices compound right-to-left, it is necessary to start at the end of the fermion flow

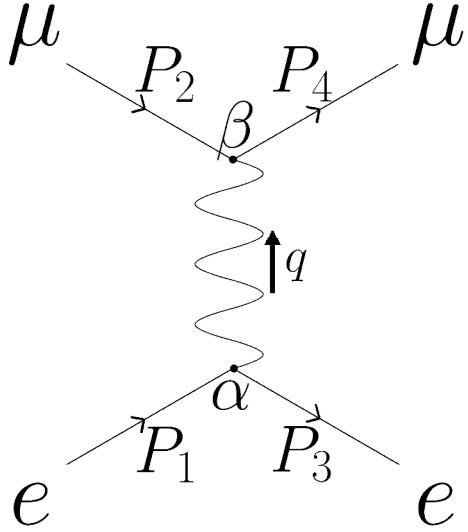


Figure C.1. Feynman diagram for electron-muon scattering.  $P_1$  and  $P_2$  are the incoming four-momenta for the electron and muon and  $P_3$  and  $P_4$  are the outgoing four-momenta.  $q$  represents the four-momentum carried by the virtual photon.

and work backwards. Figure C.2 helps to show that the scattering amplitude is

$$i\mathcal{M} = \bar{U}_4(-ieQ_\mu\gamma^\beta)U_2 \cdot \frac{i}{q^2}(-\eta_{\alpha\beta} + \frac{q_\alpha q_\beta}{q^2}) \cdot \bar{U}_3(-ieQ_e\gamma^\alpha)U_1, \quad (\text{C.1})$$

where  $U_i$  is the spinor for the  $i^{th}$  particle,  $q$  is the momentum carried by the virtual photon,  $\gamma^i$  is the  $\gamma$  matrix corresponding to vertex  $i$  in Figure C.1,  $\alpha, \beta$  denote the vertices in Figure C.1, and  $\eta_{i,j}$  is the  $(i,j)^{th}$  component of the Minkowski metric described in Section F.4.

Ignoring the multiplicative constants, Eq. (C.1) can be rearranged to

$$\mathcal{M} \propto \bar{U}_4\gamma^\beta U_2 * \frac{1}{q^2}(-\eta_{\alpha\beta} + \frac{q_\alpha q_\beta}{q^2}) * \bar{U}_3\gamma^\alpha U_1.$$

Note that the second term in the parenthesis (i.e.  $q_\alpha q_\beta/q^2$ ) vanishes. To see this, observe that when the expression is multiplied out the second term  $q_\alpha q_\beta/q^2$  becomes proportional to  $\bar{U}_4\gamma^\beta U_2 q_\beta$ . By conservation of  $P_\beta$  at vertex  $\beta$ , it can be seen that

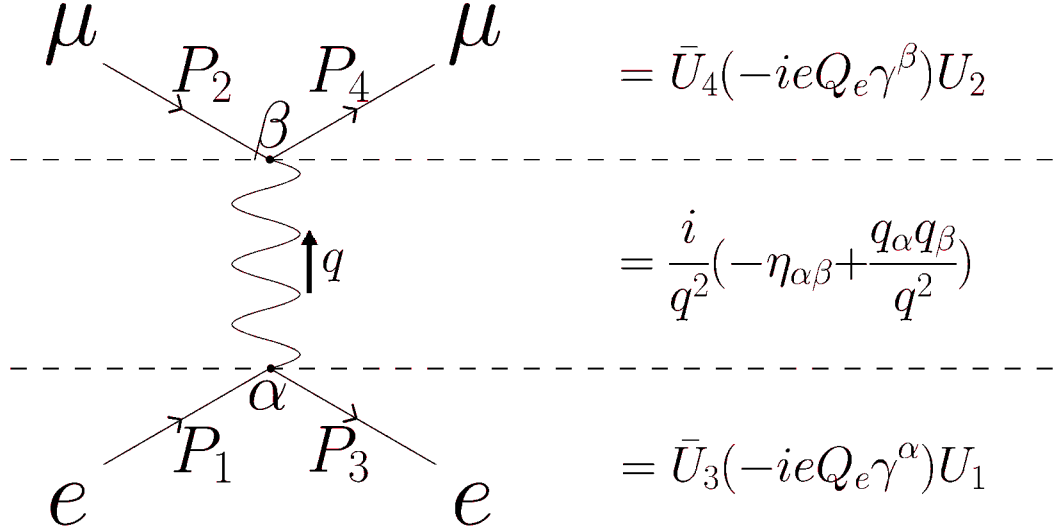


Figure C.2. Mathematical interpretation the three branches of the Feynman diagram in Figure C.1. The top part is the muon flow, the middle is the virtual photon, and the bottom is the electron flow.

$P_{2\beta} + q_\beta = P_{4\beta}$ , or more usefully  $q_\beta = P_{4\beta} - P_{2\beta}$ . Then

$$\begin{aligned} \bar{U}_4 \gamma^\beta U_2 q_\beta &= \bar{U}_4 (\gamma^\beta (P_{4\beta} - P_{2\beta})) U_2 \\ &= \bar{U}_4 (\gamma^\beta P_{4\beta} - \gamma^\beta P_{2\beta}) U_2. \end{aligned}$$

Eq. (D.2) states that  $\gamma^\alpha P_\alpha - m = 0$ , and so

$$\bar{U}_4 \gamma^\beta U_2 q_\beta = \bar{U}_4 (m_\mu - m_\mu) U_2 = 0.$$

For this reason, the second term in parenthesis vanishes entirely, leaving

$$\mathcal{M} \propto \bar{U}_4 \gamma^\beta U_2 * \frac{\eta_{\alpha\beta}}{q^2} * \bar{U}_3 \gamma^\alpha U_1.$$

Propagating the  $\eta_{\alpha\beta}$  through,

$$\mathcal{M} \propto \bar{U}_4 \gamma^\beta U_2 * \frac{1}{q^2} * \bar{U}_3 \gamma_\beta U_1.$$

The final cross section is proportional to  $|\mathcal{M}|^2$ , and so

$$|\mathcal{M}|^2 \propto \frac{1}{q^4} * \bar{U}_4 \gamma^\beta U_2 [\bar{U}_4 \gamma^\delta U_2]^* * \bar{U}_3 \gamma_\beta U_1 [\bar{U}_3 \gamma_\delta U_1]^*.$$

Since  $\bar{U}_4\gamma^\beta U_2$  is the same as  $\bar{U}_3\gamma_\beta U_1$  except for notation, from here the quantity  $\bar{U}_4\gamma^\beta U_2[\bar{U}_4\gamma^\delta U_2]^*$  is reduced and the same treatment is applied to  $\bar{U}_3\gamma_\beta U_1[\bar{U}_3\gamma_\delta U_1]^*$ .

Since  $\bar{U}_4\gamma^\delta U_2 \in \mathbb{C}$  in Dirac space,

$$\begin{aligned} [\bar{U}_4\gamma^\delta U_2]^* &= [\bar{U}_4\gamma^\delta U_2]^\dagger \\ &= U_2^\dagger \gamma^{\delta\dagger} \bar{U}_4^\dagger. \end{aligned}$$

Observe that since  $\gamma^\delta$  has the form

$$\gamma^\delta = \begin{pmatrix} A & B \\ -B & -A \end{pmatrix}$$

then

$$\begin{aligned} \gamma^0 \gamma^\delta \gamma^0 &= \begin{pmatrix} I_2 & 0 \\ 0 & I_2 \end{pmatrix} \begin{pmatrix} A & B \\ -B & -A \end{pmatrix} \begin{pmatrix} I_2 & 0 \\ 0 & I_2 \end{pmatrix} \\ &= \begin{pmatrix} A & -B \\ B & -A \end{pmatrix} \\ &= \gamma^{\delta\dagger}, \end{aligned}$$

and so

$$[\bar{U}_4\gamma^\delta U_2]^* = U_2^\dagger [\gamma^0 \gamma^\delta \gamma^0] \bar{U}_4^\dagger.$$

Recall the definition of the spinor adjoint in Eq. (D.3):

$$\bar{U} = U^\dagger \gamma^0.$$

Then

$$\begin{aligned} \bar{U}_4^\dagger &= (U_4^\dagger \gamma^0)^\dagger \\ &= \gamma^{0\dagger} U_4^{\dagger\dagger} \\ &= \gamma^0 U_4, \end{aligned}$$

which results in

$$[\bar{U}_4 \gamma^\delta U_2]^* = U_2^\dagger [\gamma^0 \gamma^\delta \gamma^0] [\gamma^0 U_4],$$

or more suggestively,

$$\begin{aligned} [\bar{U}_4 \gamma^\delta U_2]^* &= [U_2^\dagger \gamma^0] \gamma^\delta [\gamma^0 \gamma^0] U_4 \\ &= \bar{U}_2 \gamma^\delta U_4. \end{aligned}$$

This results in

$$|\mathcal{M}|^2 \propto \frac{1}{q^4} * \bar{U}_4 \gamma^\beta U_2 \bar{U}_2 \gamma^\delta U_4 * \bar{U}_3 \gamma_\beta U_1 \bar{U}_1 \gamma_\delta U_3. \quad (\text{C.2})$$

In principle, if the spinors of the muons were known (e.g. the muons were part of a polarized beam) this could be evaluated directly. However, in general the spinors are not known. As an approximation, it is necessary to average the spinors over their spins. Again, starting with the muons and extrapolating the treatment to the electrons,

$$\begin{aligned} \langle \bar{U}_4 \gamma^\beta U_2 \bar{U}_2 \gamma^\delta U_4 \rangle_{\text{spin } 2} &= \frac{1}{2} \sum_{s_2=1}^2 \bar{U}_4 \gamma^\beta U_2^{(s_2)} \bar{U}_2^{(s_2)} \gamma^\delta U_4 \\ &= \frac{1}{2} \bar{U}_4 \gamma^\beta \left[ \sum_{s_2=1}^2 U_2^{(s_2)} \bar{U}_2^{(s_2)} \right] \gamma^\delta U_4. \end{aligned}$$

Recall the completeness property of spinors (Eq. (D.4)):

$$\sum_s U^{(s)} \bar{U}^{(s)} = \gamma^\alpha P_\alpha + m.$$

Then

$$\langle \bar{U}_4 \gamma^\beta U_2 \bar{U}_2 \gamma^\delta U_4 \rangle_{\text{spin } 2} = \frac{1}{2} \bar{U}_4 \gamma^\beta (\gamma^\epsilon P_{2\epsilon} + m_\mu) \gamma^\delta U_4.$$

Averaging similarly over the spin for particle #4 yields

$$\langle \bar{U}_4 \gamma^\beta U_2 \bar{U}_2 \gamma^\delta U_4 \rangle_{\text{spin } 2, \text{ spin } 4} = \frac{1}{2} \frac{1}{2} \sum_{s_4=1}^2 \bar{U}_4^{(s_4)} [\gamma^\beta (\gamma^\epsilon P_{2\epsilon} + m_\mu) \gamma^\delta] U_4^{(s_4)}.$$

Now, spinors do not generally commute, but their components (which are scalars) do. Observing that  $\bar{U}$  is a 1x4 row vector, the bracketed term is a 4x4 matrix, and  $U$  is a 4x1 column vector, it is possible to write out the matrix multiplication as an explicit double sum over the indices  $i, j$ :

$$\begin{aligned}\langle \bar{U}_4 \gamma^\beta U_2 \bar{U}_2 \gamma^\delta U_4 \rangle_{s2, s4} &= \frac{1}{4} \sum_{s4=1}^2 \sum_{i,j=1}^4 \bar{U}_{4i}^{(s4)} [\gamma^\beta (\gamma^\epsilon P_{2\epsilon} + m_\mu) \gamma^\delta]_{ij} U_{4j}^{(s4)} \\ &= \frac{1}{4} \sum_{i,j=1}^4 \left( [\gamma^\beta (\gamma^\epsilon P_{2\epsilon} + m_\mu) \gamma^\delta]_{ij} \left[ \sum_{s4=1}^2 \bar{U}_4^{(s4)} U_4^{(s4)} \right]_{ij} \right)\end{aligned}$$

Spinor completeness (Eq. (D.4)) requires a summation over  $U\bar{U}$ , not  $\bar{U}U$ . However,  $\bar{U}U$  is still useful. Since  $A^T + B^T = [A + B]^T$ ,

$$\begin{aligned}\sum \bar{U}U &= \left[ \sum (\bar{U}U)^T \right]^T \\ &= \left[ \sum U^T \bar{U}^T \right]^T.\end{aligned}$$

Again explicitly writing the matrix multiplication,

$$\begin{aligned}\sum \bar{U}U &= \left[ \sum_{k,l}^4 \left( \sum_{k,l}^4 (U_k)^T (\bar{U}_l)^T \right) \right]^T \\ &= \left[ \sum_{k,l}^4 \left( \sum_{k,l}^4 (U_k)^T (\bar{U}_l)^T \right) \right]^T \\ &= \left[ \sum_{k,l}^4 \left( \sum_{k,l}^4 U_l \bar{U}_k \right) \right]^T \\ &= \left[ \sum_{k,l}^4 \left( \sum_{k,l}^4 U \bar{U} \right)_{l,k} \right]^T.\end{aligned}$$

Now it is possible to use spinor completeness (Eq. (D.4)):

$$\begin{aligned}\sum \bar{U}U &= \left[ \sum_{k,l}^4 (\gamma^\alpha P_\alpha + m)_{l,k} \right. \\ &\quad \left. = (\gamma^\alpha P_\alpha + m)^T. \right]\end{aligned}$$

Conclusively, if the  $i$ - $j^{th}$  component of  $\sum \bar{U}U$  is desired, then the indices of Eq. (D.4) must be exchanged:

$$\begin{aligned} \left[ \sum \bar{U}U \right]_{i,j} &= [(\gamma^\alpha P_\alpha + m)^T]_{i,j} \\ &= [(\gamma^\alpha P_\alpha + m)_{i,j}]^T \\ &= [\gamma^\alpha P_\alpha + m]_{j,i}. \end{aligned}$$

This results in

$$\langle \bar{U}_4 \gamma^\beta U_2 \bar{U}_2 \gamma^\delta U_4 \rangle_{s2, s4} = \frac{1}{4} \sum_{i,j=1}^4 \left( [\gamma^\beta (\gamma^\epsilon P_{2\epsilon} + m_\mu) \gamma^\delta]_{ij} [\gamma^\kappa P_{4\kappa} + m_\mu]_{j,i} \right).$$

Upon the concatenation of the subscripts  $i, j$  and  $j, i$ , it can be seen that

$$\langle \bar{U}_4 \gamma^\beta U_2 \bar{U}_2 \gamma^\delta U_4 \rangle_{s2, s4} = \frac{1}{4} \sum_{i=1}^4 \left( [\gamma^\beta (\gamma^\epsilon P_{2\epsilon} + m_\mu) \gamma^\delta] (\gamma^\kappa P_{4\kappa} + m_\mu) \right)_{ii}.$$

This is now the definition of a trace ( $\sum_i M_{ii} \equiv \text{Tr}(M)$ ). Then

$$\langle \bar{U}_4 \gamma^\beta U_2 \bar{U}_2 \gamma^\delta U_4 \rangle_{s2, s4} = \frac{1}{4} \text{Tr}[\gamma^\beta (\gamma^\epsilon P_{2\epsilon} + m_\mu) \gamma^\delta (\gamma^\kappa P_{4\kappa} + m_\mu)].$$

Using the addition property of traces, it is clear that there are four terms to evaluate:

- i)  $\text{Tr}(\gamma^\beta \gamma^\epsilon P_{2\epsilon} \gamma^\delta \gamma^\kappa P_{4\kappa})$
- ii)  $\text{Tr}(\gamma^\beta \gamma^\epsilon P_{2\epsilon} \gamma^\delta m_\mu)$
- iii)  $\text{Tr}(\gamma^\beta m_\mu \gamma^\delta \gamma^\kappa P_{4\kappa})$
- iv)  $\text{Tr}(\gamma^\beta m_\mu \gamma^\delta m_\mu)$ .

The derivations for the solutions to these traces can be found in Appendix F. The first term is the trace of four  $\gamma$  matrices and can be solved by using Eq. (F.9):

$$\begin{aligned} \text{Tr}(\gamma^\beta \gamma^\epsilon P_{2\epsilon} \gamma^\delta \gamma^\kappa P_{4\kappa}) &= P_{2\epsilon} P_{4\kappa} \text{Tr}(\gamma^\beta \gamma^\epsilon \gamma^\delta \gamma^\kappa) \\ &= 4P_{2\epsilon} P_{4\kappa} (\eta^{\beta\epsilon} \eta^{\delta\kappa} - \eta^{\beta\delta} \eta^{\epsilon\kappa} + \eta^{\beta\kappa} \eta^{\epsilon\delta}) \\ &= 4(P_2^\beta P_4^\delta - P_2 \cdot P_4 \eta^{\beta\delta} + P_2^\delta P_4^\beta). \end{aligned}$$

The second term is the trace of an odd number of  $\gamma$  matrices, and is equal to zero via Eq. (F.6):

$$\begin{aligned}\text{Tr}(\gamma^\beta \gamma^\epsilon P_{2\epsilon} \gamma^\delta m_\mu) &= P_{2\epsilon} m_\mu \text{Tr}(\gamma^\beta \gamma^\epsilon \gamma^\delta) \\ &= 0.\end{aligned}$$

The third term is also a trace of an odd number of  $\gamma$  matrices:

$$\begin{aligned}\text{Tr}(\gamma^\beta m_\mu \gamma^\delta \gamma^\kappa P_{4\kappa}) &= m_\mu P_{4\kappa} \text{Tr}(\gamma^\beta \gamma^\delta \gamma^\kappa) \\ &= 0.\end{aligned}$$

The final term is the trace of two  $\gamma$  matrices, and results in the Minkowski metric via Eq. (F.8):

$$\begin{aligned}\text{Tr}(\gamma^\beta m_\mu \gamma^\delta m_\mu) &= m_\mu^2 \text{Tr}(\gamma^\beta \gamma^\delta) \\ &= 4m_\mu^2 \eta^{\beta\delta}.\end{aligned}$$

Putting it all together results in

$$\langle \bar{U}_4 \gamma^\beta U_2 \bar{U}_2 \gamma^\delta U_4 \rangle_{s2, s4} = P_2^\beta P_4^\delta - P_2 \cdot P_4 \eta^{\beta\delta} + P_2^\delta P_4^\beta + m_\mu^2 \eta^{\beta\delta}.$$

The electron portion is mathematically the same. Symbolically, contravariant indices become covariant (e.g.  $\gamma^\beta$  becomes  $\gamma_\beta$ ), the mass is now the electron mass (i.e.  $m_\mu$  becomes  $m_e$ ), and the even subscripts become odd (i.e.  $P_2$ ,  $P_4$  become  $P_1$ ,  $P_3$ ). Explicitly, Eq. (C.2) becomes

$$\begin{aligned}\langle |\mathcal{M}|^2 \rangle &\propto \frac{1}{q^4} * \langle \bar{U}_4 \gamma^\beta U_2 \bar{U}_2 \gamma^\delta U_4 \rangle_{s2, s4} * \langle \bar{U}_3 \gamma_\beta U_1 \bar{U}_1 \gamma_\delta U_4 \rangle_{s1, s3} \\ &\propto \frac{1}{q^4} * (P_2^\beta P_4^\delta - P_2 \cdot P_4 \eta^{\beta\delta} + P_2^\delta P_4^\beta + m_\mu^2 \eta^{\beta\delta}) * \\ &\quad (P_{1\beta} P_{3\delta} - P_1 \cdot P_3 \eta_{\beta\delta} + P_{1\delta} P_{3\beta} + m_e^2 \eta_{\beta\delta}).\end{aligned}$$

Explicitly, the algebra is

$$\begin{aligned} \langle |\mathcal{M}|^2 \rangle \propto \frac{1}{q^4} * & [(P_1 \cdot P_2)(P_3 \cdot P_4) - (P_1 \cdot P_3)(P_2 \cdot P_4) + (P_1 \cdot P_4)(P_2 \cdot P_3) + \\ & m_e^2(P_2 \cdot P_4) - (P_1 \cdot P_3)(P_2 \cdot P_4) + 4(P_1 \cdot P_3)(P_2 \cdot P_4) - \\ & (P_1 \cdot P_3)(P_2 \cdot P_4) - 4m_e^2(P_2 \cdot P_4) + (P_1 \cdot P_4)(P_2 \cdot P_3) - \\ & (P_1 \cdot P_3)(P_2 \cdot P_4) + (P_1 \cdot P_2)(P_3 \cdot P_4) + m_e^2(P_2 \cdot P_4) + \\ & m_\mu^2(P_1 \cdot P_3) - 4m_\mu^2(P_1 \cdot P_3) + m_\mu^2(P_1 \cdot P_3) + 4m_\mu^2 m_e^2], \end{aligned}$$

with  $\eta^{\alpha\beta}\eta_{\alpha\beta} = 4$ . Gathering the like terms, this reduces to

$$\begin{aligned} \langle |\mathcal{M}|^2 \rangle \propto \frac{1}{q^4} [ & 2(P_1 \cdot P_4)(P_2 \cdot P_3) + 2(P_1 \cdot P_2)(P_3 \cdot P_4) - \\ & 2m_e^2(P_2 \cdot P_4) - 2m_\mu^2(P_1 \cdot P_3) + 4m_\mu^2 m_e^2]. \end{aligned}$$

Up until here, this is a quite general expression for two particles interacting via virtual photon exchange. For COSY, straggling and scattering are mutually exclusive processes: first the straggling routine is called and then the scattering routine is called. Therefore, for this model it must be assumed that there is no energy exchange between the muon and electron. Consequently, since the electron is bound it remains fixed and the muon scatters. This can be seen diagrammatically in Figure C.3.

Now it is clear that  $P_1 = P_3 = (m_e, 0, 0, 0)$ . Furthermore, since the total energy of the muon is conserved  $E_2 = E_4 = E_\mu$  and  $P_2 = (E_\mu, \vec{p}_2)$  and  $P_4 = (E_\mu, \vec{p}_4)$  and so

$$\begin{aligned} P_1 \cdot P_2 &= E_\mu m_e & P_1 \cdot P_3 &= m_e^2 \\ P_1 \cdot P_4 &= E_\mu m_e & P_2 \cdot P_3 &= E_\mu m_e \\ P_2 \cdot P_4 &= E_\mu^2 - \vec{p}_2 \cdot \vec{p}_4 & &= E_\mu^2 - p_\mu^2 \cos \theta \\ P_3 \cdot P_4 &= E_\mu m_e. \end{aligned}$$

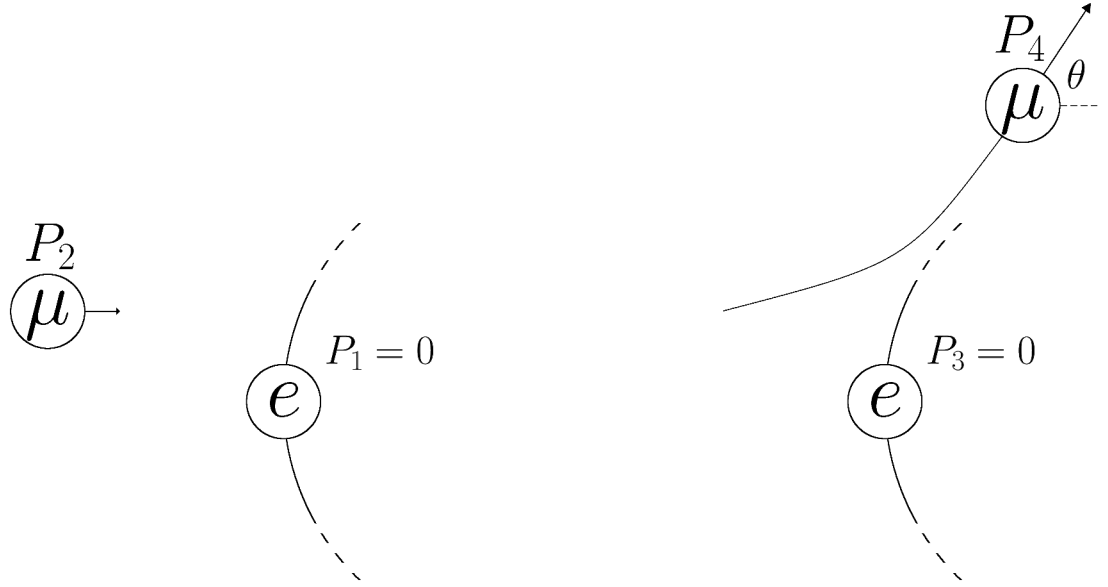


Figure C.3. COSY treatment of muon-electron scattering. Since the routines are called separately, the model assumes no straggling while scattering.

Then

$$\begin{aligned} \langle |\mathcal{M}|^2 \rangle &\propto \frac{1}{q^4} [2(E_\mu m_e)(E_\mu m_e) + 2(E_\mu m_e)(E_\mu m_e) \\ &\quad - 2m_e^2(E_\mu^2 - p_\mu^2 \cos \theta) - 2m_\mu^2 m_e^2 + 4m_\mu^2 m_e^2]. \end{aligned}$$

Factoring out the term  $2m_e^2$ ,

$$\begin{aligned} \langle |\mathcal{M}|^2 \rangle &\propto \frac{1}{q^4} (E_\mu^2 + E_\mu^2 - E_\mu^2 + p_\mu^2 \cos \theta - m_\mu^2 + 2m_\mu^2) \\ &\propto \frac{1}{q^4} (E_\mu^2 + p_\mu \cos \theta + m_\mu^2) \\ &\propto \frac{1}{q^4} (p_\mu + m_\mu + p_\mu \cos \theta + m_\mu^2) \\ &\propto \frac{1}{q^4} (2m_\mu^2 + p_\mu(1 + \cos \theta)). \end{aligned}$$

Factoring out  $2m_\mu^2$  and observing that  $p/m = \beta\gamma$  yields

$$\langle |\mathcal{M}|^2 \rangle \propto \frac{1 + \frac{(\beta\gamma)^2}{2}(1 + \cos \theta)}{q^4}.$$

Again using conservation of  $P_\beta$  at vertex  $\beta$ , it can be seen that

$$P_{2\beta} + q_\beta = P_{4\beta} \quad \rightarrow \quad q_\beta = P_{4\beta} - P_{2\beta}$$

. Then

$$\begin{aligned} q^2 &= (P_{4\beta} - P_{2\beta})^2 \\ &= ((E_4, \vec{p}_4) - (E_2, \vec{p}_2))^2 \\ &= ((0, \vec{p}_4 - \vec{p}_2))^2 \\ &= -(p_4^2 + p_2^2 - p_4 p_2 \cos \theta) \\ &= -2p_\mu(1 - \cos \theta). \end{aligned}$$

Squaring  $q^2$  and throwing out the constant  $p_\mu$ ,

$$\langle |\mathcal{M}|^2 \rangle \propto \frac{1 + \frac{(\beta\gamma)^2}{2}(1 + \cos \theta)}{(1 - \cos \theta)^2}.$$

Finally, the Mott cross section is obtained:

$$\frac{d\sigma}{d\Omega} \propto \frac{1 + \frac{(\beta\gamma)^2}{2}(1 + \cos \theta)}{(1 - \cos \theta)^2}. \quad (\text{C.3})$$

Observe that for a non-relativistic beam of muons,  $\beta\gamma \rightarrow 0$  and this reduces to the Rutherford cross section (Eq. (2.24)).

APPENDIX D  
A BRIEF REVIEW OF RELEVANT PARTICLE PHYSICS

Since this dissertation concerns only muons interacting with electrons, this brief review only covers particles with spin 1/2. This review follows [38]. Particles of four-momentum  $P = (E, \vec{p}) = (E, p_x, p_y, p_z)$  must satisfy the relativistic energy-momentum relation:

$$P^\alpha P_\alpha - m^2 = 0, \quad (\text{D.1})$$

since

$$\begin{aligned} P^\alpha P_\alpha - m^2 &= E^2 - p^2 - m^2 \\ &= E^2 - (p^2 + m^2) \\ &= E^2 - E^2 = 0. \end{aligned}$$

For particles at rest (i.e.  $\vec{p} = 0$ ), this can be written as:

$$P^\alpha P_\alpha - m^2 = (p^0 + m)(p^0 - m) = 0,$$

and so clearly the energy  $p^0 = E$  has to be either the rest mass or the negative of the rest mass (for antiparticles). However, for particles which are not at rest, if this same form is desired then it should look something like

$$P^\alpha P_\alpha - m^2 = (\gamma^\beta P_\beta + m)(\gamma^\delta P_\delta - m).$$

One may solve this equation for the coefficients  $\gamma^\beta = (\gamma^0, \gamma^1, \gamma^2, \gamma^3)$ , but no scalars solve this complex system. Dirac proposed that the various  $\gamma$ s were actually matrices, not scalars. This approach has the solution:

$$\gamma^0 = \begin{pmatrix} I_2 & 0 \\ 0 & -I_2 \end{pmatrix} \quad \gamma^j = \begin{pmatrix} 0 & \sigma^j \\ -\sigma^j & 0 \end{pmatrix},$$

where  $\sigma^j$  are the Pauli matrices. This leads to the Dirac equation for particles (for antiparticles, simply switch the sign of the mass):

$$\gamma^\alpha P_\alpha - m = 0. \quad (\text{D.2})$$

These particles can be represented by the wavefunctions for free particles,

$$\psi(x) = C e^{-(i/\hbar)p \cdot x} U^{(s)}(P),$$

where  $C$  is some amplitude,  $U$  is the spinor, and  $s$  is the spin state of the particle (in this case  $s = 1, 2$ ). Antiparticle spinors are represented by  $V$  (unused in this work).

Spinor adjoints are defined by

$$\bar{U} = U^\dagger \gamma^0 = U^{*T} \gamma^0, \quad (\text{D.3})$$

where  $*$  represents the complex conjugate and  $T$  the transpose. These spinors satisfy the Diracequation:

$$(\gamma^\alpha P_\alpha - m)U = 0,$$

they are orthogonal:

$$\bar{U}^{(1)} U^{(2)} = 0,$$

and they are normalized:

$$\bar{U} U = 2m,$$

and they are complete:

$$\sum_{s=1}^2 U^{(s)} \bar{U}^{(s)} = (\gamma^\alpha P_\alpha + m). \quad (\text{D.4})$$

These spinors are four-component column vectors, and spinors describing particles ( $U$ ) and antiparticles ( $V$ ) for spin 1/2 particles could be represented as, for instance

$$U^{(1)} = \begin{pmatrix} 1 \\ 0 \\ 0 \\ 0 \end{pmatrix} \quad U^{(2)} = \begin{pmatrix} 0 \\ 1 \\ 0 \\ 0 \end{pmatrix}$$

$$V^{(1)} = \begin{pmatrix} 0 \\ 0 \\ 1 \\ 0 \end{pmatrix} \quad V^{(2)} = \begin{pmatrix} 0 \\ 0 \\ 0 \\ 1 \end{pmatrix},$$

but are usually more complicated if unpolarized.

APPENDIX E  
EXPLICIT FORMS OF THE DIRAC GAMMA MATRICES AND PAULI  
MATRICES

From the conventions in [38] it is observed that the Pauli matrices are defined as:

$$\sigma^1 = \begin{pmatrix} 0 & 1 \\ 1 & 0 \end{pmatrix} \quad \sigma^2 = \begin{pmatrix} 0 & -i \\ i & 0 \end{pmatrix} \quad \sigma^3 = \begin{pmatrix} 1 & 0 \\ 0 & -1 \end{pmatrix}.$$

Then the Dirac matrices follow as:

$$\gamma^0 = \begin{pmatrix} 1 & 0 & 0 & 0 \\ 0 & 1 & 0 & 0 \\ 0 & 0 & -1 & 0 \\ 0 & 0 & 0 & -1 \end{pmatrix} \quad \gamma^1 = \begin{pmatrix} 0 & 0 & 0 & 1 \\ 0 & 0 & 1 & 0 \\ 0 & -1 & 0 & 0 \\ -1 & 0 & 0 & 0 \end{pmatrix} \quad (E.1)$$

$$\gamma^2 = \begin{pmatrix} 0 & 0 & 0 & -i \\ 0 & 0 & i & 0 \\ 0 & i & 0 & 0 \\ -i & 0 & 0 & 0 \end{pmatrix} \quad \gamma^3 = \begin{pmatrix} 0 & 0 & 1 & 0 \\ 0 & 0 & 0 & -1 \\ -1 & 0 & 0 & 0 \\ 0 & 1 & 0 & 0 \end{pmatrix}.$$

## APPENDIX F

## PROOFS OF USEFUL DIRAC GAMMA MATRIX TRACE IDENTITIES

### F.1 Proof of $(\gamma^5)^2 = I_4$

Let  $\gamma^5 \equiv i\gamma^0\gamma^1\gamma^2\gamma^3$ . Then explicitly carrying out the multiplication yields

$$\begin{aligned} \gamma^5 &= i \begin{pmatrix} 0 & 0 & 0 & 1 \\ 0 & 0 & 1 & 0 \\ 0 & 1 & 0 & 0 \\ 1 & 0 & 0 & 0 \end{pmatrix} \cdot -i \begin{pmatrix} 0 & 1 & 0 & 0 \\ 1 & 0 & 0 & 0 \\ 0 & 0 & 0 & 1 \\ 0 & 0 & 1 & 0 \end{pmatrix} \\ \gamma^5 &= \begin{pmatrix} 0 & 0 & 1 & 0 \\ 0 & 0 & 0 & 1 \\ 1 & 0 & 0 & 0 \\ 0 & 1 & 0 & 0 \end{pmatrix}. \end{aligned} \quad (\text{F.1})$$

Then

$$(\gamma^5)^2 = I_4. \quad (\text{F.2})$$

### F.2 Proof of $\gamma^5\gamma^\alpha = -\gamma^\alpha\gamma^5$

Let the form of  $\gamma^\alpha$  be represented as

$$\begin{pmatrix} A & B \\ -B & -A \end{pmatrix}$$

(i.e. for  $\alpha = 0$ ,  $A = I_2$  and  $B = 0$ ; otherwise  $A = 0$  and  $B = \sigma^\alpha$ ). Then using the explicit form of  $\gamma^5$  in Eq. (F.1):

$$\begin{pmatrix} 0 & I_2 \\ I_2 & 0 \end{pmatrix} \begin{pmatrix} A & B \\ -B & -A \end{pmatrix} + \begin{pmatrix} A & B \\ -B & -A \end{pmatrix} \begin{pmatrix} 0 & I_2 \\ I_2 & 0 \end{pmatrix} = \begin{pmatrix} 0 & 0 \\ 0 & 0 \end{pmatrix}.$$

Therefore,

$$\gamma^5 \gamma^\alpha = -\gamma^\alpha \gamma^5. \quad (\text{F.3})$$

### F.3 Proof of $\text{Tr}(\text{odd number of } \gamma \text{ matrices}) = 0$

Let there be the trace of an arbitrary odd number of  $\gamma$  matrices

$$\text{Tr}(\gamma^{\alpha_1} \gamma^{\alpha_2} \dots \gamma^{\alpha_n}),$$

such that  $n$  is odd. Now insert into the beginning of the trace  $\gamma^5 \gamma^5$ ,

$$\text{Tr}(\gamma^5 \gamma^5 \gamma^{\alpha_1} \gamma^{\alpha_2} \dots \gamma^{\alpha_n}),$$

and there are two cases. The first makes use of  $(\gamma^5)^2 = I_4$  (Eq. F.2), and results in

$$\begin{aligned} \text{Tr}(\gamma^5 \gamma^5 \gamma^{\alpha_1} \gamma^{\alpha_2} \dots \gamma^{\alpha_n}) &= \text{Tr}(I_4 \gamma^{\alpha_1} \gamma^{\alpha_2} \dots \gamma^{\alpha_n}) \\ \text{Tr}(\gamma^5 \gamma^5 \gamma^{\alpha_1} \gamma^{\alpha_2} \dots \gamma^{\alpha_n}) &= \text{Tr}(\gamma^{\alpha_1} \gamma^{\alpha_2} \dots \gamma^{\alpha_n}) \end{aligned} \quad (\text{F.4})$$

The next case uses the cyclic property of traces, which is  $\text{Tr}(ABCD) = \text{Tr}(BCDA) = \text{Tr}(CDAB) = \dots$ . Then

$$\text{Tr}(\gamma^5 \gamma^5 \gamma^{\alpha_1} \gamma^{\alpha_2} \dots \gamma^{\alpha_n}) = \text{Tr}(\gamma^5 \gamma^{\alpha_1} \gamma^{\alpha_2} \dots \gamma^{\alpha_n} \gamma^5).$$

Now using  $\gamma^5 \gamma^\alpha = -\gamma^\alpha \gamma^5$  (Eq. F.3):

$$\text{Tr}(\gamma^5 \gamma^5 \gamma^{\alpha_1} \gamma^{\alpha_2} \dots \gamma^{\alpha_n}) = \text{Tr}(\gamma^5 \gamma^{\alpha_1} \gamma^{\alpha_2} \dots \gamma^5 \gamma^{\alpha_n})(-1)^1.$$

Applying this  $n$  times yields

$$\text{Tr}(\gamma^5 \gamma^5 \gamma^{\alpha_1} \gamma^{\alpha_2} \dots \gamma^{\alpha_n}) = \text{Tr}(\gamma^5 \gamma^5 \gamma^{\alpha_1} \gamma^{\alpha_2} \dots \gamma^{\alpha_n})(-1)^n.$$

Since  $n$  is negative,  $(-1)^n = -1$ . Again using  $(\gamma^5)^2 = I_4$  (Eq. F.2), this yields

$$\text{Tr}(\gamma^5 \gamma^5 \gamma^{\alpha_1} \gamma^{\alpha_2} \dots \gamma^{\alpha_n}) = -\text{Tr}(\gamma^{\alpha_1} \gamma^{\alpha_2} \dots \gamma^{\alpha_n}). \quad (\text{F.5})$$

Combining Eqns. F.4 and F.5:

$$\text{Tr}(\gamma^5 \gamma^5 \gamma^{\alpha_1} \gamma^{\alpha_2} \dots \gamma^{\alpha_n}) = \text{Tr}(\gamma^{\alpha_1} \gamma^{\alpha_2} \dots \gamma^{\alpha_n})$$

$$\text{Tr}(\gamma^5 \gamma^5 \gamma^{\alpha_1} \gamma^{\alpha_2} \dots \gamma^{\alpha_n}) = -\text{Tr}(\gamma^{\alpha_1} \gamma^{\alpha_2} \dots \gamma^{\alpha_n}).$$

Since this trace is both positive and negative the only conclusion is that it must be zero:

$$\text{Tr}(\gamma^{\alpha_1} \gamma^{\alpha_2} \dots \gamma^{\alpha_n}) = 0 \quad \text{for odd } n. \quad (\text{F.6})$$

#### F.4 Proof of $\text{Tr}(\gamma^\alpha \gamma^\beta) = 4\eta^{\alpha\beta}$

$\eta^{\alpha\beta}$  is an element of the Minkowski metric, which is defined here as

$$\eta = \begin{pmatrix} 1 & 0 & 0 & 0 \\ 0 & -1 & 0 & 0 \\ 0 & 0 & -1 & 0 \\ 0 & 0 & 0 & -1 \end{pmatrix}.$$

Unlike  $\gamma^\alpha$ ,  $\eta^{\alpha\beta}$  is simply a number. For example, if  $\alpha \neq \beta$  then  $\eta^{\alpha\beta} = 0$ , if  $\alpha = \beta = 0$  then  $\eta^{\alpha\beta} = 1$ , and so on. While it can be shown explicitly, it is treated as fact that the defining algebra is

$$\gamma^\alpha \gamma^\beta + \gamma^\beta \gamma^\alpha = 2\eta^{\alpha\beta} I_4, \quad (\text{F.7})$$

which is simply to say that

$$(\gamma^0)^2 = I_4$$

$$(\gamma^{1,2, \text{ or } 3})^2 = -I_4$$

$$\gamma^\alpha \gamma^\beta = 0 \quad \text{for } \alpha \neq \beta.$$

Now, concerning the problem at hand

$$\text{Tr}(\gamma^\alpha \gamma^\beta) = \frac{1}{2}(\text{Tr}(\gamma^\alpha \gamma^\beta) + \text{Tr}(\gamma^\beta \gamma^\alpha)).$$

Using first the cyclic property of traces, the addition of two traces, and the defining algebra (Eq. (F.7))

$$\begin{aligned}\text{Tr}(\gamma^\alpha \gamma^\beta) &= \frac{1}{2}(\text{Tr}(\gamma^\alpha \gamma^\beta) + \text{Tr}(\gamma^\beta \gamma^\alpha)) \\ &= \frac{1}{2}\text{Tr}(\gamma^\alpha \gamma^\beta + \gamma^\beta \gamma^\alpha) \\ &= \frac{1}{2}\text{Tr}(2\eta^{\alpha\beta} I_4).\end{aligned}$$

Finally,

$$\text{Tr}(\gamma^\alpha \gamma^\beta) = 4\eta^{\alpha\beta}. \quad (\text{F.8})$$

### F.5 Proof of $\text{Tr}(\gamma^\alpha \gamma^\beta \gamma^\delta \gamma^\epsilon) = 4(\eta^{\alpha\beta} \eta^{\delta\epsilon} - \eta^{\alpha\delta} \eta^{\beta\epsilon} + \eta^{\alpha\epsilon} \eta^{\beta\delta})$

Using the defining algebra (Eq. (F.7)), commuting  $\alpha$  and  $\beta$  yields that

$$\begin{aligned}\text{Tr}(\gamma^\alpha \gamma^\beta \gamma^\delta \gamma^\epsilon) &= \text{Tr}((2\eta^{\alpha\beta} - \gamma^\beta \gamma^\alpha) \gamma^\delta \gamma^\epsilon) \\ &= \text{Tr}(2\eta^{\alpha\beta} \gamma^\delta \gamma^\epsilon - \gamma^\beta \gamma^\alpha \gamma^\delta \gamma^\epsilon).\end{aligned}$$

Using the same method first for  $\alpha$  and  $\delta$  and then  $\alpha$  and  $\epsilon$ ,

$$\begin{aligned}\text{Tr}(\gamma^\alpha \gamma^\beta \gamma^\delta \gamma^\epsilon) &= \text{Tr}(2\eta^{\alpha\beta} \gamma^\delta \gamma^\epsilon - \gamma^\beta (2\eta^{\alpha\delta} - \gamma^\delta \gamma^\alpha) \gamma^\epsilon) \\ &= \text{Tr}(2\eta^{\alpha\beta} \gamma^\delta \gamma^\epsilon - 2\eta^{\alpha\delta} \gamma^\beta \gamma^\epsilon + \gamma^\beta \gamma^\delta \gamma^\alpha \gamma^\epsilon) \\ &= \text{Tr}(2\eta^{\alpha\beta} \gamma^\delta \gamma^\epsilon - 2\eta^{\alpha\delta} \gamma^\beta \gamma^\epsilon + \gamma^\beta \gamma^\delta (2\eta^{\alpha\epsilon} - \gamma^\beta \gamma^\delta \gamma^\epsilon \gamma^\alpha)) \\ &= \text{Tr}(2\eta^{\alpha\beta} \gamma^\delta \gamma^\epsilon - 2\eta^{\alpha\delta} \gamma^\beta \gamma^\epsilon + 2\eta^{\alpha\epsilon} \gamma^\beta \gamma^\delta - \gamma^\beta \gamma^\delta \gamma^\epsilon \gamma^\alpha).\end{aligned}$$

Recalling the addition properties of traces and observing Eq. (F.8),

$$\begin{aligned}\text{Tr}(\gamma^\alpha \gamma^\beta \gamma^\delta \gamma^\epsilon) &= 2\eta^{\alpha\beta} \text{Tr}(\gamma^\delta \gamma^\epsilon) - 2\eta^{\alpha\delta} \text{Tr}(\gamma^\beta \gamma^\epsilon) + 2\eta^{\alpha\epsilon} \text{Tr}(\gamma^\beta \gamma^\delta) - \text{Tr}(\gamma^\beta \gamma^\delta \gamma^\epsilon \gamma^\alpha) \\ &= 8\eta^{\alpha\beta} \eta^{\delta\epsilon} - 8\eta^{\alpha\delta} \eta^{\beta\epsilon} + 8\eta^{\alpha\epsilon} \eta^{\beta\delta} - \text{Tr}(\gamma^\beta \gamma^\delta \gamma^\epsilon \gamma^\alpha).\end{aligned}$$

Now recalling the cyclic permutative properties of traces, it can be seen that  $\text{Tr}(\gamma^\beta \gamma^\delta \gamma^\epsilon \gamma^\alpha) = \text{Tr}(\gamma^\alpha \gamma^\beta \gamma^\delta \gamma^\epsilon)$ . Then it is possible to move the last term on the right side to the left side, yielding the desired outcome

$$\text{Tr}(\gamma^\alpha \gamma^\beta \gamma^\delta \gamma^\epsilon) = 4\eta^{\alpha\beta} \eta^{\delta\epsilon} - 4\eta^{\alpha\delta} \eta^{\beta\epsilon} + 4\eta^{\alpha\epsilon} \eta^{\beta\delta}. \quad (\text{F.9})$$

APPENDIX G  
REPRODUCTION OF IMPLEMENTED CODE

The following is a verbatim reproduction of the code that was implemented into COSY Infinity. This is broken up into three levels: the user input via an example script called *example.fox*, which exemplifies the correct use of the implemented routines in this work; COSYScript (inside the file *cosy.fox*); and FORTRAN (inside the file *absfox.f*). It should be noted that this appendix contains only code that was added to COSY version 9.1. As such, this section does not present a stand-alone code.

### G.1 Example COSY Deck using ABSPOLY

```
{EXAMPLE USING THE NEW ABSPOLY ROUTINE FOR COSY INFINITY}
{CREATED ON JULY 21, 2016 BY JOSIAH KUNZ FOR HIS THESIS}

INCLUDE 'COSY';

PROCEDURE RUN;
VARIABLE LEN 1;
VARIABLE NPART 1;
VARIABLE RADLEN 1;
VARIABLE RI 1000000 6;
VARIABLE SO 100 2 2;
{-----}

{CUSTOM MATERIAL ROUTINE}
{-----}

PROCEDURE SETMAT MAT R;
VARIABLE PREF 1; VARIABLE MASS 1; VARIABLE GAMMA 1; VARIABLE BETA 1;
VARIABLE Z 1; VARIABLE A 1; VARIABLE RHO 1; VARIABLE IP 1;
VARIABLE RADLEN 1; VARIABLE X0 1; VARIABLE X1 1; VARIABLE SA 1;
VARIABLE SC 1; VARIABLE SM 1; VARIABLE XS 1; VARIABLE DENS 1;
```

```

PREF:=CONS(P0); MASS:=CONS(M0);

GAMMA :=SQRT(PREF^2+MASS^2)/MASS;
BETA :=SQRT(1-1/GAMMA^2);
{MATERIAL PARAMETER FOR DENSITY CORRECTION}
XS :=LOG(BETA*GAMMA)/LOG(10);

IF (MAT='LH'); Z := 2;A := 2.016; RHO := 0.071 {0.0755};
IP := 0.0000218; RADLEN := 8.321; X0 := 0.4759;
X1 := 1.9215; SA := 0.1348; SC :=-3.2632;
SM := 5.6249;

ELSEIF (MAT='LHE'); Z := 2;A := 4.003; RHO := 0.125;
IP := 0.0000423; RADLEN := 7.56 ;
ELSEIF (MAT='LIH'); Z := 4;A := 7.95 ; RHO := 0.82;
IP := 0.0000365; RADLEN := 1.149;
ELSEIF (MAT='AL'); Z := 13;A := 26.982; RHO := 2.699;
IP := 0.000166 ; RADLEN := 0.089;
ELSEIF (MAT='BE'); Z := 4;A := 9.012; RHO := 1.85 ;
IP := 0.0000637; RADLEN := 0.351; X0 := 0.0592;
X1 := 1.6922; SA := 0.80392; SC :=-2.7847;
SM := 2.4339;

ENDIF;

IF (XS>X1);
DENS := 4.60517*XS+SC;
ELSEIF (XS>X0);
DENS := 4.60517*XS+SC+SA*(X1-XS)^SM;

```

```

ELSEIF LO(1);

DENS := 0;

ENDIF;

{WE DON'T ACTUALLY WANT A DENSITY CORRECTION!}

DENS:=0;

BBC Z A RHO IP DENS 0;

R:=RADLEN;

ENDPROCEDURE;

{-----}

{MAIN SIMULATION}

{-----}

WAS 1;

OV 5 3 0;

{MUONS WITH P=200 MEV/C}

RPM 200 0.1134289256 1;

NPART:=1000000;

LEN:=0.100;

SETMAT 'LH' RADLEN;

{GENERATE PARTICLES (FASTER)}

{-----}

BGEN NPART RI 0 0.32 0 10 0 0.32 0 10 0 0 CONS(P0) 10;

{

NPART          =      NUMBER OF PARTICLES TO GENERATE

```

```

RI      =      PUT THEM INTO PARTICLE ARRAY RI
0      =      AVERAGE X (METERS)
0.32   =      SIGMA X
0      =      AVERAGE PX (MEV/C)
10     =      SIGMA PX
0      =      AVERAGE Y
0.32   =      SIGMA Y
0      =      AVERAGE PY
10     =      SIGMA PY
0      =      AVERAGE T
0      =      SIGMA T
CONS(PO) =      AVERAGE PZ
10     =      SIGMA PZ
}

```

{READ FROM FILE (COMMENTED OUT FOR NOW)}

{-----}

{READ\_G4BL 89 NPART RI;}

{

```

89      =      READ FROM FORT.89
NPART  =      NUMBER OF PARTICLES TO READ
RI      =      PUT THEM INTO PARTICLE ARRAY RI
}

```

{ZERO TH ORDER (FLAT) ABSORBER}

S0(1,1):=0;

UM;

```
ABSPOLY S0 S0 0 LEN 1.0 RI RADLEN 1 LEN 0;
{
    S0      =      ENTRANCE SHAPE
    S0      =      EXIT SHAPE
    0       =      ORDER OF S0
    LEN     =      ABSORBER LENGTH
    1.0    =      APERTURE
    RI     =      INPUT AND OUTPUT ARRAY OF PARTICLES
    RADLEN =      RADIATION LENGTH OF MATERIAL
    1      =      NUMBER OF ITERATIONS IN PROPAGAION
    LEN    =      CELL LENGTH
    0      =      WRITE TO THIS FILE WHEN DONE (0 =NO FILE)
}
```

WRITE\_ICOOL LEN 1 NPART RI 12 1;

```
{
    LEN      =      Z POSITION
    1       =      REGION NUMBER
    NPART   =      NUMBER OF PARTICLES
    RI     =      ARRAY OF PARTICLES TO WRITE
    12    =      WRITE TO FORT.12
    1      =      APERTURE (<=0 MEANS NO APERTURE)
}
```

```
ENDPROCEDURE;
```

```
RUN;
```

```
END;
```

## G.2 COSYScript

```
FUNCTION IN1DVE SIZE VAL ;
{INITIALIZES 1D VECTOR WITH ZEROS. VECTOR VE MUST BE EMPTY}
VARIABLE TMPX SIZE ;VARIABLE SIZETMP 1 ;
VARIABLE I 1 ;VARIABLE COUNT 1 ;
TMPX :=VAL ;
{FIRST LOOP}
SIZETMP :=SIZE ;
LOOP I 0 (INT(LOG(SIZETMP)/LOG(2))-1) ;
TMPX:=TMPX&TMPX ;
ENDLOOP;
IN1DVE :=TMPX ;
TMPX := 0;
COUNT :=COUNT+2^(INT(LOG(SIZETMP)/LOG(2))) ;
SIZETMP :=SIZETMP-2^(INT(LOG(SIZETMP)/LOG(2))) ;
WHILE (COUNT<SIZE) ;
LOOP I 0 (INT(LOG(SIZETMP)/LOG(2))-1) ;
TMPX:=TMPX&TMPX ;
ENDLOOP;
IN1DVE :=IN1DVE&TMPX ;
TMPX := 0;
COUNT :=COUNT+2^(INT(LOG(SIZETMP)/LOG(2))) ;
```

```

SIZETMP :=SIZETMP-2^(INT(LOG(SIZETMP)/LOG(2))) ;
ENDWHILE ;

ENDFUNCTION ;

PROCEDURE BGEN NPART V X SX PX SPX Y SY PY SPY T ST PZ SPZ ;
{PROCEDURE TO QUICKY GENERATE A GAUSSIAN BEAM.

NPART = NUMBER OF PARTICLES
V = 2D VECTOR TO PUT PARTICLES IN
X = AVERAGE X POSITION
SX = SIGMA X
ETC.

}

VARIABLE I 1 ;VARIABLE GAM NPART 1 ;VARIABLE PV 1 12 ;
{}

{INITIALIZE VECTOR V IS NECESSARY}

IF LENGTH(V(1))#NPART ;
LOOP I 1 6 ;
V(I) :=IN1DVE(NPART,0);
ENDLOOP ;
ENDIF ;
{}

PV(1) :=X ;PV(2) :=SX ;PV(3) :=PX ;PV(4) :=SPX ;
PV(5) :=Y ;PV(6) :=SY ;PV(7) :=PY ;PV(8) :=SPY ;
PV(9) :=T ;PV(10) :=ST; PV(11) :=PZ; PV(12) :=SPZ;
GAUVEC PV 6 V NPART ;
{CONVERT BACK TO COSY COORDINATES}

```

```

V(6):=SQRT(V(2)^2+V(4)^2+V(6)^2+(CONS(M0)*AMUMEV)^2) ;{NOW V(6) IS E}
V(6):=V(6)-CONS(M0)*AMUMEV ;{NOW V(6) IS KE}
GAM(1) :=V(6)/(CONS(M0)*AMUMEV)+1 ;
V(2):=V(2)/CONS(P0) ;
V(4):=V(4)/CONS(P0) ;
V(6):=(V(6)-CONS(E0))/CONS(E0) ;{NOW V(6) IS D}
V(5):=-V(5)*CONS(V0)*GAM(1)/(1+GAM(1)) ;{ASSUMES TREF=0}
ENDPROCEDURE ;

```

```

PROCEDURE READ_G4BL FILE NPART V ;
{PROCEDURE TO READ PARTICLES FROM A G4BL-FORMATTED FILE AND PUT IT
INTO A COSY VECTOR V. INPUTS ARE:
FILE    = FILE NUMBER TO READ (E.G. THE 12 IN 'FORT.12')
NPART   = NUMBER OF PARTICLES
V      = VECTOR TO READ TO
}
VARIABLE I 1 ;VARIABLE GAM NPART ;VARIABLE MASS 1 ;
{INITIALIZE VECTOR IF NECESSARY}
IF LENGTH(V(1))#NPART ;
LOOP I 1 6 ;
V(I):=IN1DVE(NPART,0);
ENDLOOP ;
ENDIF ;
{READ FILE AT FORTRAN LEVEL}
RG4BL FILE NPART V ;
{OUTPUT IS IN (X,PX,Y,PY,T,E) SO NEED TO TRANSLATE TO COSY COORDS}
MASS:=CONS(M0)*AMUMEV ;

```

```

GAM:=V(6)/MASS ;
V(2):=V(2)/CONS(P0) ;
V(4):=V(4)/CONS(P0) ;
V(5):=-V(5)*CONS(V0)*GAM/(1+GAM) ;
V(6):=(V(6)-MASS)/CONS(E0)-1 ;
ENDPROCEDURE ;

PROCEDURE READ_ICOOL FILE NPART V ;
{PROCEDURE TO READ PARTICLES FROM AN ICOOL-FORMATTED FILE AND PUT IT
INTO A COSY VECTOR V. INPUTS ARE:
FILE    = FILE NUMBER TO READ (E.G. THE 12 IN 'FORT.12')
NPART   = NUMBER OF PARTICLES
V       = VECTOR TO READ TO
}
VARIABLE I 1 ;VARIABLE GAM NPART ;VARIABLE MASS 1 ;
{INITIALIZE VECTOR IF NECESSARY}
IF LENGTH(V(1))#NPART ;
  LOOP I 1 6 ;
    V(I):=IN1DVE(NPART,0);
  ENDLOOP ;
ENDIF ;
{READ FILE AT FORTRAN LEVEL}
RICOOL FILE NPART V ;
{OUTPUT IS IN (X,PX,Y,PY,T,E) SO NEED TO TRANSLATE TO COSY COORDS}
MASS:=CONS(M0)*AMUMEV ;
GAM:=V(6)/MASS ;
V(2):=V(2)/CONS(P0) ;

```

```

V(4):=V(4)/CONS(P0) ;
V(5):=-V(5)*CONS(V0)*GAM/(1+GAM) ;
V(6):=(V(6)-MASS)/CONS(E0)-1 ;
ENDPROCEDURE ;

PROCEDURE WRITE_ICOOL Z REG NPART V UI APE ;
{PROCEDURE TO TAKE COSY ARRAY AND WRITE IT INTO ICOOL STYLE.
Z = Z-POSITION
REG = REGION NUMBER
NPART = NUMBER OF PARTICLES
V = VECTOR TO WRITE
UI = UI TO WRITE (E.G. UI=12 WRITES TO FORT.12)
APE = APERATURE (<=0 TO TURN OFF)
VECTOR SHOULD BE NORMAL COSY VECTOR:
V = (X,A,Y,B,L,D)
}
VARIABLE GAM1 LENGTH(V(1)) 1 ;VARIABLE L1 LENGTH(V(1)) 1 ;
VARIABLE V1 LENGTH(V(1)) 6 ;

{}  

{NEED VECTOR "V1" =(X,PX,Y,PY,TOF,EI)}
V1(1) :=V(1) ;
V1(2) :=V(2)*CONS(P0) ;
V1(3) :=V(3) ;
V1(4) :=V(4)*CONS(P0) ;

```

```

V1(6) :=CONS(E0)*(V(6)+1)+CONS(M0)*AMUMEV ;
L1(1) :=V(5) ;
GAM1(1) :=V1(6)/(CONS(M0)*AMUMEV) ;
{TOF ASSUMING REF T = 0}
V1(5) :=-L1(1)*(1+GAM1(1))/(CONS(V0)*GAM1(1)) ;
WICOOL Z REG NPART V1 UI APE ;
ENDPROCEDURE ;

PROCEDURE CMSTPT CURD R1 R2 L ZST S1 S2 AX AY SS ;
{TILTED CMSTP WITH THE USUAL ARGUMENTS +TILTS IN DEGREES +STEP SIZE.
CURD = CURRENT DENSITY
R1 = INNER RADIUS
R2 = OUTER RADIUS
L = LENGTH OF MAGNET
ZST = STARTING POSITION OF MAGNET
S1 = LEFT SLICE Z-POSITION
S2 = RIGHT SLICE Z-POSITION
AX = X TILT IN DEGREES
AY = Y TILT IN DEGREES
SS = STEPSIZE (CAN BE ZERO)}}

VARIABLE I 1 ;VARIABLE CURDA 1 1 ;VARIABLE R1A 1 1 ;
VARIABLE R2A 1 1 ;VARIABLE LA 1 1 ;VARIABLE ZSTA 1 1 ;
VARIABLE XOFF 1 ;VARIABLE YOFF 1 ;VARIABLE ZOFF 1 ;
VARIABLE START 1 ;

{CORRECTION FOR X,Y (INPUT SHOULD BE SAME AS G4BL TILTS; MUST

```

TRANSLATE TO COSY. E.G. IF G4BL HAS A -3 X TILT, THIS IS +3 Y TILT.}

I:=AY;

AY:=-AX;

AX:=I;

CURDA(1):=CURD; R1A(1):=R1; R2A(1):=R2; LA(1):=L; ZSTA(1):=ZST;

DL ZST-S1+L/2 ; {GET TO CENTER OF MAGNET}

TA AX AY ;

DL -(ZST-S1+L/2) ;{BACK TO CELL'S START}

IF SS#0 ;

LOOP I S1 S2-SS SS ;

CMSTP 1 CURDA R1A R2A LA ZSTA I I+SS;

ENDLOOP ;

ELSEIF LO(1) ;

CMSTP 1 CURDA R1A R2A LA ZSTA S1 S2 ;

ENDIF ;

DL ZST-S2+L/2 ; {BACK TO MAGNET'S CENTER}

TA -AX -AY ;{TILT BACK IN LAB FRAME}

DL -(ZST-S2+L/2) ;{TO CELL'S EXIT}

ENDPROCEDURE ;

FUNCTION CEILING X ;

VARIABLE RX 1 ;

RX :=NINT(X) ;

```

IF (RX<X) ;RX :=RX+1 ; ENDIF ;{CASE FOR NINT ROUNDED DOWN}
CEILING :=RX ;
ENDFUNCTION ;

PROCEDURE ABSPOLY S1 S2 N LEN APERTURE V RADLEN SPLIT LCELL SAV ;
{-----}

VARIABLE SS1 1000 N+1 N+1 ; VARIABLE SS2 1000 N+1 N+1 ;
VARIABLE LF1 NM1 1 ; VARIABLE PATH LENGTH(V(1)) 1 ;
VARIABLE V1 LENGTH(V(1)) 6 ;VARIABLE MASS 1 ;VARIABLE SUBLEN 1 ;
VARIABLE NPART 1 ;VARIABLE J 1 ;VARIABLE V01 1 ; VARIABLE V02 1 ;
VARIABLE I 1 ;VARIABLE K 1 ;VARIABLE LF NM1 ; VARIABLE SUBCELL 1 ;
VARIABLE ZEROES 1 6 ;VARIABLE L1 LENGTH(V(1)) 1 ;VARIABLE DT0 1 ;
VARIABLE GAM1 LENGTH(V(1)) 1 ;VARIABLE GAM2 LENGTH(V(1)) 1 ;
VARIABLE SAVNUM 1 ;

{-----}

{INITIALIZE}

IF (NINT(SPLIT)#SPLIT) ;
  WRITE 6 '###ERROR IN ABSPOLY###' ;
  WRITE 6 ' >ITERATION NUMBER MUST BE INTEGER!<' ;
  QUIT 0 ;
ELSEIF ((SPLIT<0)+(SPLIT=0)) ;
  WRITE 6 '###ERROR IN ABSPOLY###' ;
  WRITE 6 ' >ITERATION NUMBER MUST BE POSITIVE!<' ;
  QUIT 0 ;
ENDIF ;

MASS :=CONS(M0)*AMUMEV ;

```

```

NPART :=LENGTH(V(1)) ;
V01 := CONS(V0) ;
LOOP I 1 6 ;ZEROES(I) := 0;ENDLOOP ;
DT0 := 0 ;

{-----}
{NEED VECTOR "V1" =(X,PX,Y,PY,TOF,EI)}

V1(1) :=V(1) ;
V1(2) :=V(2)*CONS(P0) ;
V1(3) :=V(3) ;
V1(4) :=V(4)*CONS(P0) ;
V1(6) :=CONS(E0)*(V(6)+1)+CONS(M0)*AMUMEV ;
L1(1) :=V(5) ;
GAM1(1) :=V1(6)/(CONS(M0)*AMUMEV) ;
{TOF ASSUMING REF T = 0}
V1(5) :=-L1(1)*(1+GAM1(1))/(CONS(V0)*GAM1(1)) ;

{-----}
{PROPAGATE PARTICLES FROM CELL BOUNDARY TO WEDGE BOUNDARY}

IF (LCELL-LEN)>0 ;
LOOP I 1 N+1 ;
LOOP J 1 N+1 ;
SS1(I,J) := 0;
SS2(I,J) :=-1*S1(I,J) ;
ENDLOOP ;

```

```

ENDLOOP ;

WL SS1 SS2 N 0 (LCELL-LEN)/2 LF ; {GET PATHS TRAVELED}
LF1(1) :=LF ; {REFERENCE TIME}

POLVAL 1 LF1 1 V 6 PATH 1 ;
V1(1) :=V1(1)+PATH(1)*V1(2)/SQRT(V1(6)^2-MASS^2) ;
V1(3) :=V1(3)+PATH(1)*V1(4)/SQRT(V1(6)^2-MASS^2) ;
V1(5) :=V1(5)+PATH(1)/(299792458*SQRT(V1(6)^2-MASS^2)/V1(6)) ;
DT0 := DT0+(LCELL-LEN)/(2*V01) ; {REFERENCE TIME}

ENDIF ;

{-----}

{PROPAGATE THROUGH ABSORBER}

SUBLEN :=LEN/SPLIT ;
SUBCELL :=LCELL/SPLIT ;
LOOP K 1 SPLIT ;
LOOP I 1 N+1 ;
LOOP J 1 N+1 ;
SS1(I,J) :=(1-(K-1)/SPLIT)*S1(I,J)-(K-1)/SPLIT*S2(I,J) ;
SS2(I,J) :=-(1-K/SPLIT)*S1(I,J)+K/SPLIT*S2(I,J) ;
ENDLOOP ;
ENDLOOP ; {END I,J SUBABSORBER LOOPS}

WL SS1 SS2 N 0 SUBLEN LF ; {FIND DISTANCE TRAVELED}
LF1(1) :=LF ;
POLVAL 1 LF1 1 V 6 PATH 1 ; {PATH =DETERMINISTIC LENGTH}
SAVNUM := 0;
IF ((LCELL-LEN)=0)*(K=SPLIT) ; {ONLY SAVE ON LAST SPLIT}
SAVNUM :=SAV ;

```

```

ENDIF ;

STOABS V1 MASS PATH(1) BETHEBLOHC RADLEN V1 SAVNUM APERTURE NPART ;
UM ;

WA SS1 SS2 N SUBLEN APERTURE ; {UPDATE REFERENCE PARTICLE}

UM ;

V02 := CONS(V0) ; {NEW REFERENCE VELOCITY}

DT0 := DT0+(V02-V01)*2*SUBLEN/(V02^2-V01^2) ;{NEW REFERENCE TIME}

ENDLOOP ; {END K LOOP}

```

{-----}

{PROPAGATE PARTICLES FROM WEDGE BOUNDARY TO CELL BOUNDARY}

```

IF (LCELL-LEN)>0 ;

LOOP I 1 N+1 ;
    LOOP J 1 N+1 ;
        SS1(I,J) :=-1*S2(I,J) ;
        SS2(I,J) := 0;
    ENDLOOP ;
ENDLOOP ;

WL SS1 SS2 N 0 (LCELL-LEN)/2 LF ;
LF1(1) :=LF ;
POLVAL 1 LF1 1 V 6 PATH 1 ;
STOABS V1 MASS PATH(1) ZEROES 0 V1 SAV APERTURE NPART ;
DT0 := DT0+(LCELL-LEN)/(2*V02) ;
ENDIF ;

```

{-----}

{XFORM BACK TO COSY COORDINATES}

```

V(1) :=V1(1) ;
V(2) :=V1(2)/CONS(P0) ;
V(3) :=V1(3) ;
V(4) :=V1(4)/CONS(P0) ;
V(6) :=(V1(6)-CONS(M0)*AMUMEV)/CONS(E0)-1 ;
GAM2(1) :=V1(6)/(CONS(M0)*AMUMEV) ;
V(5) :=(DT0-V1(5))*V02*GAM2(1)/(1+GAM2(1)) ;
V(5) :=V(5)+L1(1)*V02*GAM2(1)*(1+GAM1(1))/(V01*GAM1(1)*(1+GAM2(1))) ;
ENDPROCEDURE ;
SAVE 'COSY' ;

```

### G.3 FORTRAN

```

SUBROUTINE STOABS(IV1,IMA,IL,IBB,IRA,IV2,ISA,IAP,INP)
!      CALCULATES CONSTANTS FIRST WITHOUT INITIALIZING VECTORS
!
!      FOR EXPLANATION OF TERMS AND DERIVATIONS OF THEORETICAL
!      MODELS USED, PLEASE SEE JOSIAH KUNZ DISSERTATION 2016.
IMPLICIT DOUBLE PRECISION (A-H,O-Z)
DOUBLE PRECISION MASS
DOUBLE PRECISION BETHEBLOCHC(6)
INTEGER SAV,NPART
!-----MEMORY MANAGEMENT -----
PARAMETER(LMEM=1000000000,LVAR=100000000,LDIM=10000)
INTEGER NTYP(LVAR),NBEG(LVAR),NEND(LVAR),NMAX(LVAR),
*          NC(LMEM),NDIM(LDIM)

```

```

DOUBLE PRECISION CC(LMEM)

COMMON NTYP,NBEG,NEND,NMAX, CC,NC, NDIM, IDIM, IVAR,IMEM
COMMON /TYID/ NRE,NST,NLO,NCM,NVE,NIN,NIV,NDA,NCD,NTM,NGR

!
IF(NTYP(IMA).NE.NRE) CALL FOXNTY(IMA)
IF(NTYP(IAP).NE.NRE) CALL FOXNTY(IAP)
IF(NTYP(IRA).NE.NRE) CALL FOXNTY(IRA)
IF(NTYP(INP).NE.NRE) CALL FOXNTY(INP)

!
MASS = CC(NBEG(IMA))
RADLEN = CC(NBEG(IRA))
SAV = NINT(CC(NBEG(ISA)))
APE = CC(NBEG(IAP))
NPART = CC(NBEG(INP))

DO 5 I=0,6
    BETHEBLOCHC(I) = CC(NBEG(IBB+I))
5 CONTINUE
CALL STORUN(IV1,MASS,IL,BETHEBLOCHC,RADLEN,IV2,SAV,APE,NPART)
RETURN
END

! ****
SUBROUTINE STORUN(IV1,MASS,IL,BETHEBLOCHC,RADLEN,IV2,SAV,APE,
& NPART)
! TAKES PARTICLE VECTOR V1 = (X,PX,Y,PY,TOF,EI)
! THROUGH ABSORBER OF LENGTH L. THE ABSORBER HAS PROPERTIES
! DESCRIBED BY THE BETHEBLOCH ARRAY AND A RADIATION LENGTH
! OF RADLEN. OUTPUT IS THE VECTOR V2.

```

```

IMPLICIT DOUBLE PRECISION (A-H,O-Z)

DOUBLE PRECISION IP,LO,LAMBAR,LAMMAX,LATDIS,LO,MASS,MASSE,
& MAXSTEP,MPL,NA,L

DOUBLE PRECISION BETHEBLOCHC(6),MP(6),THOA(6),DA(6), BAR(6)
DOUBLE PRECISION, DIMENSION(:), ALLOCATABLE :: LV !LV(NPART)
DOUBLE PRECISION, DIMENSION(:, :), ALLOCATABLE :: V1 !V1(NPART,6)

INTEGER FLAG,I,J,LDK,LCNT,LIT,NPART,SAV

!-----MEMORY MANAGEMENT -----
PARAMETER(LMEM=1000000000,LVAR=100000000,LDIM=10000)
INTEGER NTYP(LVAR),NBEG(LVAR),NEND(LVAR),NMAX(LVAR),
* NC(LMEM),NDIM(LDIM)
DOUBLE PRECISION CC(LMEM)
COMMON NTYP,NBEG,NEND,NMAX, CC,NC, NDIM, IDIM, IVAR,IMEM
COMMON /TYID/ NRE,NST,NLO,NCM,NVE,NIN,NIV,NDA,NCD,NTM,NGR
!

INTEGER IAllocateStatus,IAllocateStatus2
ALLOCATE(LV(NPART+10),Stat=IAllocateStatus)
ALLOCATE(V1(NPART+10,7),Stat=IAllocateStatus2)

IF (IAllocateStatus /= 0) STOP "*** Not enough memory ***"
IF (IAllocateStatus2 /= 0) STOP "*** Not enough memory ***"

MP(1) = BETHEBLOCHC(1)      !Z NUMBER
MP(2) = BETHEBLOCHC(2)      !ATOMIC MASS IN g/mol
MP(3) = BETHEBLOCHC(3)*1E6 !DENSITY IN g/m^3

```

```

MP(4) = BETHEBLOCHC(4)      !IONIZATION POTENTIAL IN MeV
MP(5) = BETHEBLOCHC(5)      !DENSITY CORRECTION PARAMETER
MP(6) = BETHEBLOCHC(6)      !SHELL  CORRECTION PARAMETER

!
! GET INDIVIDUAL PATH LENGTHS AND (X, PX, ...)
!
*****  

DO 7 I=1,NPART
LV(I) = CC(NBEG(IL)+I-1)
DO 6 J=1,6
V1(I,J) = CC(NBEG(IV1+J)+I-1)
6    CONTINUE
7    CONTINUE
!
DO 18 I=1,NPART !START PARTICLE LOOP
X0    = V1(I,1)
PX0   = V1(I,2)
Y0    = V1(I,3)
PY0   = V1(I,4)
TOFO  = V1(I,5)
EIO   = V1(I,6)
LO    = LV(I)
PO    = SQRT(EIO**2-MASS**2)
PZO   = SQRT(PO**2-PX0**2-PY0**2)
!
ORIGINAL ANGLE TO ROTATE BETWEEN FRAMES
THX0 = ASIN(PX0/PO)
THY0 = ASIN(PY0/PO)
!
```

! NOTE THAT ORIGINAL COMPONENTS ARE DENOTED WITH AN '0' (E.G. XO,  
 ! AS IN 'ORIGINAL', NOT ZERO, 0). COMPONENTS ON THIS PARTICULAR  
 ! STEP OF THE SIMULATION WILL HAVE NO SUBSCRIPT (E.G. X).

X = XO

PX = PXO

Y = YO

PY = PYO

TOF = TOFO

EI = EIO

L = LO

P = PO

PZ = PZO

!

! DEFINE PHYSICAL CONSTANTS

! \*\*\*\*

C = 299792458.D0 ! SPEED OF LIGHT IN m/s

EULER = 0.5772156649015329d0

BETA = SQRT(1-(MASS/EI)\*\*2)

GAM = 1/SQRT(1-BETA\*\*2)

MASSE = 0.510998928d0 ! MASS OF ELECTRON IN MeV/c\*\*2

NA = 6.02214129d23 ! AVAGADRO

PLANCK = 1.239842d-12 ! hc IN MeV\*m

RELECTRON = 2.8179403267d-15 ! CLASSICAL ELECTRON RADIUS IN m

A0 = 0.52917721092d-10 ! BOHR IN m

PI = 3.141592653589793d0

!

DZ = 0.D0 ! PATHLENGTH CORRECTION PLACEHOLDER

```

!
!      CHECK FLAGS
!
!      *****
10    CONTINUE

FLAG = 0

IF (EI.LE.MASS .OR. EIO.NE.EIO .OR. LO.NE.LO) THEN
  FLAG = 1  !'PARTICLE STOPPED' FLAG
  GOTO 16  !TERMINATE

ELSEIF (SQRT(X**2+Y**2).GE.APE) THEN
  FLAG = 2  !'PARTICLE HIT APERTURE' FLAG
  GOTO 16

ELSEIF (L.LE.0) THEN
  FLAG = 3  !PARTICLE MISSED ABSORBER COMPLETELY
  GOTO 16

ELSEIF ((MP(1).EQ.0).OR.(MP(2).EQ.0).OR.(MP(3).EQ.0).OR.
&           (MP(4).EQ.0)) THEN
  FLAG = 5  !'DRIFT' FLAG (DEALS WITH Z=0)
  GOTO 16

ENDIF

!
!      L = 2*L/(1+CTH) !TRUE PATHLENGTH CORRECTION PLACEHOLDER
!
!
!
!      STRAGGLING
!
!      *****
15    CONTINUE

DE = STRAG(MASS,EI,L,MP)

```

```

IF ((DE.GE.EI-MASS).OR.(EI.EQ.MASS)) THEN
  FLAG = 1          !PARTICLE STOPPED
  GOTO 16
ENDIF

EI = EI-DE          !NEW TOTAL ENERGY
P = SQRT(EI**2-MASS**2) !NEW TOTAL MOMENTUM
PZ = P*PZO/PO        !ANGLE DID NOT CHANGE
PX = P*PXO/PO
PY = P*PYO/PO

!
! SCATTER
!
*****  

IF (RADLEN.LE.0) RADLEN = 100*716.4/ !CRUDE APPROXIMATION IF
& (RHO*1E-6*Z*(Z+1)*LOG(287/SQRT(Z))) !DO NOT KNOW RAD LEN
!
XD = L*PXO/PZO      !X DETERMINISTIC
YD = L*PYO/PZO

!
! 1ST ORDER HIGHLAND CORRECTION
HC1 = 0.12d0
!
! 2ND ORDER HIGHLAND CORRECTION
HC2 = 0.006d0
!
! CRITICAL ANGLE (LIKE GAUS SIGMA)
TH0 = 13.6/(BETA*P)*SQRT(L/RADLEN*
& (1+HC1*LOG(L/RADLEN)+HC2*
& (LOG(L/RADLEN)**2))
!
```

```

! PZ ROTATED, NOT IN LAB FRAME YET

PZR = SCATDIST(TH0,P)

! PT ROTATED

PTR = SQRT(P**2-PZR**2)

! DISTRIBUTE ROTATED PT INTO ROTATED PX, PY

CALL RANDOM_NUMBER(R1)

R1=R1*2*PI

PXR=PTR*SIGN(COS(R1),R1-PI)

PYR=PTR*SIN(R1)

!SCATTERED X ANGLE = ASIN(PXR/P)

PX=P*SIN(ASIN(PXR/P)+THX0)

PY=P*SIN(ASIN(PYR/P)+THY0)

!

! TRANSVERSE DISPLACEMENT

! ****

THETAC = 13.6/(BETA*P)*SQRT(1/RADLEN)

! AMOUNT OF DEFLECTION IN X

ANGDIF = ASIN(PX/P)-ASIN(PX0/PO)

! SHIFT+DETERMINISTIC+FLUCTUATION

X = X+XD+LATDIS(ANGDIF,L,THETAC)

ANGDIF = ASIN(PY/P)-ASIN(PY0/PO)

Y = Y+YD+LATDIS(ANGDIF,L,THETAC)

TOF = TOF+DTOF(EI0,P,MASS,L+DZ)

! CHECK FLAGS AGAIN

IF (FLAG.EQ.0) THEN

IF (EI.LE.MASS) THEN

```

```

!      'PARTICLE STOPPED' FLAG

FLAG = 1

ELSEIF (SQRT(X**2+Y**2).GE.APE) THEN

!      'PARTICLE HIT APERTURE' FLAG

FLAG = 2

ENDIF

ENDIF

16  CONTINUE

!      'PARTICLE MISSED ABSORBER' OR 'DRIFT' FLAG

IF ((FLAG.EQ.3).OR.(FLAG.EQ.5)) THEN

EI = EIO

X = X0+LO*PX0/PO

Y = Y0+LO*PY0/PO

TOF = TOFO+LO/(C*SQRT(EI**2-MASS**2)/EI)

!      STOPPED, APERTURE, OR DECAY

ELSEIF ((FLAG.EQ.1).OR.(FLAG.EQ.2).OR.(FLAG.EQ.4)) THEN

X = 0.DO

PX = 0.DO

Y = 0.DO

PY = 0.DO

TOF = 0.DO

EI = 0.DO

ENDIF

CC(NBEG(IV1+1)+I-1) = X

CC(NBEG(IV1+2)+I-1) = PX

CC(NBEG(IV1+3)+I-1) = Y

CC(NBEG(IV1+4)+I-1) = PY

```

```

CC(NBEG(IV1+5)+I-1) = TOF
CC(NBEG(IV1+6)+I-1) = EI
IF (SAV.GT.0) THEN
  WRITE(SAV,20) X,PX,Y,PY,TOF,EI,FLAG
ENDIF
20 FORMAT(6E22.14,I5)
21 FORMAT(1A3)
18 CONTINUE
RETURN
END

! ****
FUNCTION STRAG(MASS,EIO,LO,MP)
! DETERMINES ENERGY LOSS OF A PARTICLE TRAVELLING THROUGH
! ABSORBER WITH ALPHALAN AS THE APPROXIMATE MEAN ENERGY LOSS,
! XI AS A SCALING PARAMETER, DMAX AS THE MAXIMUM ENERGY LOSS
! (FOR THE LANDAU DISTRIBUTION), EMAX AS THE MAXIMUM ENERGY
! LOSS PER INTERACTION, AND BETA*C AS THE INCIDENT SPEED OF
! THE PARTICLE.

IMPLICIT DOUBLE PRECISION (A-H,O-Z)
DOUBLE PRECISION MP(6)
DOUBLE PRECISION PAR(6)
DOUBLE PRECISION IP,L,LAMBAR,LAMBARI,LAMMAX,LAMMAXI,LANDAU,
&           LANDAU2,LO,LLI,MASS,MASSE,NA
INTEGER J,K
!
!
! DEFINE PHYSICAL CONSTANTS

```

```
! ****
EULER = 0.5772156649015329d0
BETA = SQRT(1-(MASS/EI)**2)
GAM = 1/SQRT(1-BETA**2)
MASSE = 0.510998928d0      !MASS OF ELECTRON IN MeV/c**2
NA = 6.02214129d23        !AVAGADRO
PLANCK = 1.239842d-12      !hc IN MeV*m
RELECTRON = 2.8179403267d-15 !CLASSICAL ELECTRON RADIUS IN m
A0 = 0.52917721092d-10     !BOHR IN m
PI = 3.141592653589793d0
!
! LANDAU LAMBDA CUTOFF PARAMETERS
PAR = (/ 0.517891D0, 1.17765D0, 0.476074D0, 0.00880733D0,
&           1.15467D0 , 0.984008D0 /)
!
! DEFINE SPECIFIC MATERIAL CONSTANTS FOR ENERGY LOSS
! ****
Z   = MP(1)
A   = MP(2)
RHO = MP(3)
IP  = MP(4)
DCP = MP(5)
SCP = MP(6)
!
! CALL FLAGS FOR CALCULATING DENSITY, SHELL PARAMETERS
! ****
DF = 0.D0
SF = 0.D0
```

```

IF (DCP.EQ.0) DF = 1 !USER DID NOT SUPPLY CORRECTION PARAMETER
IF (SCP.EQ.0) SF = 1 !SO WE WILL APPROXIMATE
!
! CAN ONLY CALCULATE ONE STEP AT A TIME, SINCE E IS DYNAMIC
! (CANNOT SIMPLY SPLIT ABSORBER INTO EVEN PIECES).
! THAT IS, IF E IS TOO HIGH THE STEP MAY NOT BE A 'LANDAU' STEP
! ANYMORE, INVALIDATING THE THEORY.
!
CUL = 0.D0 !CUMULATIVE LENGTH
DE = 0.D0 !ENERGY LOSS
!
DO 25 WHILE (CUL.LT.L0) !LOOP THROUGH LANDAU-EXCLUSIVE STEPS
EF = E10-DE
GAM = EF/MASS
BETA = SQRT(1-1/GAM**2)
!
! DISABLE CRUDE APPROXIMATION FOR NOW
!
! IF (DF.NE.0) DCP = GET_DCP(BETA*GAM,MP)
! IF (SF.NE.0) SCP = GET_SCP(BETA*GAM,MP)
EMAX = 2*MASSE*(BETA*GAM)**2/(1+2*GAM*MASSE/MASS+
& (MASSE/MASS)**2)
J = 0
!
! FIND L WHICH WILL PRODUCE A LANDAU ENERGY PROFILE
!
*****DO 5 WHILE ((XI/EMAX>0.01D0).OR.(J<1))
J = J+1
L = L0/J
XI = 2*PI*RELECTRON**2*MASSE*NA*Z*RHO*L/(A*BETA**2)

```

```

    IF (J>10000) THEN !PARTICLE IS GOING TOO SLOW, FAIL IT

    STRAG = EI0+1

    RETURN

    ENDIF

5    CONTINUE

!

CUL = CUL+L

!

IF (CUL.GT.L0) THEN !ONLY USED ON THE FINAL STEP

    L = L0-(CUL-L)

    XI = 2*PI*RELECTRON**2*MASSE*NA*Z*RHO*L/(A*BETA**2)

    ENDIF

    IF (L.LE.0) GOTO 25 !PRECISION ERROR

!

!      NOW PROPAGATE PARTICLE THROUGH L

!

*****  

EBAR = XI*(LOG(2*MASSE*(BETA*GAM/IP)**2*EMAX)-2*BETA**2-DCP-
& SCP)

ALPHALAN = EBAR+XI*(BETA**2+LOG(XI/EMAX)+1-EULER)

LAMBAR = -(1-EULER)-BETA**2-LOG(XI/EMAX)

LAMMAX = PAR(1)+PAR(2)*LAMBAR+(PAR(3)+PAR(4)*LAMBAR)*

&           EXP(PAR(5)+PAR(6)*LAMBAR)

DEMAX = XI*(LAMMAX+1-EULER+BETA**2+LOG(XI/EMAX))+EBAR

DE = DE+LANDAU(ALPHALAN,XI,DEMAX)

25    CONTINUE

STRAG = DE

RETURN

```

```

END

! ****
REAL FUNCTION LANDAU(MEAN,SIGMA,DEMAX)
! Generate a random number following a Landau distribution
! with Landau parameters alphalan = mean, betalan= xi = sigma.
!
! This is a copy from the source file TRandom from SLAC.
! Originally converted by Rene Brun from CERNLIB routine
! ranlan(G110).

IMPLICIT DOUBLE PRECISION (A-H,O-Z)

DOUBLE PRECISION MEAN

INTEGER I,J,seed

DOUBLE PRECISION F(982)

F = (/
& 0. , 0 , 0 , 0 , 0 , -2.244733 ,
& -2.204365, -2.168163, -2.135219, -2.104898, -2.076740, -2.050397,
& -2.025605, -2.002150, -1.979866, -1.958612, -1.938275, -1.918760,
& -1.899984, -1.881879, -1.864385, -1.847451, -1.831030, -1.815083,
& -1.799574, -1.784473, -1.769751, -1.755383, -1.741346, -1.727620,
& -1.714187, -1.701029, -1.688130, -1.675477, -1.663057, -1.650858,
& -1.638868, -1.627078, -1.615477, -1.604058, -1.592811, -1.581729,
& -1.570806, -1.560034, -1.549407, -1.538919, -1.528565, -1.518339,
& -1.508237, -1.498254, -1.488386, -1.478628, -1.468976, -1.459428,
& -1.449979, -1.440626, -1.431365, -1.422195, -1.413111, -1.404112,
& -1.395194, -1.386356, -1.377594, -1.368906, -1.360291, -1.351746,
& -1.343269, -1.334859, -1.326512, -1.318229, -1.310006, -1.301843,
& -1.293737, -1.285688, -1.277693, -1.269752, -1.261863, -1.254024,

```

& -1.246235, -1.238494, -1.230800, -1.223153, -1.215550, -1.207990,  
 & -1.200474, -1.192999, -1.185566, -1.178172, -1.170817, -1.163500,  
 & -1.156220, -1.148977, -1.141770, -1.134598, -1.127459, -1.120354,  
 & -1.113282, -1.106242, -1.099233, -1.092255,  
 & -1.085306, -1.078388, -1.071498, -1.064636, -1.057802, -1.050996,  
 & -1.044215, -1.037461, -1.030733, -1.024029, -1.017350, -1.010695,  
 & -1.004064, -0.997456, -0.990871, -0.984308, -0.977767, -0.971247,  
 & -0.964749, -0.958271, -0.951813, -0.945375, -0.938957, -0.932558,  
 & -0.926178, -0.919816, -0.913472, -0.907146, -0.900838, -0.894547,  
 & -0.888272, -0.882014, -0.875773, -0.869547, -0.863337, -0.857142,  
 & -0.850963, -0.844798, -0.838648, -0.832512, -0.826390, -0.820282,  
 & -0.814187, -0.808106, -0.802038, -0.795982, -0.789940, -0.783909,  
 & -0.777891, -0.771884, -0.765889, -0.759906, -0.753934, -0.747973,  
 & -0.742023, -0.736084, -0.730155, -0.724237, -0.718328, -0.712429,  
 & -0.706541, -0.700661, -0.694791, -0.688931, -0.683079, -0.677236,  
 & -0.671402, -0.665576, -0.659759, -0.653950, -0.648149, -0.642356,  
 & -0.636570, -0.630793, -0.625022, -0.619259, -0.613503, -0.607754,  
 & -0.602012, -0.596276, -0.590548, -0.584825, -0.579109, -0.573399,  
 & -0.567695, -0.561997, -0.556305, -0.550618, -0.544937, -0.539262,  
 & -0.533592, -0.527926, -0.522266, -0.516611, -0.510961, -0.505315,  
 & -0.499674, -0.494037, -0.488405, -0.482777,  
 & -0.477153, -0.471533, -0.465917, -0.460305, -0.454697, -0.449092,  
 & -0.443491, -0.437893, -0.432299, -0.426707, -0.421119, -0.415534,  
 & -0.409951, -0.404372, -0.398795, -0.393221, -0.387649, -0.382080,  
 & -0.376513, -0.370949, -0.365387, -0.359826, -0.354268, -0.348712,  
 & -0.343157, -0.337604, -0.332053, -0.326503, -0.320955, -0.315408,  
 & -0.309863, -0.304318, -0.298775, -0.293233, -0.287692, -0.282152,

& - .276613, - .271074, - .265536, - .259999, - .254462, - .248926,  
 & - .243389, - .237854, - .232318, - .226783, - .221247, - .215712,  
 & - .210176, - .204641, - .199105, - .193568, - .188032, - .182495,  
 & - .176957, - .171419, - .165880, - .160341, - .154800, - .149259,  
 & - .143717, - .138173, - .132629, - .127083, - .121537, - .115989,  
 & - .110439, - .104889, - .099336, - .093782, - .088227, - .082670,  
 & - .077111, - .071550, - .065987, - .060423, - .054856, - .049288,  
 & - .043717, - .038144, - .032569, - .026991, - .021411, - .015828,  
 & - .010243, - .004656, .000934, .006527, .012123, .017722,  
 & .023323, .028928, .034535, .040146, .045759, .051376,  
 & .056997, .062620, .068247, .073877,  
 & .079511, .085149, .090790, .096435, .102083, .107736,  
 & .113392, .119052, .124716, .130385, .136057, .141734,  
 & .147414, .153100, .158789, .164483, .170181, .175884,  
 & .181592, .187304, .193021, .198743, .204469, .210201,  
 & .215937, .221678, .227425, .233177, .238933, .244696,  
 & .250463, .256236, .262014, .267798, .273587, .279382,  
 & .285183, .290989, .296801, .302619, .308443, .314273,  
 & .320109, .325951, .331799, .337654, .343515, .349382,  
 & .355255, .361135, .367022, .372915, .378815, .384721,  
 & .390634, .396554, .402481, .408415, .414356, .420304,  
 & .426260, .432222, .438192, .444169, .450153, .456145,  
 & .462144, .468151, .474166, .480188, .486218, .492256,  
 & .498302, .504356, .510418, .516488, .522566, .528653,  
 & .534747, .540850, .546962, .553082, .559210, .565347,  
 & .571493, .577648, .583811, .589983, .596164, .602355,  
 & .608554, .614762, .620980, .627207, .633444, .639689,

& .645945, .652210, .658484, .664768,  
& .671062, .677366, .683680, .690004, .696338, .702682,  
& .709036, .715400, .721775, .728160, .734556, .740963,  
& .747379, .753807, .760246, .766695, .773155, .779627,  
& .786109, .792603, .799107, .805624, .812151, .818690,  
& .825241, .831803, .838377, .844962, .851560, .858170,  
& .864791, .871425, .878071, .884729, .891399, .898082,  
& .904778, .911486, .918206, .924940, .931686, .938446,  
& .945218, .952003, .958802, .965614, .972439, .979278,  
& .986130, .992996, .999875, 1.006769, 1.013676, 1.020597,  
& 1.027533, 1.034482, 1.041446, 1.048424, 1.055417, 1.062424,  
& 1.069446, 1.076482, 1.083534, 1.090600, 1.097681, 1.104778,  
& 1.111889, 1.119016, 1.126159, 1.133316, 1.140490, 1.147679,  
& 1.154884, 1.162105, 1.169342, 1.176595, 1.183864, 1.191149,  
& 1.198451, 1.205770, 1.213105, 1.220457, 1.227826, 1.235211,  
& 1.242614, 1.250034, 1.257471, 1.264926, 1.272398, 1.279888,  
& 1.287395, 1.294921, 1.302464, 1.310026, 1.317605, 1.325203,  
& 1.332819, 1.340454, 1.348108, 1.355780,  
& 1.363472, 1.371182, 1.378912, 1.386660, 1.394429, 1.402216,  
& 1.410024, 1.417851, 1.425698, 1.433565, 1.441453, 1.449360,  
& 1.457288, 1.465237, 1.473206, 1.481196, 1.489208, 1.497240,  
& 1.505293, 1.513368, 1.521465, 1.529583, 1.537723, 1.545885,  
& 1.554068, 1.562275, 1.570503, 1.578754, 1.587028, 1.595325,  
& 1.603644, 1.611987, 1.620353, 1.628743, 1.637156, 1.645593,  
& 1.654053, 1.662538, 1.671047, 1.679581, 1.688139, 1.696721,  
& 1.705329, 1.713961, 1.722619, 1.731303, 1.740011, 1.748746,  
& 1.757506, 1.766293, 1.775106, 1.783945, 1.792810, 1.801703,

& 1.810623, 1.819569, 1.828543, 1.837545, 1.846574, 1.855631,  
& 1.864717, 1.873830, 1.882972, 1.892143, 1.901343, 1.910572,  
& 1.919830, 1.929117, 1.938434, 1.947781, 1.957158, 1.966566,  
& 1.976004, 1.985473, 1.994972, 2.004503, 2.014065, 2.023659,  
& 2.033285, 2.042943, 2.052633, 2.062355, 2.072110, 2.081899,  
& 2.091720, 2.101575, 2.111464, 2.121386, 2.131343, 2.141334,  
& 2.151360, 2.161421, 2.171517, 2.181648, 2.191815, 2.202018,  
& 2.212257, 2.222533, 2.232845, 2.243195,  
& 2.253582, 2.264006, 2.274468, 2.284968, 2.295507, 2.306084,  
& 2.316701, 2.327356, 2.338051, 2.348786, 2.359562, 2.370377,  
& 2.381234, 2.392131, 2.403070, 2.414051, 2.425073, 2.436138,  
& 2.447246, 2.458397, 2.469591, 2.480828, 2.492110, 2.503436,  
& 2.514807, 2.526222, 2.537684, 2.549190, 2.560743, 2.572343,  
& 2.583989, 2.595682, 2.607423, 2.619212, 2.631050, 2.642936,  
& 2.654871, 2.666855, 2.678890, 2.690975, 2.703110, 2.715297,  
& 2.727535, 2.739825, 2.752168, 2.764563, 2.777012, 2.789514,  
& 2.802070, 2.814681, 2.827347, 2.840069, 2.852846, 2.865680,  
& 2.878570, 2.891518, 2.904524, 2.917588, 2.930712, 2.943894,  
& 2.957136, 2.970439, 2.983802, 2.997227, 3.010714, 3.024263,  
& 3.037875, 3.051551, 3.065290, 3.079095, 3.092965, 3.106900,  
& 3.120902, 3.134971, 3.149107, 3.163312, 3.177585, 3.191928,  
& 3.206340, 3.220824, 3.235378, 3.250005, 3.264704, 3.279477,  
& 3.294323, 3.309244, 3.324240, 3.339312, 3.354461, 3.369687,  
& 3.384992, 3.400375, 3.415838, 3.431381, 3.447005, 3.462711,  
& 3.478500, 3.494372, 3.510328, 3.526370,  
& 3.542497, 3.558711, 3.575012, 3.591402, 3.607881, 3.624450,  
& 3.641111, 3.657863, 3.674708, 3.691646, 3.708680, 3.725809,

& 3.743034, 3.760357, 3.777779, 3.795300, 3.812921, 3.830645,  
& 3.848470, 3.866400, 3.884434, 3.902574, 3.920821, 3.939176,  
& 3.957640, 3.976215, 3.994901, 4.013699, 4.032612, 4.051639,  
& 4.070783, 4.090045, 4.109425, 4.128925, 4.148547, 4.168292,  
& 4.188160, 4.208154, 4.228275, 4.248524, 4.268903, 4.289413,  
& 4.310056, 4.330832, 4.351745, 4.372794, 4.393982, 4.415310,  
& 4.436781, 4.458395, 4.480154, 4.502060, 4.524114, 4.546319,  
& 4.568676, 4.591187, 4.613854, 4.636678, 4.659662, 4.682807,  
& 4.706116, 4.729590, 4.753231, 4.777041, 4.801024, 4.825179,  
& 4.849511, 4.874020, 4.898710, 4.923582, 4.948639, 4.973883,  
& 4.999316, 5.024942, 5.050761, 5.076778, 5.102993, 5.129411,  
& 5.156034, 5.182864, 5.209903, 5.237156, 5.264625, 5.292312,  
& 5.320220, 5.348354, 5.376714, 5.405306, 5.434131, 5.463193,  
& 5.492496, 5.522042, 5.551836, 5.581880, 5.612178, 5.642734,  
& 5.673552, 5.704634, 5.735986, 5.767610,  
& 5.799512, 5.831694, 5.864161, 5.896918, 5.929968, 5.963316,  
& 5.996967, 6.030925, 6.065194, 6.099780, 6.134687, 6.169921,  
& 6.205486, 6.241387, 6.277630, 6.314220, 6.351163, 6.388465,  
& 6.426130, 6.464166, 6.502578, 6.541371, 6.580553, 6.620130,  
& 6.660109, 6.700495, 6.741297, 6.782520, 6.824173, 6.866262,  
& 6.908795, 6.951780, 6.995225, 7.039137, 7.083525, 7.128398,  
& 7.173764, 7.219632, 7.266011, 7.312910, 7.360339, 7.408308,  
& 7.456827, 7.505905, 7.555554, 7.605785, 7.656608, 7.708035,  
& 7.760077, 7.812747, 7.866057, 7.920019, 7.974647, 8.029953,  
& 8.085952, 8.142657, 8.200083, 8.258245, 8.317158, 8.376837,  
& 8.437300, 8.498562, 8.560641, 8.623554, 8.687319, 8.751955,  
& 8.817481, 8.883916, 8.951282, 9.019600, 9.088889, 9.159174,

```

& 9.230477, 9.302822, 9.376233, 9.450735, 9.526355, 9.603118,
& 9.681054, 9.760191, 9.840558, 9.922186, 10.005107, 10.089353,
& 10.174959, 10.261958, 10.350389, 10.440287, 10.531693, 10.624646,
& 10.719188, 10.815362, 10.913214, 11.012789, 11.114137, 11.217307,
& 11.322352, 11.429325, 11.538283, 11.649285,
& 11.762390, 11.877664, 11.995170, 12.114979, 12.237161, 12.361791,
& 12.488946, 12.618708, 12.751161, 12.886394, 13.024498, 13.165570,
& 13.309711, 13.457026, 13.607625, 13.761625, 13.919145, 14.080314,
& 14.245263, 14.414134, 14.587072, 14.764233, 14.945778, 15.131877,
& 15.322712, 15.518470, 15.719353, 15.925570, 16.137345, 16.354912,
& 16.578520, 16.808433, 17.044929, 17.288305, 17.538873, 17.796967,
& 18.062943, 18.337176, 18.620068, 18.912049, 19.213574, 19.525133,
& 19.847249, 20.180480, 20.525429, 20.882738, 21.253102, 21.637266,
& 22.036036, 22.450278, 22.880933, 23.329017, 23.795634, 24.281981,
& 24.789364, 25.319207, 25.873062, 26.452634, 27.059789, 27.696581,
& 28.365274, 29.068370, 29.808638, 30.589157, 31.413354, 32.285060,
& 33.208568, 34.188705, 35.230920, 36.341388, 37.527131, 38.796172,
& 40.157721, 41.622399, 43.202525, 44.912465, 46.769077, 48.792279,
& 51.005773, 53.437996, 56.123356, 59.103894 /)

J = 0

```

30   CONTINUE

```

IF (SIGMA.LE.0) THEN
  WRITE(6,*) "Error in LANDAU: sigma cannot be less than zero!"
  GOTO 35
ENDIF
CALL RANDOM_NUMBER(X)
!
```

```

U = 1000*X
I = NINT(U)
U = U-I
IF ((I.GE.70.D0).AND.(I.LT.800.D0)) THEN
  RANLAN = F(I) + U*(F(I+1)-F(I))
ELSEIF ((I.GE.7.D0).AND.(I.LE. 980.D0)) THEN
  RANLAN = F(I) + U*(F(I+1)-F(I)-0.25*(1-U)*(F(I+2)-F(I+1)-F(I)
&           +F(I-1)));
ELSEIF (I.LT.7.D0) THEN
  V = LOG(X)
  U = 1/V
  RANLAN = ((0.99858950+(3.45213058E1+1.70854528E1*U)*U)/
&           (1           +(3.41760202E1+4.01244582 *U)*U))**
&           (-LOG(-0.91893853-V)-1);
ELSE
  U = 1-X
  V = U*U
  IF (X.LE.0.999D0) THEN
    RANLAN = (1.00060006+2.63991156E2*U+4.37320068E3*V)/
&           ((1           +2.57368075E2*U+3.41448018E3*V)*U)
  ELSE
    RANLAN = (1.00001538+6.07514119E3*U+7.34266409E5*V)/
&           ((1           +6.06511919E3*U+6.94021044E5*V)*U);
  ENDIF
ENDIF
LANDAU = MEAN+SIGMA*RANLAN
J = J+1

```

```

!REPICK AT MOST 100 TIMES

IF ((ABS(LANDAU).GT.ABS(DEMAX)).AND.(J.LE.100)) GOTO 30

35  CONTINUE

RETURN

END

! ****
FUNCTION GAURAN(AVG,SIG)

! SIMPLE GAUSSIAN GENERATOR

IMPLICIT DOUBLE PRECISION (A-H,O-Z)

IF (SIG.EQ.0) THEN

GAURAN = AVG

RETURN

ENDIF

45  CONTINUE

CALL RANDOM_NUMBER(R1)

IF (R1.EQ.0) GOTO 45

CALL RANDOM_NUMBER(R2)

R2 = R2*6.283185

GAURAN = AVG+SIG*SIN(R2)*SQRT(-2*LOG(R1))

RETURN

END

! ****
SUBROUTINE GAUVEC(IPV,IPN,IV,IN)

! SIMPLE GAUSSIAN GENERATOR. OUTPUT IS ARRAY X.

IMPLICIT DOUBLE PRECISION (A-H,O-Z)

INTEGER I,N

!----MEMORY MANAGEMENT -----

```

```

PARAMETER(LMEM=1000000000,LVAR=100000000,LDIM=10000)
INTEGER NTYP(LVAR),NBEG(LVAR),NEND(LVAR),NMAX(LVAR),
*      NC(LMEM),NDIM(LDIM)
DOUBLE PRECISION CC(LMEM)
COMMON NTYP,NBEG,NEND,NMAX, CC,NC, NDIM, IDIM, IVAR, IMEM
COMMON /TYID/ NRE,NST,NLO,NCM,NVE,NIN,NIV,NDA,NCD,NTM,NGR
!
!      CONSISTENCY CHECKS AND PREPARATION
!
*****  

IF(NTYP(IN) .NE.NRE) CALL FOXNTY(IN)
IF(NTYP(IPN).NE.NRE) CALL FOXNTY(IPN)
!
!      GET PARTICLE VARS
!
*****  

N    = NINT(CC(NBEG(IN)))
PN   = NINT(CC(NBEG(IPN)))
DO 7 I=1,N
  DO 6 J=1,PN
    ! V(I,J)=GAURAN(PV(J),PV(J+1))
    AVG=CC(NBEG(IPV+2*J-1))
    SIG=CC(NBEG(IPV+2*J))
    CC(NBEG(IV+J)+I-1)=GAURAN(AVG,SIG)
6    CONTINUE
7    CONTINUE
!
RETURN

```

```

END

! ****
SUBROUTINE GAUS(IAV,ISI,IX,IN)
! NOTE: DOES NOT WORK
! SIMPLE GAUSSIAN GENERATOR. OUTPUT IS ARRAY X.
IMPLICIT DOUBLE PRECISION (A-H,O-Z)
INTEGER I,N
!-----MEMORY MANAGEMENT -----
PARAMETER(LMEM=1000000000,LVAR=100000000,LDIM=10000)
INTEGER NTYP(LVAR),NBEG(LVAR),NEND(LVAR),NMAX(LVAR),
* NC(LMEM),NDIM(LDIM)
DOUBLE PRECISION CC(LMEM)
COMMON NTYP,NBEG,NEND,NMAX, CC,NC, NDIM, IDIM, IVAR,IMEM
COMMON /TYID/ NRE,NST,NLO,NCM,NVE,NIN,NIV,NDA,NCD,NTM,NGR
!
! CONSISTENCY CHECKS AND PREPARATION
! ****
IF(NTYP(IAV).NE.NRE) CALL FOXNTY(IAV)
IF(NTYP(ISI).NE.NRE) CALL FOXNTY(ISI)
IF(NTYP(IN) .NE.NRE) CALL FOXNTY(IN)
!
! GET PARTICLE VARS
! ****
AVG = CC(NBEG(IAV))
SIG = CC(NBEG(ISI))
N   = NINT(CC(NBEG(IN)))
!
```

```

DO 47 I=1,N
  IF (SIG.EQ.0) THEN
    X=AVG
  ELSE
    46  CONTINUE
    CALL RANDOM_NUMBER(R1)
    IF (R1.EQ.0) GOTO 46
    CALL RANDOM_NUMBER(R2)
    R2 = R2*6.283185
    X = AVG+SIG*SIN(R2)*SQRT(-2*LOG(R1))
  ENDIF
  CC(NBEG(IX+1)+I-1) = X
47  CONTINUE
RETURN
END

! ****
FUNCTION SCATDIST(TH0,P)
IMPLICIT DOUBLE PRECISION (A-H,O-Z)
DOUBLE PRECISION MASS
INTEGER I,J,N
A = 0.5/(1-COS(TH0))
MASS = 105.6583715
E = SQRT(P**2+MASS**2)
GAM = E/MASS
BETA = SQRT(1-1/GAM**2)
BG2 = (BETA*GAM)**2
XI1 = 4.5d0 !EMPERICAL CUTOFF BETWEEN DISTRIBUTIONS

```

```

D = 2.d0      !POWER IN DENOMINATOR (I.E. ~ 1/U^D)

U0 = 1-XI1/A

A1 = -A*BG2   !SEE THESIS

A2 = BG2*(1-D)-2*A

A3 = BG2*(A-D-1)+2*(A-D)

B = U0+(A2+SQRT(A2**2-4*A1*A3))/(2*A1)

ZETA = EXP(-A*(1-U0))*(1-U0+B)**D/(1+0.5*BG2*(1+U0-B))

G0 = ZETA*((1+BG2)*(1/(1-U0+B)-1/(2+B))+BG2/2*LOG((1-U0+B)/
& (2+B)))

GMAX = G0+(1-EXP(-A*(1-U0)))/A

CALL RANDOM_NUMBER(G)

G = G*GMAX

!

! USE GAUSSIAN -GENERATION VIA INVERSION

IF (G.GT.G0) THEN

U = 1+LOG(A*(G-G0)+EXP(-A*(1-U0)))/A

! USE MOTT -GENERATION VIA BISECTION METHOD

ELSE

ACC = 1.D-8          !+- BINWIDTH OF g (ACCURACY)

UMAX = U0

UMIN = -1

80 CONTINUE

U = (UMAX+UMIN)/2

! 'G' UPPER-CASE' GENERATOR-CDF NOT PDF

TEST = GUC_TAIL(U,ZETA,B,BG2)

IF (TEST.GT.G*(1+ACC)) UMAX = U

IF (TEST.LT.G*(1-ACC)) UMIN = U

```

```

    IF (NOT((TEST.GE.G*(1-ACC)).AND.(TEST.LE.G*(1+ACC)))) GOTO 80

ENDIF

85   CONTINUE

!

SCATDIST = P*U

RETURN

END

! ****
FUNCTION GLC_TAIL(U,ZETA,B,BG2)

! RETURNS THE TAIL OF THE PDF OF THE SCATTERING FUNCTION
! GIVEN THE SCALE, SHIFT, AND ENERGY.

IMPLICIT DOUBLE PRECISION (A-H,O-Z)

GLC_TAIL = ZETA*(1+0.5*BG2+(1+U-B))/((1-U+B)**2)

RETURN

END

! ****
FUNCTION GUC_TAIL(U,ZETA,B,BG2)

! RETURNS THE TAIL OF THE CDF OF THE SCATTERING FUNCTION
! GIVEN THE SCALE, SHIFT, AND ENERGY.

IMPLICIT DOUBLE PRECISION (A-H,O-Z)

GUC_TAIL = ZETA*((1+BG2)*(1/(1-U+B)-1/(2+B))+BG2/2*LOG
& ((1-U+B)/(2+B)))

RETURN

END

! ****
REAL FUNCTION LATDIS(THETA,Z,THC)

! RETURNS TRANSVERSE COORDINATE. BASED ON FERNOW AND

```

```

!      GALLARDO, "Muon transverse ionization cooling:
!      Stochastic approach", PHYS. REV. E 52 1039 (1995).
!      THETA IS FLUCTUATION (I.E. THETA-THETAO), Z IS ABS
!      LENGTH, AND THC IS CRITICAL ANGLE COEFFICIENT.

      IMPLICIT DOUBLE PRECISION (A-H,O-Z)

      DOUBLE PRECISION MU

      MU = THETA*Z/1.8

      SIG = THETAC/(2*SQRT(3.))

      LATDIS = GAURAN(MU,SIG)

      RETURN

      END

! ****

      FUNCTION DTOF(EI,P2,MASS,L)
!      RETURNS THE TEMPORAL DISPLACEMENT CORRECTION ASSUMING
!      AN INITIAL STRAIGHT TRAJECTORY (I.E. PZ = P).

      IMPLICIT DOUBLE PRECISION (A-H,O-Z)

      DOUBLE PRECISION L,MASS

      C = 299792458.D0           ! m/s

      P1 = SQRT(EI**2-MASS**2)

      DTOF = (P2/SQRT(P2**2+MASS**2)-P1/SQRT(P1**2+MASS**2))
      &      *2*L/(C*(P2**2/(P2**2+MASS**2)-P1**2/(P1**2
      &      +MASS**2)))

      RETURN

      END

! ****

      INTEGER FUNCTION DECAY(GAM1,GAM2,TOF)
!      RETURNS 4 IF PARTICLE DECAY OCCURED OR ZERO OTHERWISE.

```

```

IMPLICIT DOUBLE PRECISION (A-H,O-Z)

TAU = 2.197034D-6          !MEAN LIFETIME IN [s]

GAM = (GAM1+GAM2)/2        !AVG GAMMA; PROBLEM FOR LARGE STEPS

T    = TOF/GAM

CALL RANDOM_NUMBER(R1)

TEST = EXP(-T/TAU)

DECAY = 0

IF (R1.GT.TEST) DECAY = 4

RETURN

END

! ****
FUNCTION GET_DCP(ETA,MP)

IMPLICIT DOUBLE PRECISION(A-H,O-Z)

DOUBLE PRECISION KDE, MP(6)

! ADOPT DENSITY EFFECT PARAMETER FROM PDG:

! pdg.web.cern.ch/pdg/2013/AtomicNuclearProperties/adndt.pdf

! I HAVE YET TO IMPLEMENT THE 'CONDUCTORS' PORTION

HWP = 28.816*SQRT(MP(3)/(1.E6)*MP(1)/MP(2))*1.E-6 !PLAMSA ENERGY

X   = LOG10(ETA)

C   = 2*LOG(MP(4)/HWP)+1

X0 = 0.2D0

KDE = 3.D0      !K FOR THE DENSITY EFFECT

! DETERMINE X1, X0 FOR SOLIDS, LIQUIDS:

IF (MP(4).GE.0.0001D0) THEN

X1 = 3.D0

IF (C.GE.5.215D0) X0 = 0.326*C-1.5

ELSE

```

```
X1 = 2.D0

IF (C.GE.3.681D0) X0 = 0.326*C-1.0

ENDIF

! DETERMINE X1, X0 FOR GASSES:

! YET TO IMPLEMENT STATE DISTINCTION FOR COSY!

! ****
! X1 = 4.D0 !DEFAULT

! IF (C.GE.13.804D0) THEN

! X0 = 0.326*C-1.5

! X1 = 5.D0

! ELSEIF (C.GE.12.25) THEN

! X0 = 2.D0

! X1 = 5.D0

! ELSEIF (C.GE.11.50) THEN

! X0 = 2.D0

! ELSEIF (C.GE.11.00) THEN

! X0 = 1.9D0

! ELSEIF (C.GE.10.50)

! X0 = 1.8D0

! ELSEIF (C.GE.10.00)

! X0 = 1.7D0

! ELSE

! X0 = 1.6D0

! ENDIF

! ADE = (C-2*LOG(10.)*X0)/((X1-X0)**3)

!

! "TABULATED DATA" FOR HYDROGEN IS AT BUBBLE-CHAMBER CONDITIONS.
```

```

! THEREFORE A CORRECTION MUST BE MADE:

R = 1

IF (MP(1)/MP(2).EQ.1.D0/1.008D0) R = MP(3)/(0.060*1.D6)

C = C-LOG(R)

X0 = X0-0.5*LOG10(R)

X1 = X1-0.5*LOG10(R)

!

IF (X.GE.X1) THEN

DCP = 2*LOG(10.)*X-C

ELSEIF (X.GT.X0) THEN

DCP = 2*LOG(10.)*X-C+ADE*(X1-X)**KDE

ELSE

DCP = 0.D0

ENDIF

GET_DCP = DCP

RETURN

END

!
*****  

FUNCTION GET_SCP(ETA, MP)
IMPLICIT DOUBLE PRECISION(A-H,O-Z)
DOUBLE PRECISION BAR(6), MP(6)
!
ADOPT SHELL CORRECTION APPROX BY BARKAS.
!
THIS APPROXIMATION IS OUT OF DATE, AND IS THEREFORE QUITE ROUGH.
!
SEE PDG FOR MORE INFO:
!
pdg.web.cern.ch/pdg/2013/AtomicNuclearProperties/adndt.pdf
!
IF (ETA>0.13D0) THEN !ONLY GOOD FOR ETA>0.13 (MUON: KE = 0.89)
BAR = (/ 0.422377, 0.0304043, -0.00038106, 3.858019,

```

```

&           -0.1667989, 0.00157955 /)

SCP = (BAR(1)/ETA**2+BAR(2)/ETA**4+BAR(3)/ETA**6)*MP(4)**2*1.E6
&     +(BAR(4)/ETA**2+BAR(5)/ETA**4+BAR(6)/ETA**6)*MP(4)**3*1.E9

ENDIF

GET_SCP = SCP

RETURN

END

! ****
REAL FUNCTION MASSBYID(ID)
INTEGER ID
! RETURNS PARTICLE MASS IN MeV BASED ON PDG ID.
! CURRENTLY ONLY SUPPORTS MUONS (13).
IF (ABS(ID).EQ.11) MASSBYID=0.5109989461
IF (ABS(ID).EQ.13) MASSBYID=105.6583715
RETURN
END

! ****
REAL FUNCTION MASSBYIDICOOL(ID)
INTEGER ID
! RETURNS PARTICLE MASS IN MeV BASED ON PDG ID.
! CURRENTLY ONLY SUPPORTS MUONS (2).
IF (ABS(ID).EQ.1) MASSBYIDICOOL=0.5109989461
IF (ABS(ID).EQ.2) MASSBYIDICOOL=105.6583715
RETURN
END

! ****
SUBROUTINE RG4BL(IFILE, INPART, IV)

```

```

IMPLICIT DOUBLE PRECISION(A-H,O-Z)

INTEGER I

DOUBLE PRECISION MASSBYID

! READS PARTICLES FROM A G4BL-FORMATTED FILE. INPUTS ARE:
! IFILE - THE NUMBER OF THE FILE (E.G. 12 IN 'FORT.12')
! INPART - THE NUMBER OF PARTICLES TO READ
! IV - THE OUTPUT VECTOR
!
! OUTPUT VECTOR IS OF THE FORM
! V = (X,PX,Y,PY,T,E) IN m, MeV, AND s

!-----MEMORY MANAGEMENT -----
PARAMETER(LMEM=1000000000,LVAR=100000000,LDIM=10000)
INTEGER NTYP(LVAR),NBEG(LVAR),NEND(LVAR),NMAX(LVAR),
* NC(LMEM),NDIM(LDIM)
DOUBLE PRECISION CC(LMEM)
COMMON NTYP,NBEG,NEND,NMAX, CC,NC, NDIM, IDIM, IVAR, IMEM
COMMON /TYID/ NRE,NST,NLO,NCM,NVE,NIN,NIV,NDA,NCD,NTM,NGR

! CONSISTENCY CHECKS AND PREPARATION
!
! ****
IF(NTYP(IFILE).NE.NRE) CALL FOXNTY(IFILE)
IF(NTYP(INPART).NE.NRE) CALL FOXNTY(INPART)
!
! GET VARS
!
! ****
FNAME = NINT(CC(NBEG(IFILE)))
NPART = NINT(CC(NBEG(INPART)))

```

```

!
! GET RID OF FIRST THREE LINES
!
! ****
READ(FNAME,*)
READ(FNAME,*)
READ(FNAME,*)

!
! READ THE REST OF THE FILE
!
! ****
DO 5 I=1,NPART
  READ(FNAME,*,END=10) X,Y,Z,PX,PY,PZ,T,PDGID,EID,TID,PID,W
  E=SQRT(PX**2+PY**2+PZ**2+MASSBYID(NINT(PDGID))**2)
  CC(NBEG(IV+1)+I-1)=X/1000
  CC(NBEG(IV+2)+I-1)=PX
  CC(NBEG(IV+3)+I-1)=Y/1000
  CC(NBEG(IV+4)+I-1)=PY
  CC(NBEG(IV+5)+I-1)=T
  CC(NBEG(IV+6)+I-1)=E
5   CONTINUE
10  CONTINUE
END
!
! ****
SUBROUTINE RICOOL(IFILE, INPART, IV)
IMPLICIT DOUBLE PRECISION(A-H,O-Z)
INTEGER I
DOUBLE PRECISION MASSBYID
!
! READS PARTICLES FROM AN ICOOL-FORMATTED FILE. INPUTS ARE:

```

```

!      IFILE - THE NUMBER OF THE FILE (E.G. 12 IN 'FORT.12')

!      INPART - THE NUMBER OF PARTICLES TO READ

!      IV      - THE OUTPUT VECTOR

!

!      OUTPUT VECTOR IS OF THE FORM

!      V = (X,PX,Y,PY,T,E) IN m, MeV, AND s

!-----MEMORY MANAGEMENT -----
PARAMETER(LMEM=1000000000,LVAR=100000000,LDIM=10000)
INTEGER NTYP(LVAR),NBEG(LVAR),NEND(LVAR),NMAX(LVAR),
*          NC(LMEM),NDIM(LDIM)
DOUBLE PRECISION CC(LMEM)
COMMON NTYP,NBEG,NEND,NMAX, CC,NC, NDIM, IDIM, IVAR,IMEM
COMMON /TYID/ NRE,NST,NLO,NCM,NVE,NIN,NIV,NDA,NCD,NTM,NGR

!

!      CONSISTENCY CHECKS AND PREPARATION
!
*****  

IF(NTYP(IFILE).NE.NRE) CALL FOXNTY(IFILE)
IF(NTYP(INPART).NE.NRE) CALL FOXNTY(INPART)

!

!      GET VARS
!
*****  

FNAME = NINT(CC(NBEG(IFILE)))
NPART = NINT(CC(NBEG(INPART)))

!

!      READ THE FILE
!
*****  

DO 5 I=1,NPART

```

```

      READ(FNAME,*,END=10) PID,PNUM,PDGID,FLAG,T,W,X,Y,Z,PX,PY,PZ,
& SPINX,SPINY,SPINZ
      E=SQRT(PX**2+PY**2+PZ**2+(MASSBYIDICOOL(NINT(PDGID))/1000)
& **2)*1000
      CC(NBEG(IV+1)+I-1)=X
      CC(NBEG(IV+2)+I-1)=PX*1000
      CC(NBEG(IV+3)+I-1)=Y
      CC(NBEG(IV+4)+I-1)=PY*1000
      CC(NBEG(IV+5)+I-1)=T
      CC(NBEG(IV+6)+I-1)=E
5    CONTINUE
10   CONTINUE
      END

!
! *****
!
!      SUBROUTINE WICOOL(IZ, IREG, INPART, IV, IUI, IAPE)
!
!      WRITES PARTICLES TO UI IN ICOOL-STYLE. INPUTS ARE:
!
!      IZ - Z LOCATION
!
!      IREG - REGION NUMBER
!
!      INPART - NUMBER OF PARTICLES
!
!      IV - VECTOR TO WRITE
!
!      IUI - UI TO WRITE TO
!
!      IAPE - APERATURE
!
!
!      VECTOR IV MUST BE OF THE FORM
!
!      V = (X,PX,Y,PY,T,E) IN m, MeV, AND s
!
!
```

```

IMPLICIT DOUBLE PRECISION(A-H,O-Z)

DOUBLE PRECISION MASS

DOUBLE PRECISION, DIMENSION(:, :, :), ALLOCATABLE :: V ! V(NPART,6)

INTEGER IALLOCATESTATUS,I,J

!-----MEMORY MANAGEMENT -----
PARAMETER(LMEM=1000000000,LVAR=100000000,LDIM=10000)
INTEGER NTYP(LVAR),NBEG(LVAR),NEND(LVAR),NMAX(LVAR),
*          NC(LMEM),NDIM(LDIM)
DOUBLE PRECISION CC(LMEM)
COMMON NTYP,NBEG,NEND,NMAX, CC,NC, NDIM, IDIM, IVAR,IMEM
COMMON /TYID/ NRE,NST,NLO,NCM,NVE,NIN,NIV,NDA,NCD,NTM,NGR

!      CONSISTENCY CHECKS AND PREPARATION
!
! *****
IF(NTYP(IZ).NE.NRE) CALL FOXNTY(IAV)
IF(NTYP(IREG).NE.NRE) CALL FOXNTY(ISI)
IF(NTYP(INPART).NE.NRE) CALL FOXNTY(IN)
IF(NTYP(IUI).NE.NRE) CALL FOXNTY(IUI)
IF(NTYP(IAPE).NE.NRE) CALL FOXNTY(IAPE)

!
!      GET VARS
!
! *****
Z = CC(NBEG(IZ))
REG = NINT(CC(NBEG(ISI)))
NPART = NINT(CC(NBEG(INPART)))
UI = NINT(CC(NBEG(IUI)))
APE = CC(NBEG(IAPE))

```



## BIBLIOGRAPHY

- [1] C. M. G. Lattes *et al.*, *Nature*, vol. 159, 1947.
- [2] P. Gagnon, “The standard model: A beautiful but flawed theory,” 2014. [Online]. Available: <http://www.quantumdiaries.org>
- [3] D. Griffiths, *Introduction to Electrodynamics*, 3rd ed. Prentice Hall Of India Pvt. Limited, 1999.
- [4] M. Berz and K. Makino, *COSY Infinity Beam Physics Manual*, 2013, version 9.1. [Online]. Available: <http://www.cosyinfinity.org>
- [5] M. Berz, *Modern Map Methods in Particle Beam Physics*. Academic Press, 1999.
- [6] M. Berz, K. Makino, and W. Wan, *An Introduction to Beam Physics*. CRC Press, 1999.
- [7] J. Nielsen and D. McMorrow, *Elements of Modern X-ray Physics*, 2nd ed. John Wiley and Sons, 2011.
- [8] D. Griffiths, *Introduction to Quantum Mechanics*, 2nd ed. Pearson, 2005.
- [9] J. V. José and E. J. Saletan, *Classical Dynamics: A Contemporary Approach*. Cambridge University Press, 1998.
- [10] Fermi National Accelerator Laboratory, “Muon Accelerator Program.” [Online]. Available: <http://map.fnal.gov>
- [11] G. K. O’Neill, “Storage-ring synchrotron: Device for high-energy physics research,” *Phys. Rev.*, vol. 102, 1956.
- [12] D. Lichtenberg, P. Stehle, and K. R. Symon, “Modifications of Liouville’s theorem required by the presence of dissipative forces,” *MURA*, vol. 126, 1956.
- [13] Y. Ado and V. Balbekov, “Use of ionization friction in the storage of heavy particles,” *Sov. Atomic Energy*, vol. 31, 1971.
- [14] “Muon ionization cooling experiment,” repository of images and public information, Accessed August 20, 2016. [Online]. Available: [http://micewww.pp.rl.ac.uk/projects/mice/wiki/\\_Repository\\_of\\_Images](http://micewww.pp.rl.ac.uk/projects/mice/wiki/_Repository_of_Images)
- [15] D. Neuffer, “Introduction to muon cooling,” in *Proceedings of COOL’03*, 2004, pp. 26–31, doi:10.1016/j.nima.2004.06.051.
- [16] J. Beringer *et al.*, (PDG) PR D86, 010001 chpt. 31, 2013.
- [17] Particle Data Group Atomic Nuclear Properties, 2014. [Online]. Available: <http://pdg.lbl.gov/2014/AtomicNuclearProperties/>
- [18] R. Fornow *et al.*, “ICOOL,” 2012, version 3.30. [Online]. Available: <http://www.cap.bnl.gov/ICOOL/fornow/readme.html>
- [19] T. Roberts, “G4beamline,” 2014, version 2.15w. [Online]. Available: <http://www.muonsinternal.com/muons3/G4beamline>

- [20] *GEANT4 Physics Reference Manual*, CERN, 2011, version 9.5.0.
- [21] H. A. Bethe, “Scattering of electrons,” *Z. für Physik*, vol. 76, 1932.
- [22] L. Landau, “On the energy loss of fast particles by ionisation,” *J. Phys. U.S.S.R.*, vol. 8, 1944.
- [23] P. V. Vavilov, “Ionization losses of high energy heavy particles,” *Soviet Physics JETP*, vol. 5, 1957.
- [24] N. Ashcroft and N. Mermin, *Solid State Physics, HRW International Editions*, 1976.
- [25] H. Bichsel, “Straggling in thin silicon detectors,” *Rev. Mod. Phys.*, vol. 60, 1988.
- [26] H. Lewis, “Multiple scattering in an infinite medium,” *Phys. Rev.*, vol. 78, 1950.
- [27] S. Goudsmit and J. Saunderson, “Multiple scattering of electrons,” *Phys. Rev.*, vol. 57, 1939.
- [28] V. Highland, “Some practical remarks on multiple scattering,” *NIM*, vol. 129, 1975.
- [29] G. R. Lynch and O. I. Dahl, “Approximations to multiple Coulomb scattering,” *NIM*, 1991.
- [30] *GEANT - Detector Description and Simulation Tool*, CERN, 1993, version 3.21.
- [31] D. Atwood *et al.*, “The scattering of muons in low z materials,” *NIM*, vol. 251, 2006.
- [32] R. Fernow and J. C. Gallardo, “Muon transverse ionization cooling: Stochastic approach,” *Phys. Rev. E*, vol. 52, 1995.
- [33] The MICE Collaboration, “An international muon ionization cooling experiment (MICE),” Tech. Rep., 2003, proposal to the Rutherford Appleton Laboratory. [Online]. Available: <http://mice.iit.edu/mnp/MICE0021.pdf>
- [34] C. B. Do, “The multivariate gaussian distribution,” 2008, Stanford University CS 229 Lecture Notes. [Online]. Available: <http://cs229.stanford.edu/section/gaussians.pdf>
- [35] P. C. Mahalanobis, “On the generalized distance in statistics,” *Proceedings of the National Institute of Sciences of India*, vol. 2, 1936.
- [36] R. L. Borrelli and C. S. Coleman, *Differential Equations: A Modeling Perspective*, 2nd ed. John Wiley and Sons, 2004.
- [37] M. S. Livingston and H. A. Bethe, “Chapter XVI: Auxiliary data for the evaluation of experiments,” *Reviews of Modern Physics*, vol. 9, 1937, section C: Nuclear Dynamics, Experimental.
- [38] D. Griffiths, *Introduction to Elementary Particles*, 2nd ed. WILEY-VCH Verlag GmbH & Co. KGaA, 2008.